Measurement and Visualization of Electron Transfer at the Single Molecule Level

---

A Dissertation
Submitted
to the Temple University Graduate Board

In Partial Fulfillment
of the Requirements for the Degree of
Doctor of Philosophy

By
Yangjun Xing
August, 2009

ABSTRACT

Molecular electronics based on bottom-up electronic circuit design is a potential solution to meet the continuous need to miniaturize electronic devices. The development of highly conductive molecular wires, especially for long distance charge transfer, is a major milestone in the molecular electronics roadmap. A challenge presented by single molecule conductance is to define the relative influence of the molecular "core" and the molecular "interconnects" on the observed currents. Much focus has been placed on designing conductive, conjugated molecules. However, the electrode-molecule contacts can dominate the responses of metal-molecule-metal devices. We have experimentally and theoretically probed charge transfer through single phenyleneethynylene molecules terminated with thiol and carbodithioate linkers, using STM break-junction and non-equilibrium Green's function methods. The STM break-junction method utilizes repeatedly formed circuits where one or a few molecules are trapped between two electrodes, at least one of which has nanoscale dimensions. The statistical analysis of thousands of measurements yields the conductance of single molecules. Experimental data demonstrate that the carbodithioate linker not only augments electronic coupling to the metal electrode relative to thiol, but reduces the barrier to charge injection into the phenyleneethynylene bridge. The theoretical analysis shows that sulfur hybridization provides the genesis for the order-of-magnitude increased conductance in carbodithioate-terminated systems relative to those that feature the thiol linker. Collectively, these data

emphasize the promising role for carbodithioate-based connectivity in molecular electronics applications involving metallic and semi-conducting electrodes.

One of the strategies for building molecular wires that can transfer charge over long distance is to incorporate metal ions into the conductive molecular core. Peptide nucleic acid (PNA) is a great candidate for this purpose. Studying the conductivity of PNA can not only contribute to a better understanding of charge transfer through biomolecules, but can also help develop better molecular wires and other building blocks of molecular electronics. We study the charge transfer of PNA molecules using the STM break-junction technique and compare with traditional macroscopic voltammetric measurements. By measuring the resistance of different PNA molecules, we hope to develop a deep understanding of how charge transport though PNA is affected by factors such as the number and type of natural and artificial bases, embedded metal ions, pH, etc.

Self-assembled monolayers (SAMs) of porphyrins are of great interest due to their diverse applications, including molecular devices, nano-templates, electrocatalysis, solar cells, and photosynthesis. We combined a molecular level study of the redox reactions using electrochemical scanning tunneling microscopy (EC-STM) with a macroscopic electrochemical technique, cyclic voltammetry (CV), to study two redox active porphyrin molecules, TPyP (5,10,15,20-Tetra(4-Pyridyl)-21H,23H-Porphine) and 5, 10, 15, 20-tetrakis (4-carboxylphenyl)-21H, 23H-porphine (TCPP). We showed that the adsorbed oxidized TPyP molecules slowly change to brighter contrast, consistent with the appearance of the reduced form of TPyP, under reduction condition ($0.0V_{SCE}$). The time scale of the slow reduction is in the order of tens of minutes at $0.0V_{SCE}$, but accelerates at more negative potentials. We propose that protonation and deprotonation processes play

an important role in the surface redox reaction due to geometric restriction of the molecules adsorbed on the surface. EC-STM and CV experiments were performed at various pH values to investigate the mechanism of this anomalously slow redox reaction. Our results show that the increased concentration of H^+ hinders the reduction of porphyrins, a feature that has not been reported preciously. This provides insight into the details of the surface redox reaction.

ACKNOWLEDGMENTS

I greatly appreciate all the support from my research advisor, Professor Eric Borguet, for guiding me through my Ph.D research over the years. I am thankful for the help from my advisory committee members, Professor Daniel R. Strongin, Professor Stephanie Wunder and Professor Theodore W. Burkhardt. I thank all the Borguet research group members for their help, especially Dr. Yufan He and Dr. Kyoungja Seo for training on scanning probe microscopy related topics and useful discussions. I also thank all my collaborators in several research areas. Their names will be acknowledged in the corresponding chapters.

My graduate research is supported by Temple University, the National Science Foundation, the Department of Energy and the Daniel Swern Fellowship.

TABLE OF CONTENTS

PAGE

ABSTRACT....iii

ACKNOWLEDGMENTS....vi

LIST OF TABLES....viii

LIST OF FIGURES....ix

CHAPTER

1. INTRODUCTION TO SINGLE MOLECULE CHARGE TRANSFER....1
2. OPTIMIZING SINGLE MOLECULE CONDUCTIVITY WITH CONJUGATED CARBODITHIOATE LINKERS....36
3. SINGLE MOLECULE CONDUCTIVITY MEASUREMENT OF PEPTIDE NUCLEIC ACIDS....61
4. MOLECULAR SCALE VISUALIZATION OF PORPHYRIN CHARGE TRANSFER REACTIONS....80

REFERENCES....110

BIBLIOGRAPHY....129

APPENDICES....147

A. STM TIP PREPARATION FOR PNA CONDUCTIVITY MEASUREMENTS IN AQUEOUS SOLUTION....148
B. PROCEDURE FOR PREPARATION OF A GOLD BEAD....150
C. SYNTHESIS AND DEPROTECTION OF CARBODITHIOATE OPE MOLECULES....152
D. SYNTHESIS OF PNA MOLECULES....155
E. THEORETICAL SIMULATION OF THE OPE MOLECULES....156
F. LIST OF PUBLICATIONS....159

LIST OF TABLES

Table Page

1. **Table 2- 1**: Conductance Measurements of T1-T3 and C1-C3 44

2. **Table 2- 2:** Resonant current (I_m^{RES} m=HOMO/LUMO) for V=100 mV) for CTS and DTS. 54

3. **Table 3- 1:** Conductance of PNA molecules. (BK means backbone only, i.e. PNA molecule without nucleobases) 73

4. **Table 3- 2:** Conductance of same length PNA molecules with various nucleobases. 74

LIST OF FIGURES

Figure Page

1. **Figure 1- 1:** The first illustration of molecular electronics in 1958.[27] 4

2. **Figure 1- 2:** A monolayer of bistable, [2]rotaxane molecules (A) is used as the data storage elements for a memory device (B). [65].....5

3. **Figure 1- 3:** a) Scheme showing occupied levels and unoccupied levels separated by Fermi level. b) Fermi-Dirac distribution at various temperature.[86].....8

4. **Figure 1- 4:** The Marcus description of charge transfer. The Gibbs energy surfaces of an electron transfer process in a DA complex (blue line), and the charge separated D^+A^- (brown line) state. The transition from DA to D^+A^- occurs at the coordinate q_t where the energy surfaces of the two species cross. This transition can only happen when DA is activated by Δ^+G.....11

5. **Figure 1- 5:** Scheme of a one dimensional wire of length L connected by two metal electrodes, described by their own chemical potentials, μ.....16

6. **Figure 1- 6 :** (a) Chemical structure of PNA with a ferrocene group, where n = 3-7. (b) PNA molecules self-assembled on a gold surface.[126] 21

7. **Figure 1- 7 :** Techniques for single molecule charge transfer study: a) cross-wire method;[127] b) electromigrated junction;[131] c) mixed SAM/SPM method;[75] d) mechanical break-junction method.[79] 23

8. **Figure 1- 8:** The process of the nano-electrodes and m-M-m system formation in STM break-junction experiments. Two nano electrodes are formed by breaking the contact between the Au tip and the substrate (a-d). With the presence of molecules in the solution and on the surface, an m-M-m system may be created (e). It takes less than a second to repeat this process in single molecule conductivity measurements. 27

9. **Figure 1- 9:** Statistical analysis process of STM break-junction method. 30

10. **Figure 1- 10:** Histrogram analysis of over 3000 IS curves for each molecule: 1,4-benzenediamine (blue), 1,4-benzenedithiol (red), and 1,4-

benzenediisonitrile (green). (a) shows the example IS curves. (b) is semi-log plot histogram analysis.[144] 33

11. **Figure 1- 11:** a) IS curves using an STM tip showing clear gold atomic steps in STM image. These curves are from successive measurements without selection. b) IS curves using a low quality STM tip. 35

12. **Figure 2- 1:** Schematic of a metal-molecule-metal junction. (Cartoon by Dr. Yufan He) 37

13. **Figure 2- 2:** Structure of α,ω-dithiol-terminated (T1, T2 and T3) and α,ω-bis-carbodithioate-terminated π-conjugated molecules (C1, C2 and C3). 40

14. **Figure 2- 3:** STM break-junction measurement for hexanedithiol in toluene. a) Typical IS curves with clear step features. b) Histogram analysis of selected IS curves show clear peaks. c) Linear plot of measurements done at different bias voltages. 42

15. **Figure 2- 4:** a) Scheme for single molecule (C3) conductance measurements; b) Example of current-distance curves recorded with C3 in the junction at 50 mV bias; c) Histogram analysis of C3 conductance constructed from ~150 IS curves; d) Conductance of C3 is determined by fitting the measurements at different bias. 43

16. **Figure 2- 5:** a) Example of IS curves recorded with T1 in the junction at 50 mV bias; b) Histogram analysis of T1 conductance constructed from ~270 IS curves. 44

17. **Figure 2- 6:** Natural logarithmic plot of the resistance of dithiols (T1-T3, red circles) and carbodithioates (C1-C3, black diamonds) versus molecular length. The β values are calculated through the semi-logarithmic plot of resistance and molecule length based on $R = R_0 \exp(\beta L)$. The dashed blue line is for DTS and the black line is for T2 and T3 only. The green line is the β fitting for CTS. 47

18. **Figure 2- 7:** Plots of the scoring factors (Eq. 2- 1) for each molecular orbital vs MO energies. a) CT systems and b) DT systems. For both CT and DT systems, the orbitals which show the strongest contributions are labeled. 53

19. **Figure 2- 8:** An example of porphyrin based molecular wire. 59

20. **Figure 3- 1**: Structure comparison between PNA, DNA and protein.[193] 62

21. **Figure 3- 2**: Long distance charge transfer molecular wire based on PNA. (Cartoon drawn by the Achim group) 64

22. **Figure 3- 3:** AFM image of Cys-T6-Fc monolayer showing two kinds of domains with height difference ~3.5 nm.[126] 69

23. **Figure 3- 4:** Ferrocene Reaction during Cyclic Voltammetry cycles.[126] 70

24. **Figure 3- 5:** Tunneling decay constant (β) determination for Thymine (T) containing single stranded PNA molecules (error bars are smaller than symbols).[126] 71

25. **Figure 3- 6:** Molecular conductance measurement of cys-T4-cys.[217] 72

26. **Figure 3- 7:** Natural logarithmic plot of the conductance of PNA versus number of bases (a) and length (b).[217] 74

27. **Figure 4- 1:** The simplest model of electrochemical double layer.[221] 81

28. **Figure 4- 2:** STM image of the Au(111) reconstructed surface. The double strips are reconstruction lines as shown in the cartoon on the right. 82

29. **Figure 4- 3:** Schematic of EC-STM. A bipotentiostat is used to control the electrode potential in a four electrode setup, including CE: counter electrode, RE: reference electrode.[229] 83

30. **Figure 4- 4:** In-situ STM images (50 x 50 nm^2) of TPyP (A) Electrode potential 0.5 V_{SCE}; (B) Electrode potential 0.5 V_{SCE} (upper part) and -0.3 V_{SCE} (lower part); (C) -0.3 V_{SCE} (upper part) and +0.5 V_{SCE}(lower part).[261] 89

31. **Figure 4- 5:** Pre-adsorbed TPyP on Au(111) in 0.1 M H_2SO_4 at 0.1 V_{SCE} (27 x 27 nm^2) after partially oxidized.[263] 89

32. **Figure 4- 6:** Electrochemical experiments designed to probe the reduction time scale of a TPyP monolayer.[262] 90

33. **Figure 4- 7:** Chemical structure of TPyP and TCPP molecules 92

34. **Figure 4- 8:** Sub-molecular resolution STM image of TPyP monolayer acquired at 0.0 V_{SCE} in 0.1 M H_2SO_4. 93

35. **Figure 4- 9:** STM images of TPyP adlayer on Au(111) in 0.1 M H_2SO_4 under potential control. a) Multilayer, 91 nm x 91 nm, 0.0 V_{SCE}; b) Two layers, 66 nm x 66 nm 0.0 V_{SCE}; c) Mono-layer, 30 nm x 30 nm, 0.2 V_{SCE}.[268] 95

36. **Figure 4- 10:** STM images showing the growth of TPyP adlayers. a) Image acquired right after the injection of TPyP molecules into the electrochemical cell. b) 15 minutes after the injection, multilayer of TPyP formed. Both images are taken in 0.1 M H_2SO_4 at 0.0 V_{SCE} with TPyP concentration ~ 10^{-6} M.[268] 96

37. **Figure 4- 11:** TPyP adlayer formation studied by QCM in 0.1 M H_2SO_4 at 0.0 V_{SCE}. Blue trace is the frequency change for TPyP adsorption. The sharp drop at around 650 sec is due to the injection of TPyP solution (final concentration after injection is ~ 10^{-6} M). The red trace is the calculated monolayer change based on the frequency plot.[268] 97

38. **Figure 4- 12:** Two STM successive image of TPyP multilayer in 0.1 M H_2SO_4 at 0.0 V_{SCE} (50 nm x 50 nm) separated by ~ 200 sec. Red circles show vacancy holes in the first image (a) being filled in the second image (b), while green circles show molecules leaving the surface.[268].....98

39. **Figure 4- 13:** STM images of TPyP adlayer on Au(111) in 0.1 M H_2SO_4 at 0.0 V_{SCE} (setpoint 0.1 nA). The center part of the image was previously scanned at 0.3 nA for several images.....99

40. **Figure 4- 14:** The slow reduction of TPyP on an Au(111) surface in 0.1 M H_2SO_4 solution (30 x 30 nm^2). A: Oxidized TPyP monolayer at 0.2 V_{SCE}, B: 12 minutes of reduction at 0.0 V_{SCE}. C: 56 minutes of reduction at 0.0 V_{SCE}.[268] 100

41. **Figure 4- 15:** TPyP monolayer in neat 0.1 M H_2SO_4, sample potential 0.0 V_{SCE}, 20 x 20 nm^2, 2 hours after reduction started.[268].....101

42. **Figure 4- 16:** (A) TCPP arrays in 0.01 M $HClO_4$ at potential of E = 0.1 V_{SCE} without any reduced form molecules. (B) Lower part, TCPP arrays in 0.01 M $HClO_4$ at potential of 0.1 V_{SCE} with only several reduced TCPP (bright spots) marked by white circles. Upper part, TCPP arrays immediately became brighter after potential change from 0.1 V_{SCE} to 0.0 V_{SCE} in the middle of image.[271] 103

43. **Figure 4- 17:** (A) TCPP arrays in 1 M $HClO_4$ at potential of E = -0.05 V_{SCE} without bright spots. (B) Sequence STM images after (A) with several bright spots (marked by white circles) at potential of -0.15 V_{SCE}.[271] 104

44. **Figure 4- 18:** Proposed mechanism of TCPP reduction on Au(111) in an acidic medium.[271] 106

LIST OF ABBREVIATIONS

ET: electron transfer

CMOS (complementary metal–oxide–semiconductor)

STM: scanning tunneling microscope

SPM: scanning probe microscopy

AFM: atomic force microscopy

NDR: negative differential resistance

DBA: donor-bridge-acceptor system

LUMO: lowest unoccupied molecular orbital

HOMO: highest occupied molecular orbital

m-M-m: metal-molecule-metal

PNA: peptide nucleic acid

SAM: self-assembled monolayer

CV: cyclic voltammetry

OPE: oligo(phenyleneethynylene)

CT: carbodithioate-terminated

DT: dithiol-terminated

CTS: carbodithioate-terminated systems

DTS: dithiol-terminated systems

NEGF: non-equilibrium Green's function

DFT: density functional theory

EC-STM: electrochemical scanning tunneling microscopy

UHV: ultra high vacuum

TPyP: 5,10,15,20-Tetra(4-Pyridyl)-21H,23H-Porphine

TCPP: 5, 10, 15, 20-tetrakis (4-carboxylphenyl)-21H, 23H-porphine

CHAPTER 1

INTRODUCTION TO SINGLE MOLECULE CHARGE TRANSFER

1. Importance of Understanding Charge Transfer

1.1. General Interest of Charge Transfer Study

Electron transfer (ET) is one of the most important chemical processes.[1] The electron is the smallest unit of charge in chemical processes and all chemical bonds involve electrons. ET is the essential step of all electron transfer reactions, which can be seen in physical, inorganic, biological and organic chemistry. ET has great impact in our every day life. For example, ET reactions between iron and oxygen are responsible for corrosion of steel, which costs billions of dollars each year. ET reactions are the crucial step in many biological processes,[1] for instance, protein-protein ET reactions[2-5], biological energy transduction processes[1, 6], light-harvesting in biological systems[1, 7-9], etc. In a number of redox enzymes that are critical for biological systems, electrons transfer efficiently over a long distance in a very short time.[5] Many reactions in organic chemical systems involve radical ions, which are generated by removing or adding one electron from/to a neutral molecule, a result of electron transfer.[1]

Understanding, manipulating and utilizing electron transfer in a variety of systems are important research tasks in chemistry. There have been tremendous research effects in this field.[1] ET study is also one of the broadest research areas in chemistry, present in almost every aspect of chemistry.[1] In particular, ET study in molecular electronics has drawn great attention in the past several decades.[10-17]

1.2. Motivation: Molecular Electronics

One of the most famous and influential speeches in the history of nanotechnology, "There is plenty of room at the bottom", given by Dr. Feynman in 1959, will have its 50th anniversary this year.[18] The past half century has seen tremendous progress in the field of microelectronics and molecular electronics, as Dr. Feynman foresaw. Indeed, there is plenty of room at the bottom. The continuous decrease of transistor size has been guided by Moore's law [19-21] in the past half century. However, there is a fundamental limit in CMOS based microelectronics: doping levels (< 1%) in solid-state semiconductor devices, the key to building field-effect transistors, result in, on average, a fraction of a doping atom per junction at the nanoscale, making the behavior of devices unpredictable.[22-24] As the scaling of conventional CMOS (complementary metal–oxide–semiconductor) based electronic devices faces increasing challenges on going to smaller and smaller sizes[25, 26], molecular electronics is one of the solutions that could meet the need to miniaturize electronic devices.[22]

Imagine that all electronic units are constructed of single molecules and connected by molecular wires, which have feature sizes down to a few nanometers. Imagine that those molecular units self assembling to form electronic devices. Imagine how the addition or removal of a single electron controls the response of electronic devices. Molecular electronics has the potential to transform the world of electronics. The beauty of using single molecules as electronic units is that each molecule has its own characteristic electrical (or mechanical, optical, magnetic, and more) properties that are sensitive to the molecular structure. The capability of designing and synthesizing a variety of molecules using advanced organic synthesis techniques enables us to build all possible electronic units using single molecules.

1.2.1. History of Molecular Electronics

In 1958, the US Air Force and Westinghouse coined the term "molecular electronics" in a collaborative program to build monolithic integrated circuits.[27] **Figure 1- 1**, drafted by an Air Force colonel in 1958, is similar to most illustration charts used nowadays. Lacking of sufficient theoretical and experimental foundation, the program was too pioneering at that time and eventually failed.[27] However, driven by the desire to build a new electronics platform beyond silicon ICs, the effort to develop molecular electronics was never stopped.

Due to the lack of advanced experimental techniques in early times, theorists took the leading role in the development of molecular electronics. Considered as the founding statement of molecular electronics, the paper published by Dr. Aviram and Dr. Ratner in 1974,[28] "Molecular Rectifiers", is purely theoretical. At that time, even the authors did not know how to solve the problem of manufacturability.[27] Without the support of experimental results, molecular electronics was seen by its critics as a scientific fantasy that could not be realized.[27] It was not until the late 1980s, with the advent of the scanning tunneling microscope (STM), that molecular electronics research accelerated dramatically.[27, 29] It is the capability of directly measuring the properties of single molecules that stimulated research in molecular electronics in the late 1980s. In addition, scanning probe microscopy (SPM), including STM and AFM (atomic force microscopy), is not limited to the characterization of molecular devices. It can also serve as a tool for nano scale modification and fabrication.

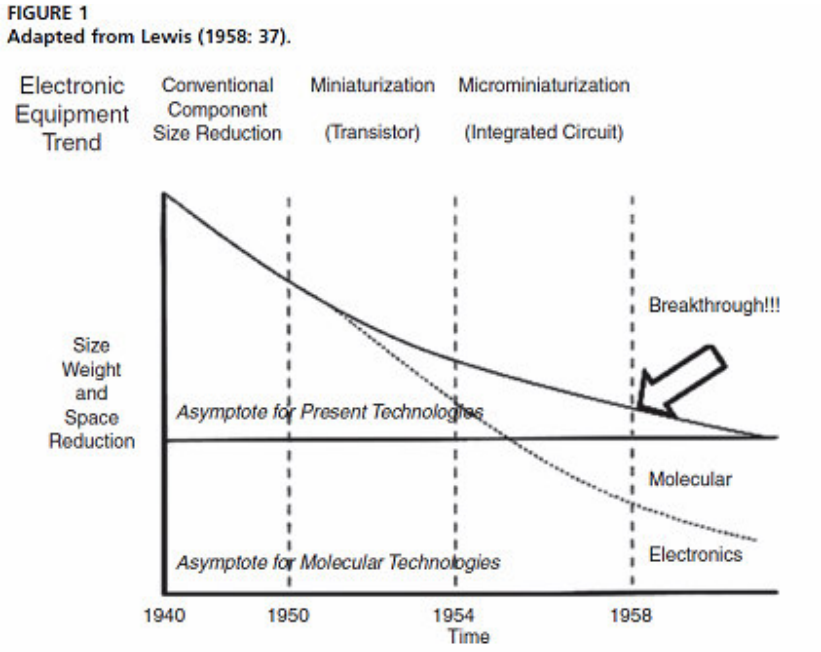

Figure 1- 1: The first illustration of molecular electronics in 1958.[27]

1.2.2. Recent Progress in Molecular Electronics

There has been tremendous progress in the field of molecular electronics, both in theory and in experiments, for example, on molecular rectifiers[30, 31], molecular switches[13, 32, 33], molecular wires[12, 34-43], and molecular memory[44-46]. It has been shown experimentally that single molecules can behave as Esaki diodes when negative differential resistance (NDR) is observed in a number of molecular systems.[47-50] The NDR effect refers to a region of current decrease with increasing voltage in the I-V characterization of a device, which can be used for many applications, including low power memory cells.

Taking advantage of the diverse properties of molecular systems, a number of special molecular devices have also been demonstrated. For example, the interaction between single molecules and light leads to the development of molecular light switches based on photochromic behavior[45, 51-53], fluorescence[54, 55], and other effects.[56-

59] Many other molecular systems, like the molecular abacus[60, 61], molecular oscillators[62], molecular motors[63, 64], etc. have also been demonstrated.

Most importantly, real molecular electronic devices have been built,[65, 66] suggesting that molecular electronics is not science fiction, but something that can be achieved. For example, a high density molecular memory (**Figure 1- 2**),[65] made by bistable [2]rotaxane, was built using a cross-bar setup.[67, 68] Although the demonstrated device is not a pure molecular device, but a hybrid of traditional methods and a molecular approach, it is still promising enough to show that we can expect molecular electronics to be realized in the near future. Using molecular devices to improve current electronics devices is a reality at the present time.

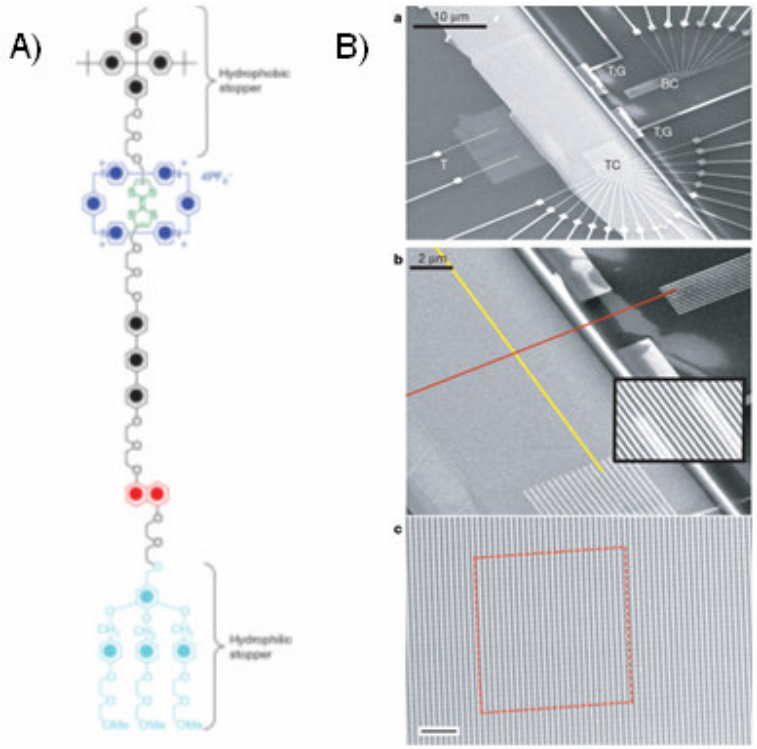

Figure 1- 2: A monolayer of bistable, [2]rotaxane molecules (A) is used as the data storage elements for a memory device (B). [65]

1.3. Molecular Wires

The development of conductive molecular wires that function as electronic components in miniaturized electronic devices is a major milestone in the molecular electronics roadmap. The molecular wire, the connection between active electronic units, is one of the key elements in molecular electronics. The synthesis, characterization and understanding of molecular wires that have high conductance and low β values (β is the coefficient describing how molecular conductance decreases with increased length) is of great interest for researchers in this field. Recent years have seen great progress in this field both theoretically[69-74] and experimentally.[34, 43, 75-81]

Because of the exponential decay of conductivity in saturated σ-bonded systems, due to the tunneling nature of electron transfer in such molecular systems, alkane chains are not suitable for charge transport in molecular electronics.[10, 75, 81] It has been suggested that molecules with delocalized, conjugated π backbones possess much higher conductance and much smaller β values than saturated σ-bonded systems.[10, 41, 82] There has been much focus on developing molecular cores based on π-conjugated building blocks, giving β values in the range of 0.2-0.6 $Å^{-1}$.[10, 41, 82] Recently, a few single molecule junction measurements with highly conjugated, low band gap oligomers have demonstrated an efficient long range charge transport with very small β values (≤ 0.2 $Å^{-1}$).[42, 83-85] For example, butadiyne bridged porphyrin oligomers display a very low β of 0.04 $Å^{-1}$, suggesting that both superexchange and hopping mechanisms (section 2.2.1) may be present within one system.[84] Notably, Choi et al. demonstrated that in the systematic molecular length increase of conjugated oligophenyleneimine (OPI) oligomers allows one to observe the theoretically predicted transport mechanism transition from tunneling to thermally activated hopping with molecular length in the metal-molecule-metal (m-M-m) junctions.[40] The extent of π-conjugation, band gap,

and length of the molecular cores are important in transporting charges efficiently over long distances and even to control transport mechanisms.

2. Charge Transfer Theory

The basic challenge in molecular electronics is to understand and control charge transfer in molecular systems. Before further discussion, it is important to review some of the basic principles of charge transfer.

2.1. General Theory

2.1.1. Fermi Energy

In molecular electronics, to control or test molecular devices, the molecules have to be connected to external systems, usually metal electrodes. This is very similar to a classical view of electronics, where electronic devices are connected using metal wires. However, at the molecular dimension, the classical theory of charge transfer, for example Ohm's law, does not work anymore. All electronics have to be described using quantum mechanics. The first important concept is the Fermi Level (or Fermi Energy).

The Fermi-Dirac distribution function *f*(E) describing the occupation of electrons when they are treated as non-interacting particles is given by

$$f(E) = \frac{1}{\exp[(E - E_F)/k_B T] + 1} \qquad \text{Eq. 1- 1}$$

where *f*(E) is the probability of an energy level E being filled by an electron. When E = E_F, *f*(E) = 0.5, which means Fermi level is an energy level that has a 50% probability of being empty and 50% probability of being filled. In metals, since the energy states fill a continuous band, the Fermi level refers the energy level that separates the filled and unoccupied states.

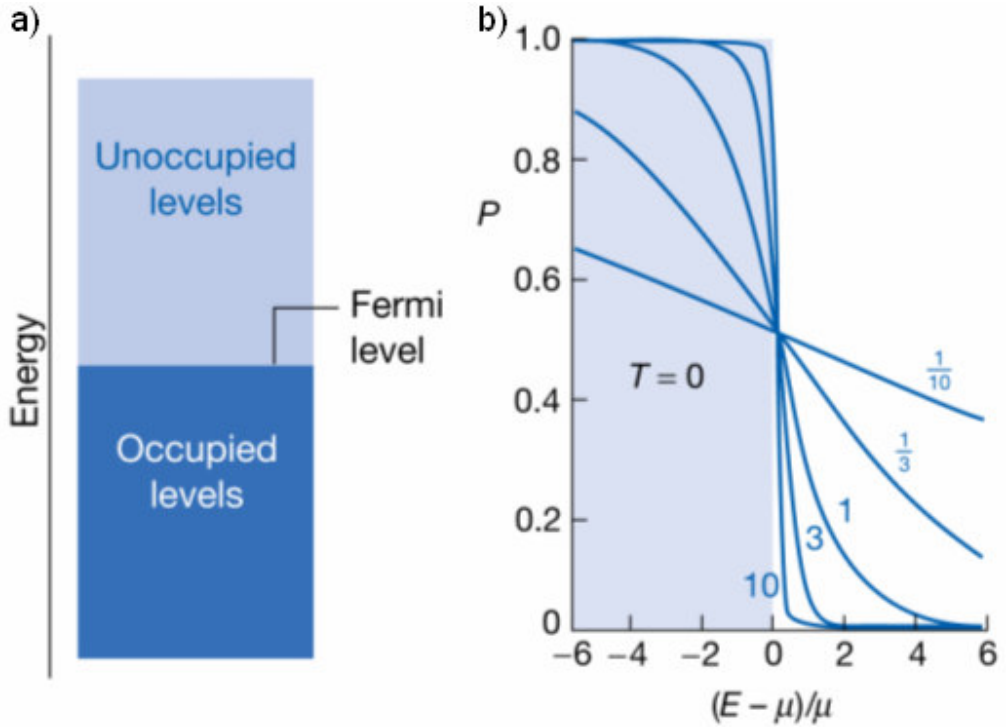

Figure 1- 3: a) Scheme showing occupied levels and unoccupied levels separated by Fermi level. b) Fermi-Dirac distribution at various temperature.[86]

The Fermi level is an important concept and we will mention it repeatedly in later discussion of charge transfer through single molecules which are connected to metal electrodes.

2.1.2. Fermi's Golden Rule

One of the central problems in quantum mechanics is to solve the time dependent Schrödinger equation, which describes the evolution of the system. For molecular electronics, a practical problem is to describe the electron transfer between energy states. For that, it is important to understand Fermi's golden rule, which deals with the transition rate from an energy state to another.

For a system described by a Hamiltonian *H,* the Schrödinger equation is:

$$H\psi = i\hbar \frac{\partial}{\partial t}\psi \qquad \text{Eq. 1- 2}$$

where $H = H_0 + H'$ is a combination of an initial, time independent Hamiltonian H_0 and a time dependent perturbation H'.

At time zero, when there is no perturbation, the eigenfunctions satisfy the following condition:

$$H_0\psi_n = E_n\psi_n \qquad <\psi_a \mid \psi_b >= \delta_{ab} \qquad \text{Eq. 1- 3}$$

The initial state ψ_0 can be described as

$$\psi_0 = \sum_n a_n\psi_n \qquad \text{Eq. 1- 4}$$

where ψ_n is a possible eigenstate and $|a_n|^2$ is the probability of finding the system in the n^{th} eigenstate. Since ψ_n forms a complete basis set, the system can also be described as a sum of eigenstates when the time dependent perturbation is introduced.

$$\psi(t) = \sum_n C_{nk}(t)e^{-iE_nt/\hbar}\psi_n \qquad \text{Eq. 1- 5}$$

where the index *nk* refers to transitions from the n^{th} state to k^{th} state under perturbation. The probability of this transition is $|C_{nk}|^2$. The transition rate is given by

$$w_{nk} = \frac{d}{dt} \mid C_{nk}(t) \mid^2 \qquad \text{Eq. 1- 6}$$

Substituting equation Eq. 1- 5 in to Eq. 1- 2 and using the condition in Eq. 1- 3, we can obtain:

$$i\hbar \frac{dC_{k'k}(t)}{dt} = \sum_n <\psi_{k'} \mid H'(t) \mid \psi_n > C_{nk}(t)e^{-i(E_{k'}-E_n)t/\hbar} \qquad \text{Eq. 1- 7}$$

Eq. 1- 7 is not easy to solve, and perturbation theory is used to obtain an approximate solution in which H' is considered much smaller than H_0. The order *(p+1)* approximation is found from the order *(p)* solution by:

$$i\hbar \frac{dC_{k'k}^{(p+1)}(t)}{dt} \approx \sum_n < \psi_{k'} \mid H'(t) \mid \psi_n > C_{nk}^{(p)}(t) e^{-i(E_k' - E_n)t/\hbar} \qquad \text{Eq. 1- 8}$$

The 0^{th} order approximation is $i\hbar \frac{dC_{k'k}^{(0)}(t)}{dt} = 0$. If H' is fixed and does not change during the transition process. Eq. 1- 8 takes the form:

$$i\hbar C_{k'k}(t) = 2H'_{k'k}\, e^{-i(E_{k'} - E_k)t/2\hbar} \left(\frac{\sin(-(E_{k'} - E_k)t/2\hbar)}{-(E_{k'} - E_k)/\hbar}\right) \qquad \text{Eq. 1- 9}$$

From Eq. 1- 9 and Eq. 1- 6, in the time limit $t \rightarrow \infty$ the transition rate is:

$$w = \int \rho(k') w_{k'k} dE_{k'} = \frac{2\pi}{\hbar} \mid H'_{k'k} \mid^2 \rho(k) \qquad \text{Eq. 1- 10}$$

where $\rho(k)$ is the density of states near E_k. Thus, $|H'_{kk}|$ is a measure of coupling strength between the k and k' states.

2.1.3. The Marcus Theory

Attempts to understand electron transfer theoretically began over a half century ago.[1, 87] The first theory that systematically interpreted electron transfer in molecular systems was the Marcus theory, initially developed by R.A. Marcus,[87] and further extended by N.S. Hush.[88] Marcus received the Nobel Prize for chemistry in 1992 for his contribution to electron transfer theory. The Marcus theory describes the electron transfer rate between a donor (D) and an acceptor (A) when D and A are close to each other:[86]

$$DA \rightarrow D^+ A^- \qquad \nu = k_{et}[DA] \qquad \text{Eq. 1- 11}$$

The electron transfer rate, $k_{et,}$ is determined by 1) the distance between D and A; 2) the reaction Gibbs energy ΔrG; 3) the reorganization energy, which is the energy cost incurred by the rearrangement of the D, A, and solvent molecules, since the D, A molecule always have solvation shells in solution.

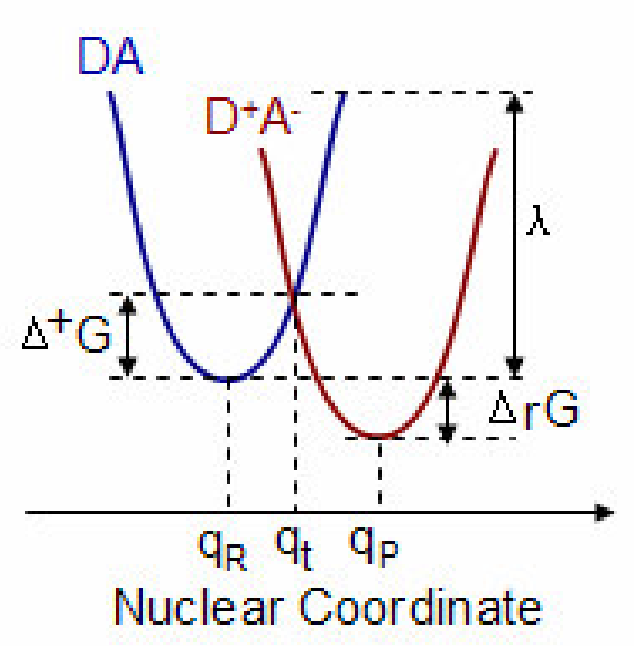

Figure 1- 4: The Marcus description of charge transfer. The Gibbs energy surfaces of an electron transfer process in a DA complex (blue line), and the charge separated D^+A^- (brown line) state. The transition from DA to D^+A^- occurs at the coordinate q_t where the energy surfaces of the two species cross. This transition can only happen when DA is activated by Δ^+G.

As shown in **Figure 1- 4**，the charge transfer process involves the reorganization energy λ, and the reaction Gibbs energy ΔrG. As described by Fermi's golden rule, the transition happens when the initial and final states have the same energy in the absence of an external light field. For the DA system, as shown in **Figure 1- 4**, the transition only occurs at a coordinate q_t (t means transition), where the energy surfaces of DA and D^+A^- cross. An activation energy

$$\Delta^+G = \frac{(\Delta_r G + \lambda)^2}{4\lambda} \qquad \text{Eq. 1- 12}$$

is required to trigger the transition. Usually, the activation energy comes from thermal fluctuations, which change the nuclear coordinate from q_R (reactant) to q_t and in turn trigger the electron transfer. The electron transfer rate is

$$k_{et} = \frac{2\pi}{\hbar} | H_{DA} |^2 \left[\frac{1}{4\pi\lambda k_B T} \right]^{1/2} e^{-(\Delta_r G + \lambda)^2 / 4\pi\lambda k_B T} \qquad \text{Eq. 1- 13}$$

where $|H_{AD}|^2$ is the coupling between donor and acceptor, which depends exponentially on the distance (R_{DA}) between D and A:

$$H_{DA} \propto \exp(-\beta R_{DA}) \quad \rightarrow k_{et} \propto \exp(-\beta R_{DA}) \qquad \text{Eq. 1- 14}$$

Eq. 1- 13 only holds in the regime of weak coupling between the donor and acceptor orbitals. Moreover, Eq. 1- 13 should not be used at temperatures to low for thermal fluctuations to activate the transition.[86]

2.2. Donor-bridge-acceptor System

The Marcus theory has been extensively used to describe electron transfer in solutions. It has also been applied to systems where the donor and acceptor are connected by a molecular bridge to form donor-bridge-acceptor system (DBA), where the bridge can be free space, solvent or a rigid molecular linker. The DBA system is an important concept, which connects the experimental verifications and electron transfer theories.[89] Many DBA systems with various length of bridge have been developed for years, and the electron transfer is studied by spectroscopic techniques.[89] R.A. Marcus compared the experimental and theoretical results for several DBA systems.[89] The dependence of the electron transfer rate on the length of bridge was investigated, and Eq. 1- 14 was verified in many molecular systems. Eq. 1- 14 is a fundamental relation which plays a central role in electron transfer research and the search for better molecular wires.

The attenuation factor (or decay constant) β is an important quantity for different molecular bridges, and it will be discussed over and over again in this thesis.

The DBA system has been extensively studied by Ratner[29], and his theoretical work provides a detailed analysis of electron transfer in molecular systems. The DBA concept was broadened to a wider range of systems, where D and A are not only molecular structures, but can also be metal electrodes, nanoparticles, etc. The mechanism of electron transfer mediated by bridges was well explained. Depending on the nature of DBA systems, for example, the length of bridge, the energy level overlap between bridge and donor or acceptor, and the property of chemical bonds in the bridge, the electron transfer can be dominated by superexchange or a hopping mechanism.[10, 29]

2.2.1. Electron Transfer Mechanisms: Superexchange and Hopping

For DBA systems in which the bridge is free space, the electron transfer mechanism is relatively simple. There is only one possible mechanism, which is quantum mechanical tunneling. In this case, it is easy to understand that the electron transfer rate follows Eq. 1- 14, since quantum mechanical tunneling decays exponentially with increasing distance. When the bridge is a molecular system, the electron transfer is mediated by the molecular bridge, and the rate of electron transfer can be increased. Depending on the nature the DBA system, electron transfer mechanisms can be very different.[10]

Superexchange. The superexchange mechanism is very similar to quantum mechanical tunneling, except that the tunneling is not directly through space, but mediated by the energy levels of the bridge. However, those levels are not intermediate states in the charge transfer process, i.e. the electrons do not populate those energy levels.[1] The energy states of bridges are usually much higher than the donor and acceptor levels. A simple model for the superexchange mechanism is to consider

electrons in the donor as free particles and treat the energy state of bridge as a tunneling barrier. The tunneling decay constant for the model can be written as:[90]

$$\beta = 2\frac{\sqrt{2m^*(E_{Barrier} - E_{Electron})}}{\hbar} \qquad \text{Eq. 1- 15}$$

This is an extension of the quantum mechanical picture of electron tunneling to the DBA systems with little modification. m^* is not the mass of an electron, but an effective mass. $E_{Barrier}$ is the energy of LUMO (lowest unoccupied molecular orbital) or HOMO (highest occupied molecular orbital) of the bridge, depending on which one mediates the electron transfer. Since the LUMO or HOMO is lower than vacuum level, the β in DBA systems with a molecular bridge is lower than tunneling through space, usually 0.2 to 0.8 $Å^{-1}$. Electron tunneling decay through space is associated with a β ~2 $Å^{-1}$, for an energy gap ~5 eV.

Although in the superexchange mechanism, the intermediate states D^+-B^--A or D-B^+-A^- do not actually exist, it is still important to discuss the energy levels or configurations of the two virtual states. If the D^+-B^--A configurations mix strongly with D-B-A and D^+-B-A^- configurations, the electron transfer process is considered to be an electron transfer mechanism.[1] If the D-B^+-A^- configurations mix more strongly, the electron transfer process is considered to be a hole transfer mechanism.

Hopping mechanism. When the bridge in a DBA system becomes longer, the probability of superexchange will decreases. The energy levels of the bridge are increasingly involved in the electron transfer process, and electrons populate those levels. Electrons (or holes) are injected into the orbitals of the bridge from the donor (or acceptor) before being transferred to the other end. The orbitals of the bridge can be delocalized, so that the electrons hop through the whole bridge at once. In many cases the bridge orbitals are localized, especially for long molecules, so that the electron transfer is completed by multiple-step hopping through the localized sites. When this

diffusive hopping dominates, the length dependence of electron transfer deviates from the tunneling picture, i.e. the electron transfer does not depend exponentially on the bridge length. Instead, it becomes ohmic, and the transfer rate depends linearly on the number of hopping sites, which is usually proportional to the length of the bridge. The hopping mechanism is important in many biological systems, especially for electron transfer through DNA chains, which are generally much longer than other molecular bridges.[91-94]

2.2.2. Metal-Molecule-metal Systems (m-M-m)

The metal-molecule-metal system is a special kind of DBA system, where both the donor and the acceptor are metals. The key difference between metal and molecular units is that the metal can be treated as an electron reservoir, and removing or adding electrons does not change the property of the metal electrodes. If the metal electrodes on both ends are identical, there is no distinction between donor and accepter in the m-M-m system. The electron transfer direction is determined by a voltage bias applied between the two metal electrodes.

The experimental realization of the m-M-m system was a crucial step toward molecular electronics. It became possible to measure electronic properties of molecular devices, for example, conductivity. The experimental progress in molecular devices, for example molecular wires, molecular switch, etc. relies, in large part, on the experimental studies of m-M-m systems experimentally. It was not until the late 1980s when it became possible to manipulate molecular systems at the nanoscale, particularly with the help of STM, that the conductivity of single molecules was experimentally measured.[27] Studies of m-M-m systems mainly focuses on a accessible property, the conductivity, instead of the electron transfer rate. Similar to Eq. 1- 14, a simple model for the dependence of conductivity on the length of molecular wire is given by $R=R_0\exp(\beta L)$,

where R_0 is the contact resistance, β is the decay constant, and L is the length of molecule.[10, 11, 90]

2.3. The Landauer Formula

2.3.1. The Landauer Interpretation of Nanoscale Electron Transfer

Electron transfer in molecular electronics is a nanoscale process. Therefore, only nanoscale charge transfer theories can be applied. The Landauer formula has been proved to be central to the understanding of electron transfer in nanoscale systems. It is the standard model for the interpretation of ballistic transport in one-dimensional wires (**Figure 1- 5**), especially for the m-M-m system.

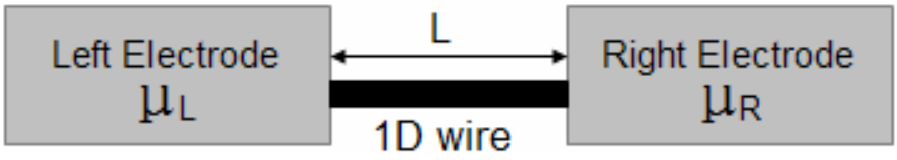

Figure 1- 5: Scheme of a one dimensional wire of length L connected by two metal electrodes, described by their own chemical potentials, μ.

The Landauer formula treats electron transfer in nanoscale systems as quantum mechanical tunneling with a transmission coefficient T. For example, the conductance, G, of the m-M-m system shown in **Figure 1- 5** under a small voltage bias is given by:

$$G = \frac{2e^2}{h} MT \qquad \text{Eq. 1- 16}$$

where M is the number of electron transfer channels, which can only be an integral number; T is the transmission coefficient, or efficiency, ranging from 0 to 100%. In an

ideal situation, when there is no dissipation during the electron transfer process, T = 100%, i.e. there is no scattering during the ET process. The conductance is (when M=1):

$$G = \frac{2e^2}{h} = 77.5\mu S = 1G_0 \text{ (corresponding resistance:12.9 k}\Omega\text{)} \qquad \text{Eq. 1- 17}$$

G_0 is the unit of conductance quantum, which we will use throughout this thesis.

2.3.2. The Conductance Quantum: G_0

G_0 is not only an important unit, but also a very useful concept that connects experiment and theory. It can be derived by simple quantum mechanical calculation and the absolute value of the calculated conductance has been confirmed by many experimental results.[81, 95] Considering an m-M-m system shown in **Figure 1- 5** with an ideal wire with length L, the Landauer formula treats the electron transfer process as electron injection from left electrode (assuming $\mu_L > \mu_R$), an electron reservoir, followed by electrons being transported to the right electrode. The tunneling current from the left electrode to the molecular wire is:

$$I_L = e\int_0^{\infty} v(k) f(E) n(k) dk \qquad \text{Eq. 1- 18}$$

where *n(k)* is the density of states per unit length of the one dimensional wire, $n(k)dk = 2\frac{1}{L}\frac{L}{2\pi}dk = \frac{1}{\pi}dk$; *v(k)* is the electron group velocity, $v(k) = \frac{\hbar k}{m}$; *f(E)* is the Fermi-Dirac distribution function. Eq. 1- 18 can reorganized as:

$$\begin{aligned} I_L &= e\int_0^{\infty} \frac{\hbar k}{\pi m} f(E) \frac{dk}{dE} dE = e\int_0^{\mu_L} \frac{\hbar k}{\pi m} \frac{dk}{dE} dE \\ &= e\int_0^{\mu_L} \frac{\hbar k}{\pi m} \frac{1}{\hbar} \frac{m}{\hbar k} dE = \frac{2e}{h}\int_0^{\mu_L} dE \end{aligned} \qquad \text{Eq. 1- 19}$$

The electron tunneling from the wire to the right electrode can be written in the same way:

$$I_R = \frac{2e}{h}\int_0^{\mu_R} dE \qquad \text{Eq. 1- 20}$$

The overall current, or the electron transfer, through the 1D nanowire is:

$$I = I_L - I_R = \frac{2e}{h}\int_{\mu_R}^{\mu_L} dE = \frac{2e}{h}(\mu_L - \mu_R) = \frac{2e^2}{h}V \qquad \text{Eq. 1- 21}$$

Therefore, the conductance of the system is

$$G = \frac{I}{V} = \frac{2e^2}{h} = G_0 \qquad \text{Eq. 1- 22}$$

G_0 has been measured experimentally, and the good agreement between the theory and experimental results highlights the importance of the Landauer formula in interpreting nanoscale electron transfer.[96, 97]

Ballistic transport. It should be noted that the conductance quantum does not depend on the length of the 1D wire. This length independence suggests an important feature of an ideal 1D wire - ballistic electron transport. In this regime, electrons pass through the 1D wire as a wave without scattering or energy loss and the wire simply serves as a waveguide, instead of offering resistance like a traditional wire. This feature has been observed by experiments. For example, the conductance of nanoscale gold wires in the STM break-junction experiments (which we will introduce later in this chapter) shows a clear length independence when the length of a nanowire is changed by mechanical force.[81]

In real systems when two electrodes are connected by a nanowire, the precondition for the observation of quantized conductance is to have the diameter of the nanowire small enough, comparable with the Fermi wavelength of the electrons in that system.[98, 99] In such circumstances, the nanowire can be treated as a 1D wire. For example, the Fermi wavelength of gold is about 0.5 nm, comparable to the separation

between atoms. Therefore, a few atom wide gold chain behaves as a 1D wire, and the conductance quantum can be easily observed.[81]

Since the conductance of a 1D wire does not depend on the length, the resistance of the wire can be understood as a contact resistance, i.e. the resistance is only introduced by the contacts between the wire and each of the electrodes. It should be pointed out that the idea of contact resistance may only be useful for comparing two nanowire systems. In quantum mechanical systems, the total resistance of two connected resistors (the contacts and the wire here) can not be a simple summation.[11, 100] In a practical point of view, one can never measure the conductance of a wire without connecting it to electrodes. Therefore, the contact resistance and the wire resistance can not be considered separately. However, if two nanowire systems show difference contact resistance values, it may imply an intrinsic difference between the two systems.

3. Measurement of Charge Transfer in Molecular Systems

3.1. Traditional Methods for Charge Transfer Study in Molecular Systems

In macroscopic systems, the electron flow can be easily measured with an ammeter. However, in molecular systems, it is not easy to wire a nanoscale connect between two electrodes to measure the electrical current. Charge transfer research in molecular systems has been performed for decades without modern nanoscale manipulation techniques. Spectroscopic and electrochemical techniques are two of the most important techniques used.

3.1.1. Traditional Spectroscopic Techniques for Charge Transfer Study

A variety of traditional spectroscopic techniques have been used to study charge transfer for decades.[1, 16] Although these techniques measure the average property of an ensemble of molecules, they are very useful in identifying molecular structures before

and after charge transfer. One of the most widely used techniques is simply measuring the absorption spectrum (UV-Vis or IR) to determine the changes in the properties of the molecular species during the electron transfer process.[1, 34, 101-103] More sophisticated experiments involve pump-probe laser techniques, which can provide ultrafast time resolution, so called transient absorption spectroscopy.[34, 103]

Fluorescence quenching is another widely used spectroscopic technique to study electron transfer in biological systems.[1, 104-109] After a chromophore linked to a molecular bridge has been excited by absorbing an excitation photon, it can fluoresce only if the absorbed energy is not dissipated. The fluorescence signal is quenched when there is electron transfer through the molecular bridge. Time-dependent fluorescence spectroscopy can be used to probe the kinetics of the charge transfer process. One example is a chromophore-linker-quencher system, where the other end of the molecular bridge is a unit with low-lying excited states, ready to perform a redox reaction and to quench the fluorescence, for example, in ferrocenes,[110-112] and fullerenes,[113, 114] etc.[111, 115-118]

3.1.2. Electrochemical Methods for Charge Transfer Study

Electrochemical methods have long been used to study interfacial charge transfer at solid-liquid interfaces, as well as the redox behavior of molecules adsorbed on an electrode surface. Generally, a self-assembled monolayer of the molecule of interest is grown on an electrode surface, blocking any direct charge transfer from the solution to the electrode. Therefore, the current observed in electrochemical measurement is due to the charge transfer through the molecules. A redox probe, which is used as a charge transfer indicator, can be added to the electrolyte solution [119-121] or attached to other end of the molecule in the SAM.[122-125] An example of the latter is shown in **Figure 1- 6**, where a redox active probe, ferrocene (brown part in **Figure 1- 6**), is attached to

peptide nucleic acid (PNA) molecules. Thiol terminated cysteine groups on the other end (blue part in **Figure 1- 6**) help the PNA molecules form an ordered self-assembled monolayer (SAM) as shown in the left side of **Figure 1- 6**b. Charge transfer through PNA molecules can by studied using electrochemical methods in an electrolyte solution by probing the kinetics of the ferrocene redox reaction. Details of this approach will be discussed later in Chapter 3 of this thesis for PNA charge transfer study.

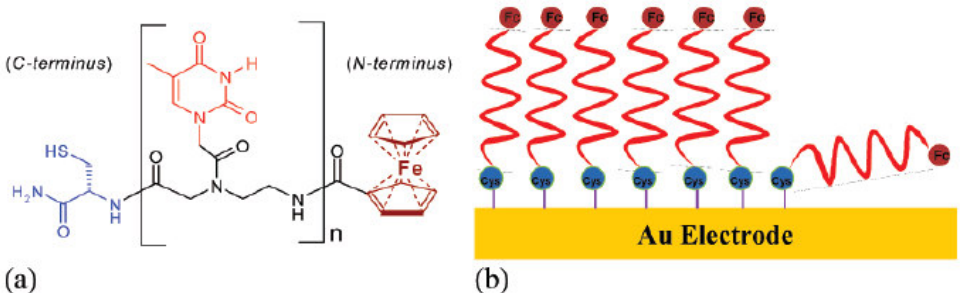

Figure 1- 6 : (a) Chemical structure of PNA with a ferrocene group, where n = 3-7. (b) PNA molecules self-assembled on a gold surface.[126]

The application of electrochemical methods is limited by the requirement of a good SAM formation. As shown on the right side of **Figure 1- 6**b, if a molecule is lying down on the electrode surface, the electron required to oxidize or reduce the ferrocene group can transfer directly between ferrocene and electrode surface, without passing through the molecular chain. Therefore the electron transfer through the molecule of interest is not probed. In the work presented in [126], a technique is used to separate the response from ferrocene groups that are close to the surface and those are lifted away from the surface. The details will be discussed in Chapter 3.

Similar to spectroscopic techniques, electrochemical methods also measure an averaged signal from an ensemble of molecules, not single molecule signals. In addition, the molecules in a closed packed SAM are adjacent to each other. Electrons can be transferred between molecular chains, instead of directly passing through the molecule.

This multiple possibility of electron transfer routes in the electrochemical measurements complicates for the interpretation of experimental results.

3.2. Single Molecule Charge Transfer Measurements

In molecular systems, it is difficult to measure the electronic properties of a single molecule. To measure, one must link the molecule between two nanoscale electrodes and record the electrical current. Several experimental setups can be used to dtudy single molecule charge transfer. The key element is the method to fabricate two nanoscale electrodes, or at least one of the electrodes in the nanoscale, in order to limit the number of molecules linked between the electrodes.

3.2.1. Cross-wire Method

Strictly speaking, the cross-wire method (**Figure 1- 7**a) is not a single molecule technique. However, it comes quite close to the goal of measuring current through a small number of molecules using a traditional setup which can be performed in many laboratories. Two thin Au wires (~10 μm in diameter) are placed perpendicular to each other, one coated with the molecule of interest, and are slowly brought into contact. The I-V characteristics of the contact are determined by the electronic properties of a limited number of molecules.[14, 127-130] The molecular conductance is estimated by dividing the measured conductance by the number of molecules in the junction, which is calculated (estimated) to be ~1000 per junction. Although far from ideal, this has been a useful approach for single molecule charge transfer studies.

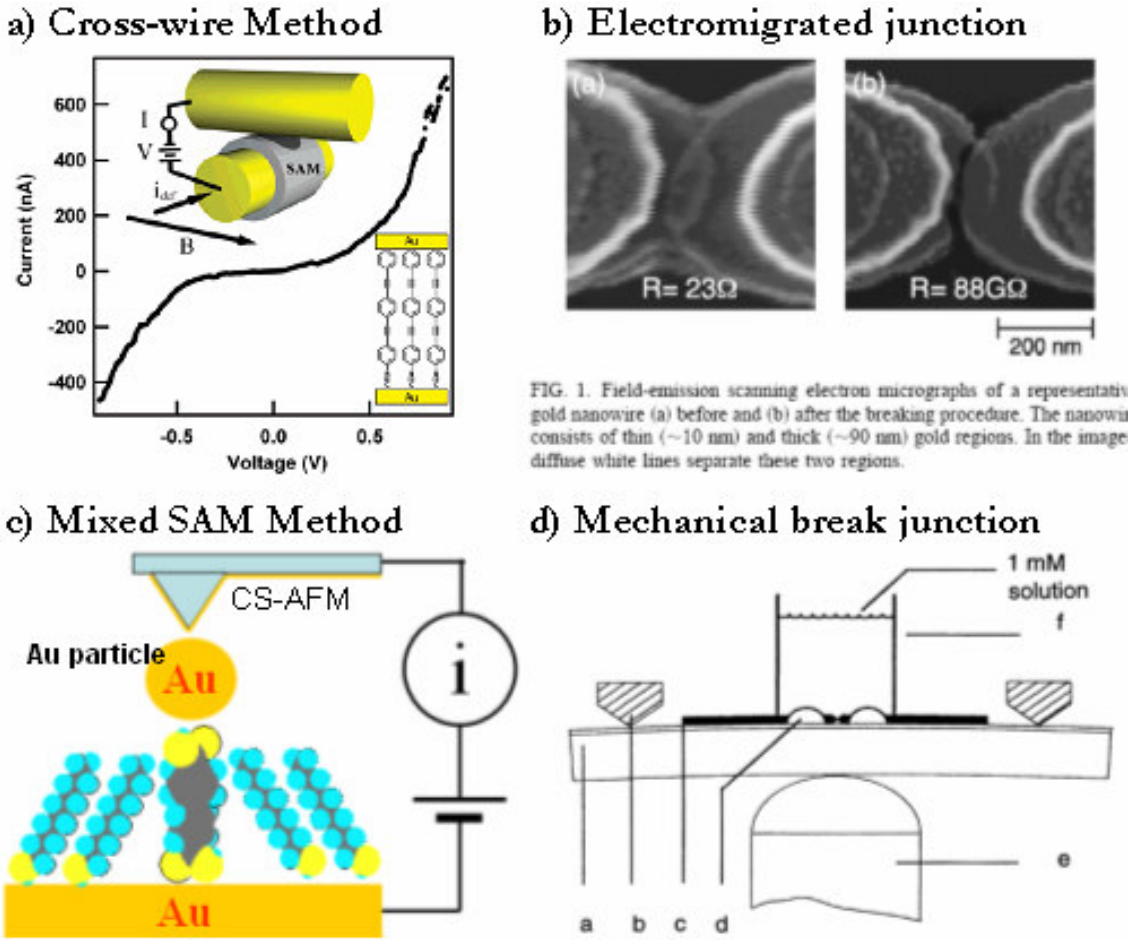

Figure 1- 7 : Techniques for single molecule charge transfer study: a) cross-wire method;[127] b) electromigrated junction;[131] c) mixed SAM/SPM method;[75] d) mechanical break-junction method.[79]

3.2.2. Electromigrated Junction Method

The electromigrated junction (**Figure 1- 7**b) is one of the few techniques that utilize true nanoscale electrodes for the m-M-m system.[131-133] The atomic motion of metal under a large electric field, a process called electromigration, is used to break down nanowires and to create nanoscale electrodes.[131-133] Electromigration, which is responsible for most failures in microelectronic circuits,[134] is a useful tool for the development of molecular electronics. Briefly, a thin gold nanowire is formed using traditional methods, and a nanoscale gap is produced by passing a high density current through the nanowire, which causes gold atoms to migrate and leads to the breakdown of the wire. Once the wire breaks, a nanoscale gap is created, and no more current can pass through unless the gap is bridged by molecules. The drawback of this technique is that the distance between the two nano electrodes can not be tuned freely, limiting the application to measure the conductance of molecules with a variety of lengths.

3.2.3. Mixed SAM/SPM Method

Atomic force spectroscopy (AFM) usually has poorer spatial resolution than STM. However, in single molecule conductivity measurements, AFM has some advantages over STM. When the AFM is operating in contact mode, an AFM tip can be used to generate true contact between the tip and the molecules, while STM usually involves a tunneling gap. With a metal coated conductive tip, AFM can be used to measure both mechanical and electrical properties of the molecules of interest.[43] To help AFM access the properties of single molecules, a mixed SAM method (**Figure 1-7**c) is used to generate metal-single molecule-metal systems.[43, 75, 90, 124] Briefly, a mixed self-assembled monolayer (SAM) on gold surface is formed by doping an insulating SAM, usually alkanethiols, with the molecular wire, which has metal binding

linker groups on both ends. The low concentration of molecular wire in the SAM results in isolated molecule wires surrounded by non-conducting alkanethiol matrix. A gold nanoparticle is attached to the other end of the molecular wire to help create a well defined electrical contact with the conductive AFM tip. The gold substrate, molecular wire, gold nanoparticle and conductive AFM tip, together, form an electrical circuit for the conductivity measurement of the molecular wire. It was reported that the I-V curves show quantized behavior of the conductance.[75, 90, 124] This provides strong evidence that single molecule conductance is probed using this technique.

3.2.4. Mechanical Break-junction Method

In the mechanical break-junction method, (**Figure 1- 7**d) a gold nanowire (a few hundred nanometers in width) is constructed on an elastic substrate by lithography. [15, 79, 135, 136] Nanoscale electrodes are created by elongating and eventually breaking the nanowire when the substrate is bent. The distance between the two electrodes is controlled by the bending of the substrate, which can be very accurate since a piezo-electric material is used to control the bending.

The mechanical break-junction was first used to study the tunneling between two electrodes.[136] Reed et al. modified the method by adding molecules to the nano junction to measure electronic properties of single molecules.[79] Molecules of interest are added to the junction by dropping a solution containing the molecule to the substrate and then rinsing after a few seconds, allowing the molecule to link to the electrodes. Conductivity measurements, usually performed in vacuum, reveal the electronic property of the molecule. Evidence for the formation of a nanoscale m-M-m system comes from the observation of weak dependence of the current on the gap distance in a certain distance range, indicating that the two nano-electrodes are linked by flexible molecules. It was shown that the I-V curves are asymmetric when measuring asymmetric molecules,

supporting the idea that single (or a few) molecule is present in the junction.[135] The conductance quantum of metal is also measured using this method, providing strong evidence of the formation of nanoscale m-M-m system.[137]

3.2.5. STM Break-junction Method

In contrast to macroscopic measurements, the results of single molecule conductivity experiments can be affected by many factors and fluctuate dramatically. These factors include the condition of the electrodes, the bond angle between linker and electrode, the environment of the molecule wire, etc. To make a reliable measurement of single molecule conductivity, it is important to repeat the measurement a large number of times that provides statistical significance. Note that every single measurement of the conductivity involves three steps: 1) the formation of two nanoscale electrodes; 2) linking the molecular wire to the two electrodes; 3) measurement of the current flow, which is usually in the order of nano-amperes or less. For all the techniques described above, it is not easy to repeat the three steps with a rate that can provide a large number of measurements in a reasonable time.

The STM break-junction method,[81] one of the most widely used techniques for measuring single molecule conductivity, is designed to create, repeatedly and rapidly, nanoscale m-M-m systems so that thousands of experiments can be conducted in a few hours or less. The STM break-junction method utilizes the accurate distance control and the small current measuring capability of an STM instrument. In this method, a gold tip is brought into contact with the surface by an STM scanner and withdrawn at a rate of ~20 nm/s, while measuring the current in a solution containing the molecular wire. Two nanoscale electrodes are formed during the pulling process (**Figure 1- 8**a-d), and the molecules in solution can enter the gap between the two electrodes (tip-substrate gap), generating an m-M-m system (**Figure 1- 8**e). The distance the STM tip moves to form

and break a contact is usually less than 10 nm. Therefore, with a tip moving rate of ~20 nm/s, this process can be repeated thousands of times in an hour, and a current-distance curve is recorded each time. When a molecule bridges the tip-substrate gap (**Figure 1-8**e), the current-distance curve shows step-like features instead of a simple exponential decay. Statistical analysis of the curves showing quantized current peaks yields information on the conductance of single molecules.

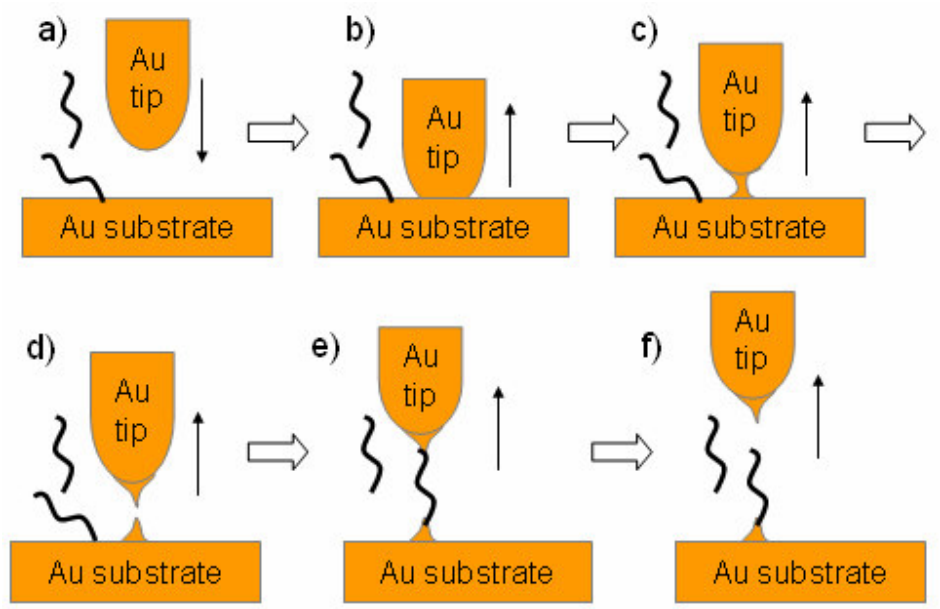

Figure 1- 8: The process of the nano-electrodes and m-M-m system formation in STM break-junction experiments. Two nano electrodes are formed by breaking the contact between the Au tip and the substrate (a-d). With the presence of molecules in the solution and on the surface, an m-M-m system may be created (e). It takes less than a second to repeat this process in single molecule conductivity measurements.

Unlike the other methods, the STM break-junction technique focuses on the separation of m-M-m system. When the STM tip is pulled away from the surface, there may be many molecules in the junction between tip and surface, including solvent and contaminant molecules. However, only the molecules that strongly bond to the two

electrodes can survive the pulling process and stay in the junction for a reasonable amount of time for the current measurement. If there are several molecules bound to the electrodes, it is impossible for those connections to be broken at the same time, i.e. one of them will last until the end of this process. Therefore, the separation process ensures the formation of metal-single molecule-metal systems. In addition, the STM break-junction method can be performed in solution, where the molecules of interest can be introduced conveniently.

3.3. STM-break Junction Method

The STM break-junction method has been used to study a variety of molecules,[83, 138-140] including several π-conjugated structures[85, 141, 142] which are expected to have high conductance and small tunneling decay constants (β) due to their delocalized π systems. It has become one the most important techniques for single molecule charge transfer studies.

3.3.1. Some Technical Details for STM Break-junction Method

The STM break-junction method has been used under a variety of conditions, including organic and aqueous solutions, air, and vacuum. In the solution based experiments, usually a diluted solution of molecular wire is used in order to reduce the possibility of multiple molecules binding to the electrodes at the same time. For the experiments without solution, a low coverage preadsorbed SAM is prepared for the same purpose.

Usually, a gold tip and a gold surface are used to perform STM break-junction measurements because of the following reasons. 1) Gold is an inert and noble metal, and a clean gold surface can be easily prepared by chemical cleaning followed by flame annealing; 2) Many linker groups for molecular wires form strong chemical bonds with

gold, especially the most widely used thiol linker group; 3) Gold is relatively soft and can easily be stretched to form nano wires for the preparation of nano electrodes.

The tip withdrawal rate is one of the key parameters to be adjusted in the STM break-junction experiments. It was shown that fast stretching rates result in a longer step compared to slow stretching rates, and the breakdown of junction is mainly due to mechanical stretching.[143] At slow stretching speeds, thermal activation is responsible for the breakdown, i.e. the breaking of the bond is due to the thermal movement of the molecule.[143] In the STM break-junction measurements, it is important to have current-distance curves with clear steps, that are as long as possible. However, the data acquisition rate may limit the speed of the experiment. Generally, 20 – 40 nm/s is a practical range of operating stretching rate.

3.3.2. Statistical Analysis

In contrast to traditional, steady state conductivity measurements, the STM break-junction method is a dynamic measuring technique. The result for each measurement is not a simple current value for the calculation of conductivity. Instead, each measurement returns a current-distance (IS) curve, in which the y-axis is the measured current and the x-axis is the displacement of the STM tip. A typical IS curve is shown in **Figure 1- 9**a, in which the step like feature represents the period of time that the molecular wire links the two electrodes. In that period, even though the tip is moving away from the surface, the current stays constant. The number of data points in the steps is related to how long the molecule stays in the m-M-m system. Before the formation of m-M-m junction in each IS curve, the current drops exponentially due to quantum mechanical tunneling. After the junction breaks down, the current continues to flow the exponential decay. Since the current value before the formation of m-M-m system and after the breakdown is continuously dropping, there will be many more data points, in a given current range, at

the current step which is related to the conductance of the molecular wire. As shown in **Figure 1- 9**c, there are many more data points around 25 nA, associated with the steps in IS curve (**Figure 1- 9**a), than data points in the current range above 40 nA, where the current decays exponentially.

The statistical analysis of thousands of IS curves is performed by binning each curve by the y-axis, as show in **Figure 1- 9**. **Figure 1- 9**a shows some IS curve examples, some of which have clear steps. Those IS curves that show clear current steps are selected (**Figure 1- 9**b) for further analysis. As show in **Figure 1- 9**c, the data points of current measurements are populated at the steps and the histogram analysis with proper bin size shows well defined peaks in the histogram plot (**Figure 1- 9**d) in which the current of the second peak is about twice the first. This suggests that the first current peak corresponds to single molecule junctions, while the second peak corresponds to pairs of molecules.[81]

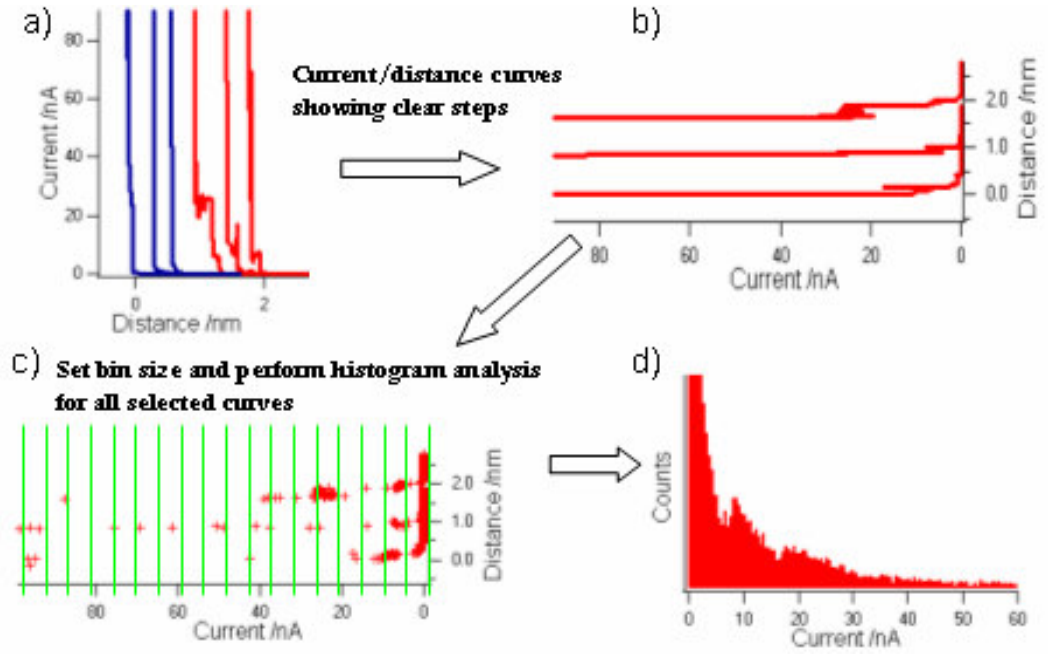

Figure 1- 9: Statistical analysis process of STM break-junction method.

3.3.3. Data Selection

It should be noted that the data selection is necessary for the clear observation of well defined peaks in the histogram analysis in our experiments. However, one should be very careful not to allow the pre-screening process to bias the interpretation of experiment results. A control experiment should be carried out under the same conditions as in the molecular conductivity measurements. It is important to check that the control experiment in solutions that do not contain the molecular wires yields no clear peaks in the histogram. This control result indicates that the appearance of clear peaks in the histogram analysis is due to the molecule of interest in the solution, not from the data selection process.

Another piece of evidence for the observation of single molecule conductance is that the multiple peaks in histogram show quantized behavior. For example, the second peak shown at ~19 nA in Figure 1- 9d is at twice the current of the first (at ~ 9nA). This quantized behavior is due to the binding of one or two molecules in the m-M-m system. In some experiments, a third peak at the three times the current of the first is observed.[81]

In most experiments reported to date, data selection was used to remove noisy curves and curves without any clear features.[83, 85, 138-142] Based on our experience, analysis without pre-screening usually generates a smooth curve which only shows the exponential decay of tunneling current, presenting as the background of the measurements. The current peaks for molecular wires are probably buried under the background because the noise signal collected in thousands of curves. In the histogram analysis, every data point in the IS curves is binned, and the background and associated noise accumulates if no data selection is performed. In addition, there are a large number of noisy curves that have many more data points than normal exponential decay curves,

in which the current drops so fast that very few data points are collected. Inclusion of the noisy curves makes it more difficulty to observe single molecule features.

Current peaks in a histogram can be observed without data selection by careful design of the instrument with low noise levels and by acquiring current over a broad current range.[138, 144] However, the current peaks shown in [138, 144] may be a collection of all possible conformations of one, two or multiple molecular connections and the broad peaks near 0.04 G_0 may not represent the actual conductance of a single molecule(red line in **Figure 1- 10**b for benzendithiol). Nevertheless, the position of the peak can be used to compare the conductance of different molecular systems. In addition, the width of the peaks observed in [138, 144] contains very useful information about the stability of the molecule-electrode contact. This information may be lost during the data selection process. Since the current peaks shown in [138, 144] span a wide current range, it is important to have a state-of-the-art experiment setup with several current preamplifers to measure current values over a wide range from pico-amperes to micro-amperes. For the experiments performed using a single current preamplifier, with an intrinsically limited current range, data selection process for histogram analysis is necessary.

The high background signal in the histogram analysis without data selection originates from three major factors. The first is instrumental noise in the current measurements, which, in principle, does not contribute significantly to the overall background because the noise is usually a few picoamperes or less using a 10 nA/V current amplifier. The second is that there are many noisy IS curves due to the instability of the m-M-m system, which is related to a number of factors, including tip condition, surface condition, pulling speed, solvent, etc. The third, and probably the most important factor, is that most of the IS curves (65-95%, various by research groups and experimental conditions) show only exponential decay without any current step features.

This is an intrinsic characteristic of STM break-junction method because a low coverage of the molecules on the substrate surface is needed to have only one or a few molecules trapped in the tip-substrate gap for each IS curve.

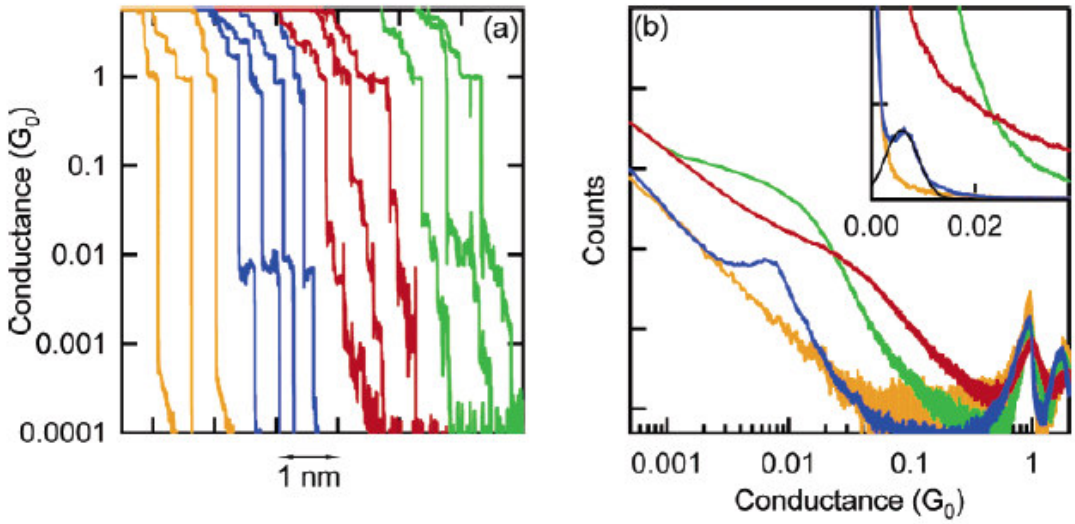

Figure 1- 10: Histrogram analysis of over 3000 IS curves for each molecule: 1,4-benzenediamine (blue), 1,4-benzenedithiol (red), and 1,4-benzenediisonitrile (green). (a) shows the example IS curves. (b) is semi-log plot histogram analysis.[144]

3.3.4. Measurement of Conductance Quantum G_0

One of the key control experiments for the STM break-junction method is the observation of conductance quantum G_0, which can only be observed for a very thin metal nanowire. In the case of gold electrodes, the measurement of 1 G_0 indicates the formation of a one gold atom wide nanowire, which ensures that two nanosized electrodes form when the nanowire breaks. The observation of clear conductance quantum peaks in the histogram analysis is a precondition for further single molecule measurements. For the IS curves of single molecule measurements, data selection is

needed due to the small percentage of IS curves that show clear current steps. For the IS curves in gold conductance quantum measurements, usually over 90% of the IS curves show clear steps with proper experimental conditions. Therefore, data selection is not necessary for the measurement of gold quantized conductance.

The quality of the gold tip is the key controlling factor for the generation of good IS curves with well defined gold quantized conductance steps for the measurement of G_0, and for the measurement of single molecule conductivity as well. The nanoscale sharpness of an STM tip can be judged by the quality of STM images in situ. In the gold tip-gold substrate (Au(111)) system, the observation of clear, ~2.5 Å high, gold atomic steps can be used to evaluate the quality of gold STM tip.

As shown in Figure 1- 11a, most the IS curves from successive measurements show clear gold quantized conductance steps using a good STM tip, which gives clear gold atomic steps in STM images. It should be pointed out that, for those good IS curves, the current saturates the amplifier with a moderate "crash" (usually 3 to 4 nm), indicating a well established tip-substrate connection. Here, "crash" means that the STM tip establishes an ohmic connection with the substrate, and we arbitrarily select a threshold current of 4 G_0. The quantitative measure of the level of "crash" is the distance required to move the STM tip from it original position (usually in the tunneling regime, 0.5 to a few nm above the surface) towards the surface until the current amplifier saturates. The response saturates because of the high conductance of the metal-metal contact and a 1 μA/V current preamplifier, which saturates at 10 μA, is used to measure the gold conductance quantum, which is in the order of μA with a small bias (e.g. 50 mV).

A low quality STM tip which shows no clear feature in STM imaging mode generates many noisy IS curves which have no clear step (Figure 1- 11b). In addition, those noisy curves do not saturate the current preamplifier even with a "crash" distance over 9 nm. In some cases, a low quality STM tip may initially generate normal IS curves

with well defined steps, but quickly lose its ability to perform after a few hundred curves, while a high quality tip can last a few thousand.

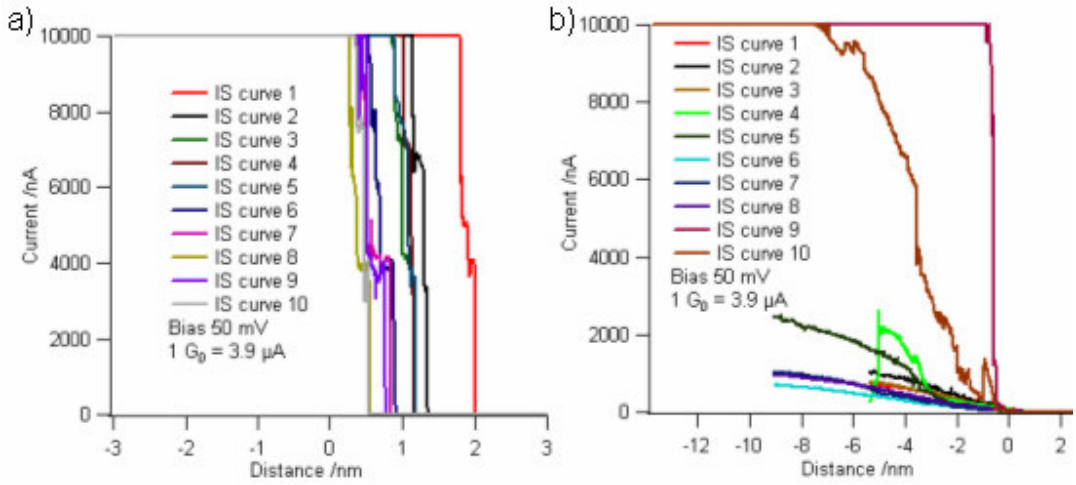

Figure 1- 11: a) IS curves using an STM tip showing clear gold atomic steps in STM images. These curves are from successive measurements without selection. b) IS curves using a low quality STM tip.

It should be noted that gold quantized conductance steps can only be seen in the IS curves with saturated current, i.e. the nano electrodes only form after well established tip-substrate connection (Figure 1- 11). In addition, the current value usually drops from saturation to close to zero within a few nanometers. This provides important experimental guidance for the experiment since the quality of tip continuously degrades during the experiment. When the tip degrades, more contact is needed to maintain the tip-substrate connection. Therefore, the "crash" distance should be frequently adjusted during an experiment, and when the distance adjustment fails to work, a new tip is needed to continue the measurement.

CHAPTER 2

OPTIMIZING SINGLE MOLECULE CONDUCTIVITY WITH CONJUGATED CARBODITHIOATE LINKERS

1. Introduction

Schematically, the metal-molecule-metal (m-M-m) junction can be divided into three parts: the molecular core and two metal-molecule contacts on either side (**Figure 2-1**).[145] Similar to the macroscopic view of electrical contact by alligator clips, the quality of the contacts has a large influence on the overall performance of the electrical linkage. However, as discussed previously, on the molecular level the overall resistance is not a simple summation of the contributions of the contacts and the molecular core. Charge transport through the molecular wire may be governed by the electronic interaction between the molecule and the electrodes. The magnitude of this interfacial electronic coupling, combined with properties of the molecular core, determine the performance of a molecular wire.[16, 22, 41]

A challenge presented by single molecule conductance is to distinguish between the relative influence of the molecular "core" and the molecular "interconnects" on the observed currents. Much focus has been placed on designing conductive, conjugated molecules. However, the electrode-molecule contacts can dominate the responses of metal-molecule-metal devices. The charge transport through molecular wires in metal-molecule-metal (m-M-m) junctions has been investigated by measuring conductance (or resistance) as a function of length.[10, 17, 40, 41, 74, 82, 84, 85, 141, 146, 147] In the tunneling regime where the behavior of molecular junctions normally belongs,[10, 41, 82] a junction resistance R displays an exponential dependence upon molecular length

with, $R = R_0 \exp(\beta L)$, where R_0 is an effective contact resistance, L is the molecular length, and β is a decay constant.

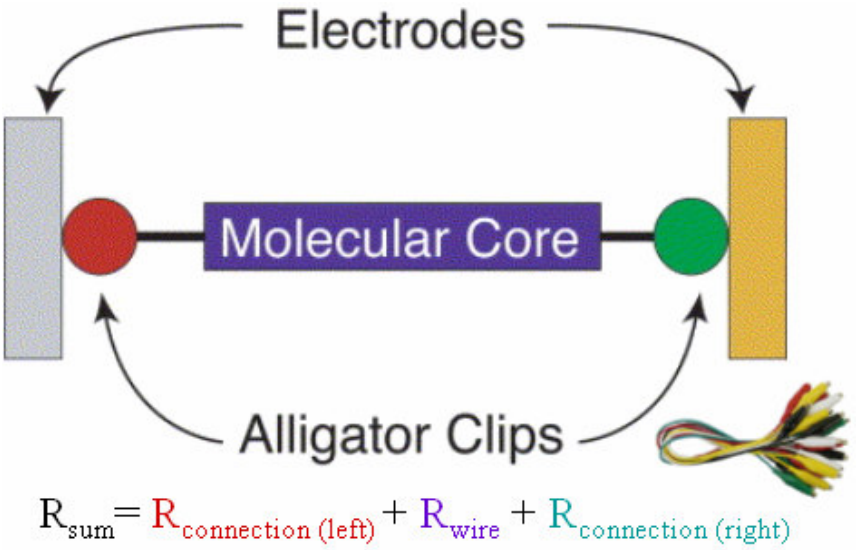

Figure 2- 1: Schematic of a metal-molecule-metal junction. (Cartoon by Dr. Yufan He)

1.1. Molecular Anchor Groups to Metal Electrodes

Besides a variety of π-conjugated molecular cores studied, the high affinity to gold surfaces and synthetic flexibility of thiolated compounds has led to their wide use as contact linkers to interconnect the molecular cores and the electrodes of the m-M-m junctions.[41] However, a gold-thiol contact appears to result in weak interfacial orbital interactions between the molecular frontier orbitals and the gold electronic states.[39, 41, 148] In addition, the relatively poor thermal stability of thiol-gold linkage may limit its usage in molecular electronics. Hence, the quest for better contacts has become one of main area of research in molecular electronics. Several studies with different linkers and metal electrodes in the m-M-m junctions other than a thiol-gold contact have been

studied.[17, 39, 81, 127, 138, 146, 149-156] It was reported that there is less variability in the conductance values of molecules with amine linker groups than those with thiol linker groups.[138] However, the conductance value of amine terminated molecules is smaller than the conductance of thiol terminated ones, indicating a less effective electrical connection between amine linkers and electrodes, possibly a result of the weaker binding.[17, 138]

1.2. Carbodithioate Linker Group

Recently, we showed that carbodithioate linkers increase single molecule conductance through a biphenyl moiety by a factor of 1.4 relative to that provided by thiol.[124] Despite the potential of the carbodithioate linkers, no further conductance measurements with carbodithioate-functionalized molecules have been reported since then [124]; not only do the strong basic conditions, necessary to introduce the carbodithioate moieties, restrict the synthesis of a variety of carbodithioate-terminated π-conjugated molecules but also the characteristic instability and the arduous isolation procedure of carbodithioic acid compounds or their salt forms may limit their broad application.[157-159]

Highly π-conjugated oligo(phenyleneethynylene)s (OPEs) have been an archetypal structure in the field of molecular electronics.[38, 47, 49, 83, 160-163] Most OPE-based molecular wires have featured thiol functional groups as linkers and have been assembled to m-M-m junctions, usually by unmasking an acetyl protecting group that enables the construction of π-conjugated oligomers via cross-coupling reactions and prevents free thiols from oxidation to disulfides. Like the acetyl protection for thiol compounds, it has been shown that with (trimethylsilyl)ethyl (TMSE) protecting group it is possible to build carbodithioate-terminated OPEs via Sonogashira cross-coupling reactions, and to functionalize gold nanoparticle surfaces by deprotecting the TMSE

group without isolating intractable carbodithioates.[158] Thus, it is possible and interesting to compare the conductance of m-M-m junctions based upon a classic OPE molecular wire motif that features thiol- and carbodithioate-termini.

We measured the conductance of thiol and carbodithioate-terminated OPEs using the STM break-junction method, and investigated the length dependence of the molecular conductance with two different linkers. Our collaborators performed non-equilibrium Green's function simulations to evaluate the effect of the linker groups on the charge transport in the OPE molecular systems. Experimental results show that the carbodithioate linkers not only increase the molecular conductance compared to their thiol counterparts but also provide a quasi-linear length dependence of conductivity for the OPE molecular wires, a feature that was not evident in measurement with the thiol linkers. The simulations identify the contributions of individual orbitals to the conductivity, revealing that the carbodithioate linkers facilitate the electronic coupling between the OPE molecular orbitals and the electrodes as well as reduce the contact resistance with respect to the thiol linkers. Our results highlight the importance of linker groups to the overall performance of molecular wires.

2. Experimental Section

This work is in collaboration with the synthetic group of Professor Michael J. Therien and theoretical group of Professor David N. Beratan at Duke University. Dr. Tae-Hong Park in the Therien group synthesized most of the OPE molecules used in this study. Dr. Ravindra Venkatramani and Dr. Shahar Keinan in the Beratan group performed the computational study, which provides deep insight into the mechanisms that contribute to the conductance improvement of OPE molecules with carbodithioate linkers.

2.1. Materials

Two series of OPE molecules were studied in this work (**Figure 2- 2**), carbodithioate-terminated (CT) systems (CTS) and dithiol-terminated (DT) systems (DTS). For convenience, the thiol terminated molecules are denoted by T1, T2 and T3, where the numbers refer to the number of phenyl rings in the molecules. Similarly, the carbodithioate terminated molecules are denoted by C1, C2, and C3.

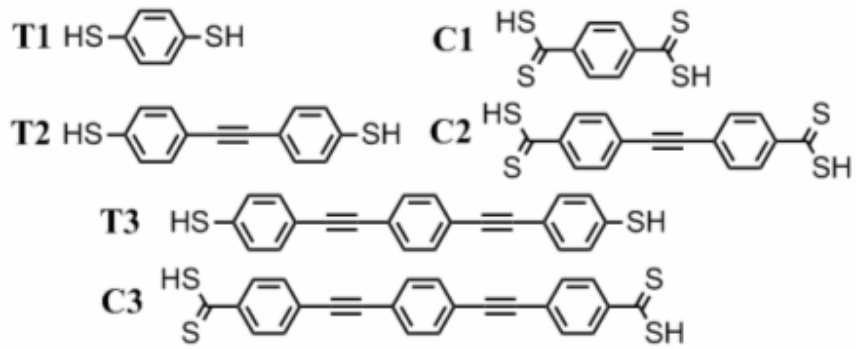

Figure 2- 2: Structure of α,ω-dithiol-terminated (T1, T2 and T3) and α,ω-bis-carbodithioate-terminated π-conjugated molecules (C1, C2 and C3).

1,4-Benznedithiol (T1) was purchased from Alfa Aesar and used as received. The rest of the molecules were synthesized by Tae-Hong Park in the Therien research group at Duke. The acetyl-protected versions of dithiol T2 and T3[38, 164] and the TMSE esters of C2 and C3[158] were synthesized according to literature procedures. The synthesis and characterization of 2-(Trimetylsilyl)ethyl ester of C1 were performed using the procedure described in the APPENDICES.

2.2. Self-assembled Monolayer (SAM) Preparation

A gold bead was prepared using Clavilier's method[165] and cleaned by piranha solution (H_2SO_4:H_2O_2 = 3:1) **(Caution! The piranha solution is a very strong oxidizing agent and extremely dangerous)** and hydrogen flame annealed in air. After cooling, the gold bead was immersed in a THF solution containing 100 μM of the target molecule (**Figure 2- 2**) for 15-30 minutes to prepare a self-assembled monolayer (SAM). The adsorbate solutions were prepared by deprotection of the precursor molecules and used immediately (The deprotection procedure is described in the APPENDICES). The sample was rinsed by THF and dried under a nitrogen stream, then put into the liquid cell of a PicoPlus SPM (Molecular Imaging, Tempe, AZ) system and covered with toluene.

2.3. Conductivity measurements

A freshly cut gold tip (0.25 mm, 99.999%, Alfa Aesar, MA) was used to image a SAM covered gold bead surface immersed in toluene, and the quality of the tip was judged by its ability to resolve gold atomic steps in STM images. Then the tip was brought into contact with the surface and withdrawn at a rate of ~20 nm/s, while measuring the current. This process was repeated thousands of times, and a current-distance curve was recorded each time. When a molecule bridges the tip-substrate gap, the current shows step-like features instead of a simple exponential decay. Statistical analysis of the curves that showing quantized conductance peaks reflects the conductance of single molecules.

A control experiment is to repeat the conductivity measurement of a well known molecule as a standard or calibration. For the single molecule conductance measurements, alkanedithiols can server as the standard sample as they have been studied extensively by a number of research groups.[12, 77, 81, 90, 144, 166, 167] **Figure 2- 3** shows the control experiment in which the conductance of hexaneditiol was measured. **Figure 2- 3**a shows some typical IS curves with clear step features. A histogram analysis

performed using the procedure described in the previous chapter is shown in **Figure 2-3**b. Linear fitting of the measurements at multiple bias yields the conductance of the hexanedithiol molecule.

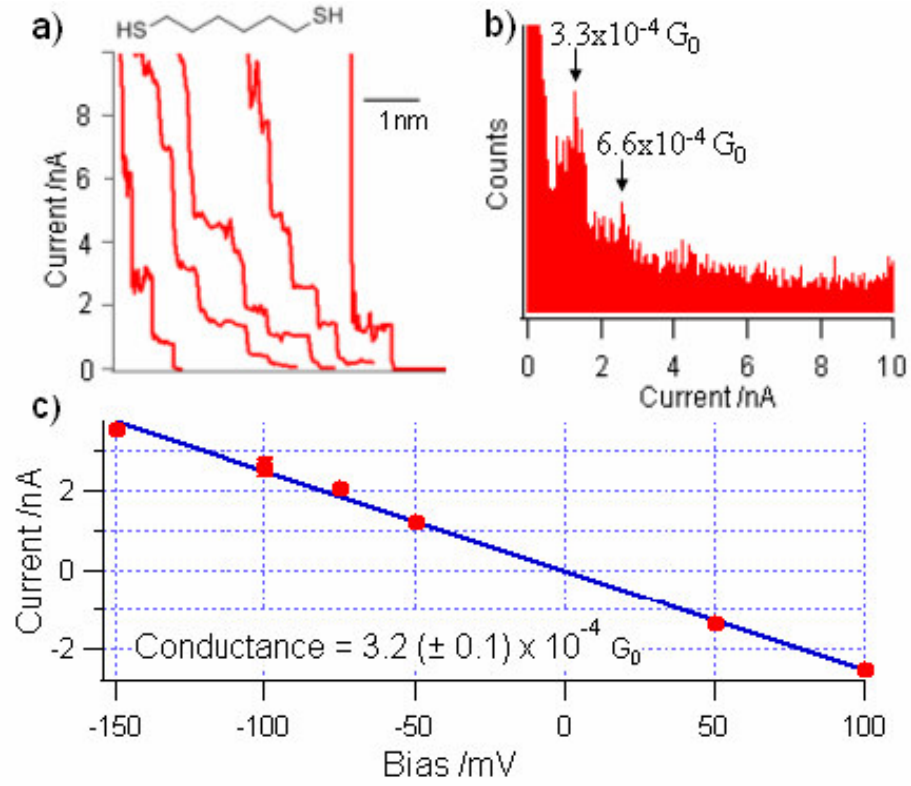

Figure 2- 3: STM break-junction measurement for hexanedithiol in toluene. a) Typical IS curves with clear step features. b) Histogram analysis of selected IS curves show clear peaks. c) Linear plot of measurements done at different bias voltages.

3. Experimental Results and Discussion

The single-molecule conductance of π-conjugated organic molecules with thiol or carbodithioate linkers (**Figure 2- 2**) was measured via the STM break-junction method[81] (**Figure 2- 4**a). Typical current-distance curves, showing clear conductance steps, are shown for C3 in **Figure 2- 4**b. The histogram analysis (**Figure 2- 4**c) shows

well defined peaks in which the current of the second peak is about twice the first. This suggests that the first current peak corresponds to single molecule junctions, while the second peak corresponds to pairs of molecules.[81] Linear fitting of the current peaks acquired at multiple biases reveals the C3 conductance to be 2.5 (± 0.3) x 10^{-3} G_0.

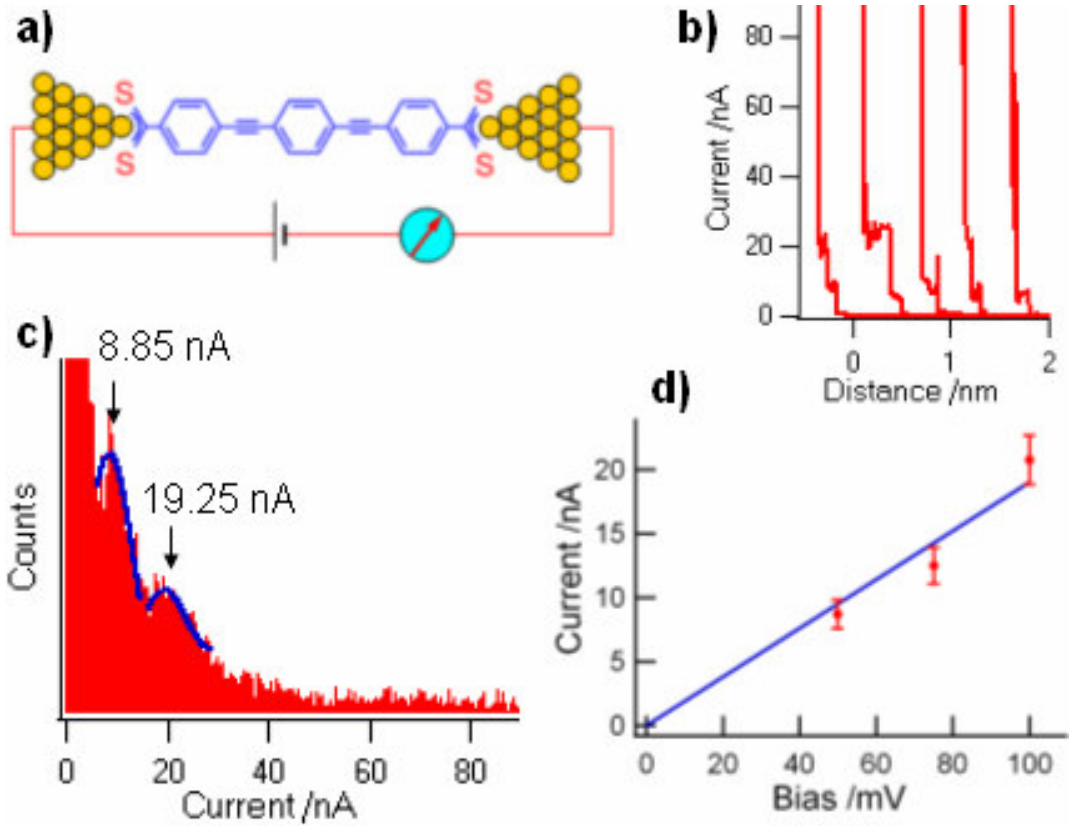

Figure 2- 4: a) Scheme for single molecule (C3) conductance measurements; b) Example of current-distance curves recorded with C3 in the junction at 50 mV bias; c) Histogram analysis of C3 conductance constructed from ~150 IS curves; d) Conductance of C3 is determined by fitting the measurements at different bias.

Following the same procedure, the conductance of all the OPE molecules shown in **Figure 2- 2** were measured. Another example of measurement is shown in **Figure 2- 5** for T1, benzenedithiol. There are three clear current peaks in the histogram analysis,

suggesting that the first peak represents the conductance of single benzenedithiol molecules. The measured conductance of T1 is 8.3 (± 0.7) x10^{-3} G_0. It should be pointed out that the conductance of T1 measured in our lab is similar to the reported value in literature, which is 1.1 x10^{-2} G_0.[168] The good agreement between independent measurements in different labs confirms the reproducibility of the STM break-junction method for single molecule conductivity.

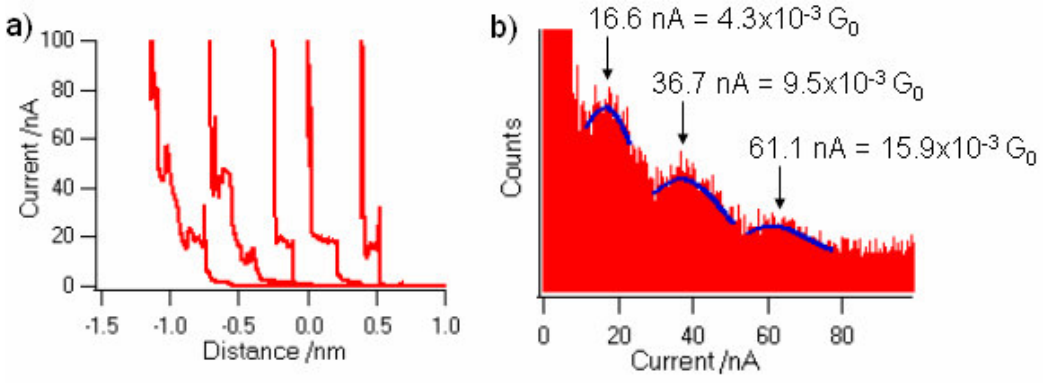

Figure 2- 5: a) Example of IS curves recorded with T1 in the junction at 50 mV bias; b) Histogram analysis of T1 conductance constructed from ~270 IS curves.

Table 2- 1: Conductance Measurements of T1-T3 and C1-C3

	Conductance /G_0	**Conductance /nS**	**Resistance /MΩ**
T1	8.3 (± 0.7) x10^{-3}	639 ± 54	1.6 ± 0.13
T2	2.6 (± 0.4) x10^{-4}	20 ± 3	50 ±7.6
T3	1.3 (± 0.3) x10^{-4}	10 ± 2	100 ± 25
C1	4.8 (± 0.5) x10^{-3}	367 ± 39	2.7 ± 0.3
C2	3.2 (± 1.1) x10^{-3}	246 ± 54	4.1 ± 0.9
C3	2.5 (± 0.3) x10^{-3}	193 ± 23	5.2 ± 0.6

$G_0 = 2e^2/h = 77\ \mu S = 13\ k\Omega$.

The conductivities of all the DT and CT molecules (**Figure 2- 2**) were measured and the results are summarized in **Table 2- 1**. It appears that, except for benzene-based C1 and T1, the carbodithioate linker enhances the conductance of OPE molecules by an order of magnitude relative to the corresponding phenyleneethynylenes with thiol connectors.

Before discussing the difference between the linkers, it is important to understand why the benzene-based C1 and T1 display similar conductance while the other OPE molecules behave quite differently, depending on the kind of linkers. The computational results reported in reference [74] suggest a significant deviation of the conductance of benzenedithiol from what would be expected based on longer OPE dithiols. The large conductance of benzenedithiol is attributed to the significant delocalization of the terminal sulfur p-orbitals over the carbons in the benzene ring induced by the coupling to the gold contacts at either end, affecting the conductance of benzenedithiol more than other molecules because of its short molecular length.[74] Our collaborators have theoretically calculated the conductivity of the dithiol systems used in the current study by assuming a weak sulfur-electrode coupling at contacts and found that the calculated conductivity of benzenedithiol follows the decay trend of dithiol-terminated systems with increasing chain length (*vide infra*). However, even in this study, which does not explicitly model the gold contacts, in contrast to reference [74], the computation suggests that the weak coupling of the sulfur atoms to the gold electrodes can give rise to a conducting channel, despite the characteristic localization of terminal sulfur orbitals. The contact-induced coupling between the terminal sulfur orbitals is predicted to be maximal for the molecule with the smallest sulfur-sulfur separation and to diminish as the molecular length increases. It should be noted that reference [74], by explicitly modeling the contacts, captured this effect quantitatively, which is missed in our theoretical calculations. Our experimental results indicate that the conductance of benzenedithiol

(T1) does not follow the decay trend of T2 and T3 (**Figure 2- 6**). Therefore, it is reasonable to exclude benzenedithiol from the decay analysis of OPE dithiols.

Comparing the conductance between C2-C3 and T2-T3 (**Table 2- 1**), it is clear that the carbodithioate linker improves the conductance of OPE molecules by over an order of magnitude. This highlights the importance of optimizing the molecule-electrode junction to enhance molecular conductivity and to access the intrinsic conductivity of the core, rather than a value reflecting the resistive bottleneck that the linkers appear to represent. The order of magnitude improvement in the conductivity of OPEs observed by changing to the carbodithioate linker is significantly greater than the 1.4-fold conductance enhancement in the biphenyl junctions.[124] Since the biphenyldithiol is shorter than T2 in this study, we think that its relatively short molecular length may play a role in the observed small carbodithioate conductivity improvement reported in ref [124] as discussed above for T1. Nevertheless, our result is in qualitative agreement with previous reports that carbodithioate linker improves the charge transport through molecular wires.[39, 124] It also confirms that there are significant complicating issues for short molecules.

A widely accepted picture of electron transport though molecular wires is that it occurs by quantum mechanical tunneling from the Fermi level (E_F) of one electrode, through the LUMO (lowest unoccupied molecular orbital) or the HOMO (highest occupied molecular orbital) of the molecule, to the Fermi level of the other electrode.[90] The tunneling decay constant is given by $\beta = 2(2m^*\varphi_0/\hbar^2)^{1/2}$, where m* is the effective mass of the electron, and φ_0 is the tunneling barrier, with $\varphi_0 = E_{LUMO} - E_F$ for tunneling through the LUMO and $\varphi_0 = E_F - E_{HOMO}$ for tunneling through the HOMO. An ideal linker will shift the LUMO or/and HOMO level(s) closer to the metal E_F, lowering the tunneling barrier and therefore β. In addition, optimal linkers also decrease the contact

resistance, so that the conductivity of the intrinsic molecular core dominates the metal-molecule-metal (m-M-m) junction response.

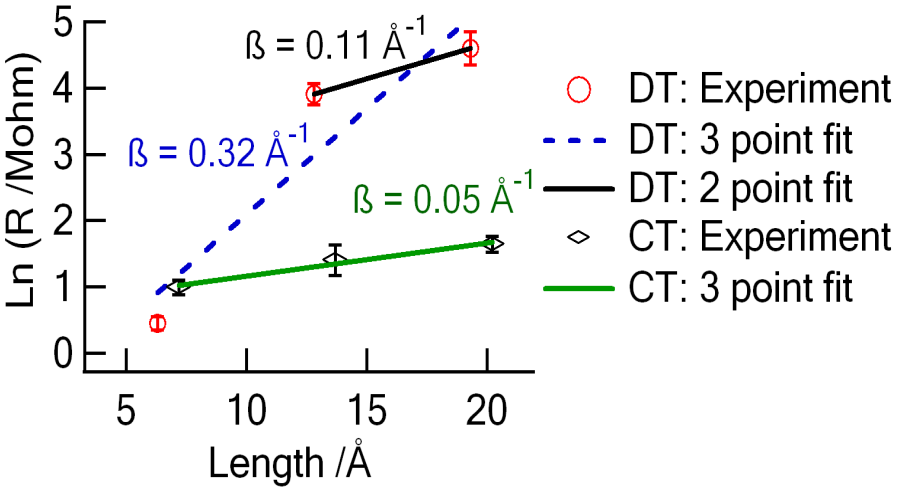

Figure 2- 6: Natural logarithmic plot of the resistance of dithiols (T1-T3, red circles) and carbodithioates (C1-C3, black diamonds) versus molecular length. The β values are calculated by fitting the semi-logarithmic plot of resistance and molecule length to $R = R_0\exp(\beta L)$. The dashed blue line is for DTS, and the black line is for T2 and T3 only. The green line is the β fitting for CTS.

The β value determined from the length dependence of T1-T3 resistances is 0.32 ± 0.10 $Å^{-1}$ (blue dashed line, **Figure 2- 6**). As the data, however, deviate significantly from the fitting line, because of the atypical behavior of T1 discussed above, the T2 and T3 data excluding the T1 resistance suggest β = 0.11 ± 0.06 $Å^{-1}$ (black line, **Figure 2- 6**) which is much lower than the theoretical estimate of 0.27 $Å^{-1}$ for dithiol OPE wires,[74] and rather close to tunneling decay constants determined for other α,ω-dithiol-terminated π-conjugated molecules using the STM break junction methods.[83, 85, 141] Despite a pronounced difference in experimental system configurations and charge injection to the bridge between a photoinduced intramolecular electron/energy transfer and a direct

charge transport along the single molecule, these processes involve electron exchange interactions which generally depend on distance exponentially.[169] It is, thus, interesting to find that the OPE display a wide range of attenuation factors ($0.10 \leq \beta \leq 0.47$) for the triplet-energy transfer process with variation of the donor-bridge energy gap in donor-bridge (OPE)-acceptor (D-B-A) systems, implying that β is not a bridge parameter but a system-specific parameter.[169] It is also known that the geometric modifications at the contact and the stretching of the molecule in the STM break-junction methods[39] could alter the alignment of the Fermi level and HOMO/LUMO levels,[42, 170] and the extent of π-conjugation of the probed molecule,[83, 85] probably causing the discrepancy between theoretical and experimental values.[11]

It is surprising, on the other hand, that carbodithioate-terminated C1-C3 show an even lower β of 0.05 ± 0.01 $Å^{-1}$ (green line, **Figure 2- 6**) than their dithiol analogs and other dithiol π-conjugated oligomers do. [83, 85, 141] Although there are a few reports of conjugated organic bridges displaying $\beta \leq 0.1$ from photoinduced electron transfer measurements,[34, 171-173] values of β as low as 0.05 $Å^{-1}$ from single molecule conductance measurements have been realized only with dithiol-terminated butadiyne-bridged porphyrin oligomers ($\beta = 0.04 \pm 0.006$ $Å^{-1}$).[84] It is noted that these very conductive bridges have significantly lower HOMO-LUMO gaps by extension of π-conjugation, reducing the gap between the donor and the bridge states in the donor-bridge-acceptor systems or between the electrode Fermi level and the bridge states in m-M-m junctions. As argued in reference [84], the electronic coupling between the contacts and the porphyrin oligomer, however, is crucial to obtain the ultralow attenuation in the porphyrin junction, because energetically the porphyrin bridge is off resonance in the low bias voltage window examined. We found that the HOMO-LUMO gaps for the CTS are lower than that of the DTS with the same molecular unit from the DFT calculations (vide infra) and from the lowest π-π transitions in electronic absorption spectra,[158] but these

gaps for the CTS are much larger than those of the butadiyne-bridged porphyrin oligomers. In order for the CTS to exhibit β as low as the porphyrin oligomers in the m-M-m junctions, therefore, the carbodithioate-mediated electronic coupling between the contacts and the bridge states should exceed that of thiol-mediated coupling in the porphyrin and OPE junctions. We also envisage that the π-conjugated two sulfur atoms of the carbodithioate group would modify the contact considerably compared to the thiol function, probably altering the alignment between the Fermi level and the HOMO/LUMO of the OPE in a different way with linkers. It has been reported that the end group effect on the alignment of molecular states and the Fermi level can explain the different decay constants for the thiol and pyridine-terminated carotenoid molecular junctions.[42] In addition, the evaluated contact resistance, R_0 for the CTS (C1-C3, 1.94 MΩ) is much smaller than that for DTS (T2 and T3, 12.02 MΩ), providing further evidence of improved electronic coupling at the contacts enhancing the conductivity of the CTS relative to the corresponding DTS. These results show the critical importance of the nature of the molecule-to-metal contact upon the bridge electronic structure, and suggest that the OPE core is more conductive than previously thought. A β value of 0.05 $Å^{-1}$ translates to an effective barrier height < k_BT for the carbodithioate-terminated OPEs, indicating that tunneling transport likely competes with thermally activated carrier injection processes.[40, 84] Recent studies indicate that conformational fluctuations can bias individual members of an ensemble toward one mechanism or another.[92, 174-176]

4. Theory Simulations and Discussion

4.1. Introduction

Over the past decade, non-equilibrium Green's function (NEGF) has become the method of choice in theoretical molecular electronics studies.[74, 177-182] The NEGF formalism[177] combined with ab initio DFT (Density functional theory) electronic

structure calculations calculate coherent transport properties for modeled m-M-m systems.[178, 179] The DFT-NEGF approach is parameter free, although the neglect of several physical features can impose serious limitations, most of which are related to the approximate nature of the exchange correlational functional (XCF) used.[183-188] Li and Kosov[189] studied the enhancement of molecular conductance of a biphenyl molecular core when carbodithioate functional groups are used in place of thiols to attach the molecule to Au electrodes. They used the DFT-NEGF approach in the strong molecule-electrode coupling limit. However, it is not obvious or well established that the gold-thiol linker coupling is strong. In fact, it has been proposed that the nature of the thiol-Au interactions are structural rather than chemical, i.e. there is negligible charge transfer, and that interactions with the electrodes are unlikely to significantly modify the energy and electron occupation of sulfur 3p orbitals,[150] which was also noted by Li and Kosov.[148] While we cannot completely discount the possibility of strong electrode-molecule couplings in these systems, in light of the above evidence, it is reasonable to explore the conductivity for the OPE systems in the weak electrode-molecule coupling regime.[190] In this limit, the influence of the electrode is only to broaden the molecular eigenstates and since the broadening is sufficiently small, the eigenstates do not lose their symmetry or qualitative charge distribution characteristics. As described below, our model parameterizes the Fermi energy and the electrode-molecule coupling strength so that we can analyze the dependence of absolute and relative conductances, contact resistance, and distance dependent conductance decay on these modeling parameters. Moreover in the weak coupling limit, the conductances can be analyzed in terms of the isolated molecule properties, leading to physical insights into the influence of the linker on molecular conductivity. These insights into the molecular contribution for conductances are independent of the type of electrode and are

transferable to other m-M-m systems where the electrode is made of metals other than gold or is even semiconducting, provided that the weak-coupling limit holds.

4.2. Methods

In order to assess the differences in resistances (conductances) for the thiol- and carbodithioate-terminated OPE structures, our collabrators performed electrical transport calculations using the non-equilibrium Green's function (NEGF) method[177] on DFT optimized structures. As opposed to the conventional DFT-NEGF method, which includes parts of the electrode in the DFT calculation, here the work is done in the weak coupling limit, using DFT to calculate the geometry of the isolated molecule (core plus linker) and using molecular orbitals information (as calculated by INDO/s) as an input to NEGF calculations. The effect of the electrodes is considered through a molecule-electrode coupling parameter, which broadens the density of states of the isolated molecule. The energy at which charge is injected at the molecule electrode junction corresponds to by the Fermi energy of the electrodes, which is also an adjustable parameter. Details of the methods are shown in the APPENDICES.

4.3. Calculations of Molecular Conductances

Computations using the non-equilibrium Green's function (NEGF) method[177] on DFT optimized structures were performed to study the origin of improved conductance and the weak dependence on length of OPE by changing to carbodithioate linkers. In the following section we first analyze the conductance of CTS and DTS in the two limits of deep tunneling and the resonant transport regime. Connections to the experiments are then made in calculations that link the two regimes and where either or both mechanisms are operative.

4.3.1. Tunneling Currents

In the tunneling regime the Fermi level of the electrode lies in the gap between filled and empty molecular orbitals. The Fermi level is far enough (energetically) from the HOMO/LUMO that the dominating contribution to the current (Eq. E-4, APPENDICES) arises from transmission near the Fermi energy. The tunneling current is thus given by:

$$I^{Tun}(V) = \left(\frac{q^2 V}{h}\right) \times T(E = E_F) \qquad \text{Eq. 2- 1}$$

with $T(E = E_F) = \sum_m SF_m^{Tun}$ and $SF_m = \sum_n \frac{\Gamma_{mn}^L \Gamma_{nm}^R}{(E_F - E_m)(E_F - E_n)}$

where, n and m sum over all MOs. Here the transmission coefficient in Eq. E-2 (and the current) has been decomposed into contributions from specific molecular orbitals m given by the scoring factor SF_m.

The calculated resistances for DTS are about an order of magnitude larger than for CTS. The values for β are comparable for both systems (0.42 $Å^{-1}$ for CTS and 0.43 $Å^{-1}$ for DTS), while the evaluated contact resistance R_0 for the CTS (C1-C3, 1.94 MΩ) is almost an order of magnitude smaller than that for DTS (T2 and T3, 12.02 MΩ), providing evidence that improving the coupling at the contacts enhances the conductivity of the CTS relative to the corresponding DTS.

Figure 2- 7 shows the scoring factor as a function of MO energy. While the barrier for hole injection is lower than that for electron injection in both systems, the electron current through empty states cannot be disregarded (relative to the hole current) for CTS. Both electron and hole transport contribute comparably in CTS (the sum of contributions from filled states exceeds that from empty states by a factor of 2 at most), while hole transport dominates for DTS (filled state contributions exceed those from empty states by at least a factor of 6). For these systems, the frontier orbitals need not

dominate the coupling contributions, and it would be misleading to correlate conductance with the HOMO and LUMO energies alone. Furthermore, even if the frontier orbitals are strongly coupled to the electrodes, they can have low scoring factors because contact-induced couplings to neighboring orbitals can lead to destructive interference. Contact-induced couplings (cross terms in Eq. 2- 1) further enable these orbitals to boost the contribution of energetically close orbitals, which are more weakly coupled to the electrodes.

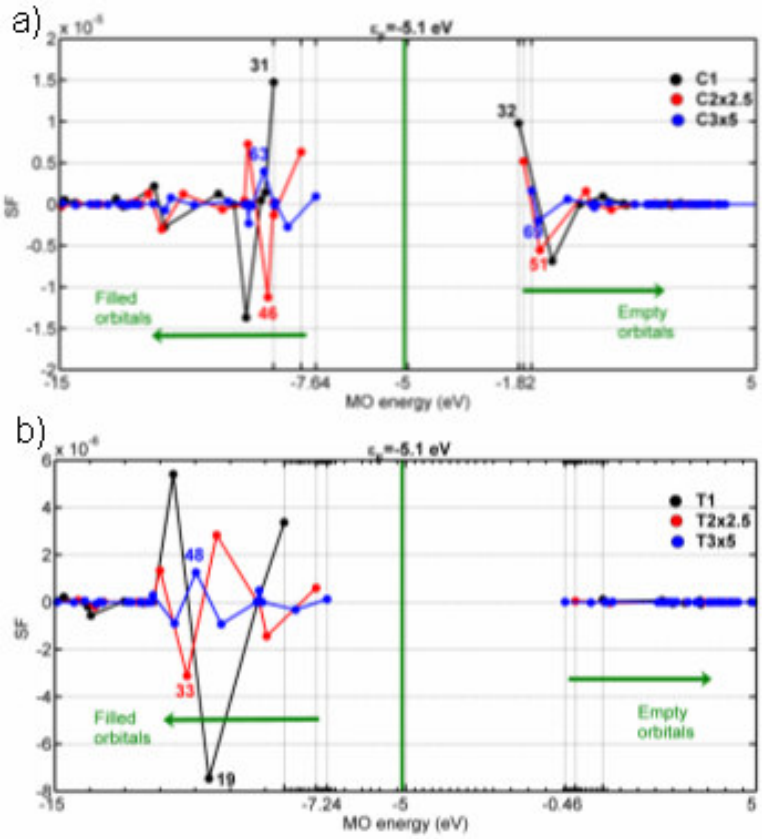

Figure 2- 7: Plots of the scoring factors (Eq. 2- 1) for each molecular orbital vs MO energies. a) CT systems and b) DT systems. For both CT and DT systems, the orbitals which show the strongest contributions are labeled.

The contribution of the HOMO to the tunneling current in CTS is much larger than in DTS, despite the higher barrier for hole injection in CTS (**Figure 2- 7**). For CTS, the additional terminal sulfur, double bonded to the terminal carbon, forms a π-mediated coupling pathway to the Au surface. The contribution of this π pathway to the current is much larger than that from the single bonded sulfur pathway. Since the carbodithioate linker is delocalized, it is plausible that the coupling for the delocalized system is intermediate between the single and double bonded sulfur coupling. This may explain why the contact resistance is decreased by an order of magnitude in CTS, as opposed to the two order of magnitude decrease seen in our calculations.

4.3.2. Resonant Currents

Table 2- 2: Resonant current (I_m^{Res} m=HOMO/LUMO) for V=100 mV) for CTS and DTS.

System	$I_{m=HOMO}^{Res}$ **(μA)**	**System**	$I_{m=HOMO}^{Res}$ **(μA)**
C1	74	T1	37
C2	26	T2	4.1
C3	24	T3	0.7
System	$I_{m=LUMO}^{Res}$ **(μA)**	**System**	$I_{m=LUMO}^{Res}$ **(μA)**
C1	42	T1	2.4
C2	35	T2	0.1
C3	25	T3	23

In the resonant regime the electrode Fermi levels are resonant with MO energies, and a ballistic current flows through the molecule. Intuitively, the current should then depend only on the contact resistance as defined by the coupling strength of each MO to

the electrodes. In the resonant regime, the conductance depends only on the strength of the broadening matrix elements and contributions from off resonant cross terms ($n \neq m$) are negligible. This further simplifies the picture as the currents in the resonant regime may be considered to be the intrinsic currents of orbital m, free of any interference from other MOs. If the Fermi level lies in the HOMO/LUMO gap and it gets energetically closer to either of HOMO or LUMO level to be resonant, only a single orbital, the one nearer to E_F, will contribute to ballistic transport. The data in **Table 2- 2** clearly indicate that each HOMO for CTS is more strongly coupled to the electrodes than that for corresponding DTS, producing higher ballistic currents in the resonant regime.

4.3.3. Mixed Mechanisms: Combination of Tunneling and Resonant Currents

The measured β value of 0.05 $Å^{-1}$ for CTS translates to an effective barrier height < k_BT for the carbodithioate-terminated OPEs, indicating that tunneling transport likely competes with thermally activated carrier injection processes.[40, 84] Recent studies indicate that conformational fluctuations can bias individual members of an ensemble toward one mechanism or another.[92, 174-176] Thus, we calculate the full (with tunneling and ballistic contributions) coherent transmission and current. E_F is restricted to values in the HOMO/LUMO gap and more than 0.4-0.6 eV away from the HOMO/LUMO, so that the current/voltage dependence in the applied bias range of 100 mV is linear and the conductance can be calculated directly from the slope of the I-V plots. The sulfur-gold coupling parameter γ is varied over a range of several orders of magnitude, while maintaining the weak coupling limit (i.e., the molecular energy levels are only broadened with negligible shifts and do not mix with each other).

Our results show that while the β values for the two linker systems remain close, varying from 0.45 to 0.15 at E_F values of $–6.5 < EF < –2.5$, it is noted that the CTS system is theoretically capable of achieving very low β (< 0.1) even in the weak sulfur-

gold coupling limit (γ = 0.1 eV) when E_F approaches the HOMO of C1. Moreover, the relative contact resistance value (R_0) of CTS is always lower (ranging from 5-180 times) than that of DTS for all values of E_F. These observations are consistent with the order of magnitude increase in resistance of DTS relative to CTS seen in our experiments. The computations suggest that in the weak coupling limit the relative differences in resistance can be increased (decreased) by shifting the electrode Fermi level E_F, using metals other than gold, for instance, towards the LUMO (HOMO).

4.3.4. Combining Simulation and Experimental Results

Having explored the dependence of the conductance, contact resistance and decay constant on our modeling parameters, we address the question of whether the theoretical approach in the weak sulfur-electrode coupling regime can explain our experimental data. The experiments show rather low β values (~0.11 $Å^{-1}$ for DTS and ~0.05 $Å^{-1}$ for CTS), which is possible when the Fermi energy E_F is close to either the HOMO/LUMO, and both tunneling and resonant currents contribute. It should be noted that β values as low as ~0.05 $Å^{-1}$ for the CTS can be realized only if the Fermi level lies close to the HOMO for the CT OPEs. While the ordering of the LUMO for the CT OPEs (C1 < C2 < C3) tends to make β large as E_F shifts towards the LUMO, the ordering of the HOMO for both CT and DT OPEs (C1 > C2 > C3 & T1 > T2 > T3) tends to reduce β as E_F shifts energetically towards the HOMO. Since both linker systems couple to the electrode through a sulfur-gold bond, we would expect the Fermi levels for both systems to be close energetically and probably lying close to the HOMO. However, as E_F shifts toward the HOMO levels of both systems from E_F = –5.5 eV in our calculation, the CTS show a larger β than the DTS at the same E_F, in contrast to the experimental values. This suggests that the Fermi level might be pinned at different energies for CT and DT OPEs. The physical basis of this assumption arises from the differences at the linker-electrode

interface: We envisage that the π-conjugated sulfur atoms of the carbodithioate group would modify the contact considerably with respect to the thiol function, altering the alignment between the Fermi level and the HOMO/LUMO of the OPE in a different way with linkers. Both the delocalization and the number of terminal sulfurs connected to the conjugated molecular cores differ in DTS and CTS, leading to differences in the orbital symmetry and energy levels that mediate the coupling at the contacts. The end group effect on the alignment of molecular states and the Fermi level has been invoked before to explain the different decay constants for the thiol and pyridine-terminated carotenoid molecular junctions.[42] Finally, it is also known that the microscopic configuration variations of molecule-electrode contacts in the STM break junction which are difficult to consider appropriately in computational approaches, as well as the conformational heterogeneity of the OPE molecules in solution can account for differences in Fermi level alignment with MOs .[11, 42, 84, 148]

5. Conclusion and Future Work

5.1. Conclusions

Combining experiments and theory, we have probed single molecule conductance of phenyleneethynylene molecules terminated with thiol and carbodithioate linkers, using STM break-junction and non-equilibrium Green's function methods. Our experimental data demonstrate that the carbodithioate linker not only augments the electronic coupling to the metal electrode relative to thiol, but reduces the barrier to charge injection into the phenyleneethynylene bridge, making possible mixed tunneling/hopping transport mechanisms, and underscoring that these structures are more conductive than originally appreciated. The theoretical analysis highlights the importance of amplified coupling and multiple electrode-linker contacts in CT OPEs and captures the key differences between molecule-electrode injection barriers associated with thiol and carbodithioate linkages

(even if charge transport does not proceed by a pure tunneling mechanism). Our calculations suggest that the experimental data can be explained in the weak coupling limit and that the Fermi energies are shifted by different amounts for CT and DT OPEs to lie close (~0.3 - 0.4 eV) to the HOMO of the C3/T3 systems, where a mix of tunneling and resonant transport mechanisms are operative. Our modeling data show that CT OPEs show enhanced conductivity relative to DT OPEs for all values of the Fermi energy in the HOMO/LUMO gap and for all values of the coupling parameter. Thus, we predict that this trend of higher conductance for CT OPE relative to DT OPE molecules will be hold in general for other metal/inorganic electrodes which couple weakly with the molecule. Collectively, these data, both experimental and theoretical, emphasize the promising role for carbodithioate-based connectivity in molecular electronics applications involving metallic and semi-conducting electrodes.

5.2. Future Work

5.2.1. Varying the Molecular Core

We have found that the carbodithioate linker improves the molecule-electrode contact, and the carbodithioate terminated OPE molecules have the potential to be ideal molecular wires. However, it is not clear that this trend will continue over longer distances. To address this it is necessary to synthesize longer carbodithioate terminated OPE molecules and perform the conductivity measurements. In principle, as the length of the OPE molecules increases, the band gap will decrease. In addition, the hopping mechanism may start to dominate the conductance. The performance of OPE molecular wire may be better than estimated from our existing measurements.

There are many more potential molecular wires that can be studied with the carbodithioate linker. For example, a porphyrin based molecular wire is shown in **Figure 2- 8**. The low energy redox centers of the metal porphyrins can serve as hopping stops

for electrons, helping the electrons to travel very long distances without dissipation. The light dependence of electronic properties of the porphyrin based molecular wires is also an interesting research topic.

Figure 2- 8: An example of porphyrin based molecular wire.

5.2.2. Varying the Linker Groups

Although the carbodithioate linker group is promising, there are other linker groups that may provide stronger linking between the molecular wire and the electrodes. We have compared the carbodithioate linker with thiol linker groups. It is important to know how carbodithioate compares to other linker groups. For example, Se, Te and isonitrile may provide stronger connection between the molecule and gold surface; a molecule with multiple connections at one end may perform better than a single connection.

5.2.3. Molecular Switch

There have been some doubts about the switching effect observed in some molecular systems. It was suggested that the switching effect may due to the instability of the contact between the molecular core and the electrodes.[191, 192] Solving this problem is important for the development of molecular switches and to do that we need

much more stable molecular connections than thiol linkers. The carbodithioate linker is a good candidate for this purpose.

5.2.4. I-V Curve Measurements

The conductance experiments presented here only measure current peaks in histograms at fixed bias values. In order to study the performance of the molecular wires at a different bias, we need to change the bias and perform a new measurement all over again. With the proper experimental setup, the STM break-junction can be upgraded to measure the I-V characteristics of single molecules, i.e. change bias while measuring current with the molecular wire bridging the two electrodes. With I-V curve measurements one can observe other electronic properties of the molecule, for example, NDR. With varying bias, the distance between the tip and the substrate has to be fixed at a certain value with the molecules trapped between them. The key issue is to have a sensitive and well controlled feedback system so that the tip movement can be stopped at any current value that indicates m-M-m formation, so that the I-V measurement can be performed.

CHAPTER 3

SINGLE MOLECULE CONDUCTIVITY MEASUREMENT OF PEPTIDE NUCLEIC ACIDS

1. Introduction

1.1. Peptide Nucleic Acid (PNA)

Peptide nucleic acid (PNA) is an artificial analog of DNA.[193, 194] In contrast to DNA, PNA has a pseudo-peptide backbone instead of a sugar-phosphate backbone. PNA was initially synthesized to be the recognition ligand for DNA. The advanced knowledge of peptide chemistry allows such precise control of the PNA structures and the synthesized PNA mimics DNA structure so well that it can form a duplex with complementary PNA and with complementary DNA. The double stranded PNA (or PNA-DNA duplex) has a very similar structure to the DNA duplex, yet the properties are very different. The peptide backbone of PNA can not be cleaved by nucleases or proteases enzymes. PNA duplexes are also more stable than DNA duplexes over a wider pH and temperature range due to the neutral backbone. In addition, PNA can form a stable triplex with double stranded PNA or DNA. All these unique properties of PNA open a wide range of applications, including molecular biology, diagnostics, and therapeutic treatments. [193]

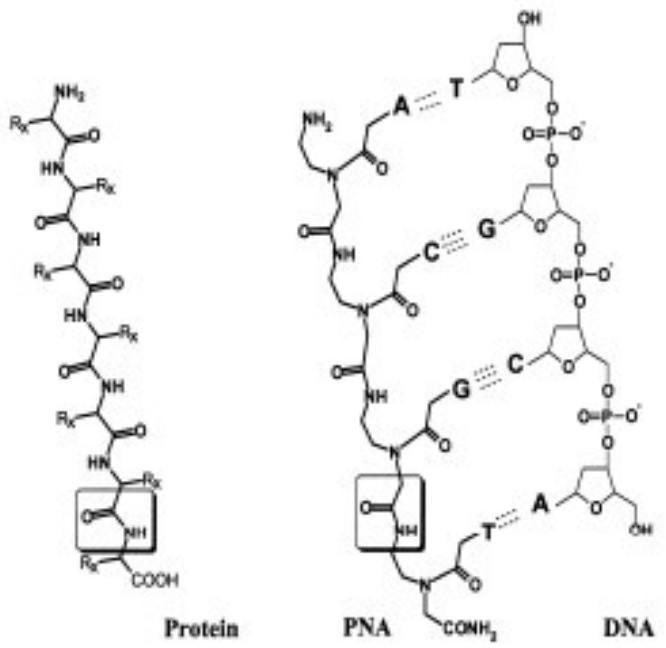

Figure 3- 1: Structure comparison between PNA, DNA and protein.[193]

1.2. Charge Transfer Study of PNA

1.2.1. DNA Charge Transfer Studies

There has been an enormous amount of research in the area of charge transfer through DNA due to its importance in biological systems.[91-93, 195-200] Electron transfer in DNA systems can cause redox reactions and may results in mutation.[201, 202] It is important to understand charge transfer through DNA for these reasons as well as possible applications in molecular electronics.[13, 94, 200, 203-205] It was proposed that the π stacking of nucleobases in DNA provides a better pathway for electron transfer than σ carbon bonds and that DNA could serve as a molecular wire with little or no distance dependence. It was shown that electrons transfer in DNA by a mixed mechanism of superexchange (tunneling) in short distance and hopping over several nanometers.[29]

1.2.2. The Advantages of PNA

Although charge transfer through DNA has been extensively studied and is relatively well understood, the ability to control charge transport, especially over long distance, remains a challenge. In part this is due to the difficulty in forming compact SAMs of DNA and distinguishing electron transport from ion transport.[77] This limitation arises from an intrinsic property of DNA, the charged phosphate backbone. Therefore, a challenge in nucleic acid charge transfer studies using electrochemical probes is to promote the formation of a close-packed SAM to have a uniform thin film. The close-packed SAM also ensures rigidity of nucleic acid molecules in the SAM and limits the diffusion of molecules in the SAM.[1] In contrast, PNA has a neutral backbone and can potentially form more compact SAMs than DNA for charge transfer studies. It was shown that the growth of PNA SAMs is similar to the two-step formation of alkanethiol SAM.[206-209] Initially, adsorbed PNA molecules lie down on the surface at low coverage. When the surface coverage increases to a certain percentage, the PNA molecules stand up normal to the surface to form compact monolayers.[206-208] The formation of compact SAM of PNA enables charge transfer to be studied by electrochemical techniques.

In principle, the advantage of more compact SAM formation of PNA is not beneficial for the STM break-junction measurement of PNA conductivity, since STM break-junction method usually requires a low density SAM. However, the higher stability of PNA duplex over DNA is still a factor to be considered in the break-junction methods. For the development of molecular electronics, the most important advantage of using PNA comes from the modifiability of the PNA chain. The well-established solid phase peptide synthetic chemistry enables researchers to modify the PNA chain easily. The most important feature for molecular electronics is that metal binding ligands can be

inserted into PNA chains. When metal ions are incorporated into the PNA structure, PNA becomes a good candidate for an ideal molecular wire for long distance charge transfer.

1.2.3. Building Molecular Wires Using PNA

One of the strategies for building molecular wires that can transfer charge over long distances is to incorporate metal ions with easily accessible redox states into the conductive molecular core.[10, 210] It has been shown that the exchangeable protons of DNA can be replaced by small radius metal ions to form a metal-DNA complex.[211] However, the position of the DNA metal binding sites can not be controlled. Also, there is no metal ion specificity in the binding process. The specific binding of particular metal ions is critical for the purpose of improving charge transfer. It has been shown that difference between the metal spin selections rules of Co and Ru results in a big difference in charge transfer rates.[212]

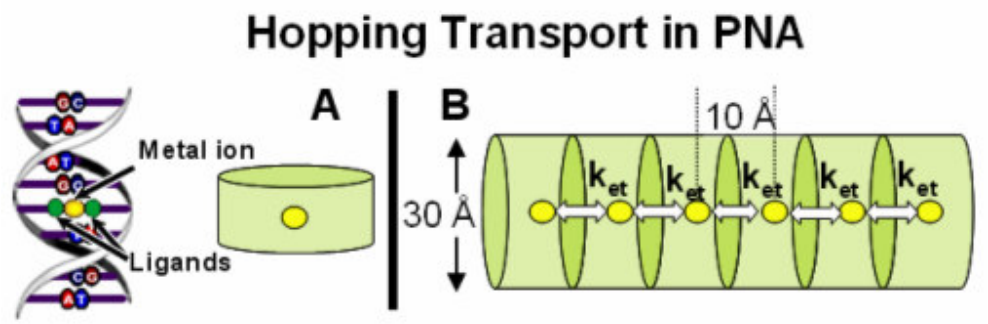

Figure 3- 2: Long distance charge transfer molecular wire based on PNA. (Cartoon drawn by the Achim group)

PNA, an artificial analog of DNA, is a great candidate for the specific and position controlled binding of metal ions.(**Figure 3- 2**) The neutral backbone of PNA minimizes the repulsive force between the two PNA chains, providing enhanced stability

of the PNA duplex. The metal binding ligands inserted into the PNA chain ensures specific binding to certain metal ions of interest, and the position of ligands determines the position of metal ions.

2. Experimental section

The PNA work is a collaborative effort of several institutions, including the Achim group at Carnegie Mellon University, the Waldeck group at the University of Pittsburgh, the Beratan group at Duke University and the Borguet group at Temple University. Silva Bezer, Richard M. Watson, and Paul Lund synthesized all the PNA molecules used in this study. Amit Paul in the Waldeck group performed electrochemical measurements. Ravindra Venkatramani in the Beratan group provided theoretical support. The Temple group did the AFM imaging work and the single molecule STM break-junction measurements.

2.1. PNA synthesis

PNA oligomers were synthesized by solid phase synthesis (Boc protection strategy).[213] Details of synthesis procedure are described in the APPENDICES.

PNA stock solutions were prepared in nanopure water, and their concentrations were determined by UV-Vis spectrophotometry (ε_{260} = 8600 cm^{-1} M^{-1} per T-monomer). PNA solutions for electrode incubation were then prepared in 50% acetonitrile, 10 mM sodium phosphate buffer (pH 7.0), typically with 20 μM ssPNA.

2.2. Electrode Preparation

2.2.1. Gold Bead For AFM Imaging and STM Break-junction Measurements

The ultra-flat Au(111) facet on a gold bead (see APPENDICES for an STM image of typical Au(111) facet) is a perfect substrate for AFM and STM experiments. The Au bead electrode was made by melting 0.6 mm Au wire (99.999%, Alfa Aesar, MA) in a hydrogen flame, followed by a cleaning procedure to remove contaminates. Details of the procedure are described in the APPENDICES.

Prior to the experiments the substrate was cleaned by immersion in hot piranha solution (1:3 H_2O_2 and 98 % H_2SO_4) **(Caution! The piranha solution is a very strong oxidizing agent and extremely dangerous)** for 1 hour. After each step the sample was rinsed by sonication in ultrapure water produced by a Barnstead, Nanopure Infinity system. After the chemical cleaning, the crystal was hydrogen flame annealed and allowed to cool in air.

2.2.2. Gold Electrode for Electrochemical Measurements

A gold wire (0.5 mm diameter, 99.999%) (purchased from Alfa Aesar, MA) was cleaned by reflux in nitric acid (70%) at 130^{o}C for 2 hours and then washed with deionized water. The tip of the gold wire was heated to form a ball. The exposed wire was sealed in a soft-glass capillary tube. The gold ball was reheated in the flame until glowing, then slowly cooled down and finally quenched in deionized water (18 MΩ.cm). This annealing process was performed more than fifteen times to make a smooth clean ball electrode. The area of the electrode was ~0.1 cm^2.

2.3. Electrochemical Measurements

Clean gold electrodes were incubated in PNA solutions at 35^{o}C or 40^{o}C, typically for 40 hours. After incubation the gold electrodes were washed with nanopure water and directly used for electrochemical studies. This study showed that the PNA SAM was exceptionally stable. After incubation, electrodes were kept in nanopure water, and

experiments could be performed more than ten days after incubation without significant changes in the response.

Cyclic Voltammetry (CV) was carried out on a CH Instrument Electrochemical Analyzer 618B (Austin, TX). A three-electrode electrochemical cell was used, which is consisted of an Ag/AgCl (3 M KCl) reference electrode, a platinum wire as counter electrode, and a SAM coated gold ball electrode as the working electrode. All experiments were performed in 1 M $NaClO_4$ (pH=7-8) aqueous electrolyte solution at room temperature. The uncompensated solution resistance was measured by AC impedance and found to be less than 5 Ω, so that iR drop was not important for these measurements. The coverage of the PNA-Fc SAM was calculated by integrating the charge under the voltammetric peaks.

2.4. Atomic Force Microscopy (AFM)

Atomic Force Microscopy was carried out on an Agilent 5500 AFM (formerly Molecular Imaging PicoPlus) (Tempe, AZ) instrument. A tapping mode silicon cantilever AFM tip (Resonant frequency 170 kHz, Force constant 40 N/ m MikroMasch, Estonia) was used. Experiments were done at room temperature under atmosphere conditions. The AFM images are shown without any treatment except for necessary flattering. Cross-section analysis of AFM images were performed using PicoScan software.

2.5. STM Break-junction Measurements

The STM break-junction setup for PNA single molecule conductivity measurements is similar to previously described in chapter 1 and chapter 2. Usually, a diluted solution of PNA (~ 10 μM) was used for the measurements. Since the PNA measurements were performed under aqueous conditions, the gold tips were coated by an

insulating material to prevent current passing through the solution, as well as unwanted faradaic current, instead of the molecules. The gold STM tips were prepared and coated following the procedure described in the APPENDICES.

3. Result and Discussion

3.1. AFM imaging of PNA SAM

Tapping mode Atomic Force Microscopy imaging was performed on a gold bead Au(111) surface for the SAM of Cys-T6-Fc. A typical AFM topography image is shown in **Figure 3- 3**. Two distinct regions of the monolayer were observed, one of them is significantly higher than the other. The cross-section analysis showed that the height difference between the two regions is ~3.5 nm. Given that the length of Cys-T6-Fc is about 3 nm, it is possible that the higher region is the self-assembled monolayer of Cys-T6-Fc with PNA molecules standing normal to the surface and the lower region is the substrate surface. However, based on the mechanism of PNA SAM formation proposed by Martin-Gago[206-208], it is not likely that PNA forms well organized SAM in one region, while leaving other regions blank. A more reasonable picture is that PNA initially grows the surface with very low coverage and as the self-assembly proceeds, PNA molecules stand up to form higher domains. This growth mechanism suggests that the two regions in AFM images refer to two different phases of PNA SAM: a lying-down phase and a standing-up phase.

The two-phase structure is also supported by electrochemical measurements which reveal two distinct charge transfer species present, one slow and one fast.[126] If the electrochemical signal is dominated by the lying down phase which transfers electrons directly to the substrate without passing them through the PNA chain, charge transfer probed by the CV (cyclic voltammetry) method does not reflect the intrinsic property of PNA.

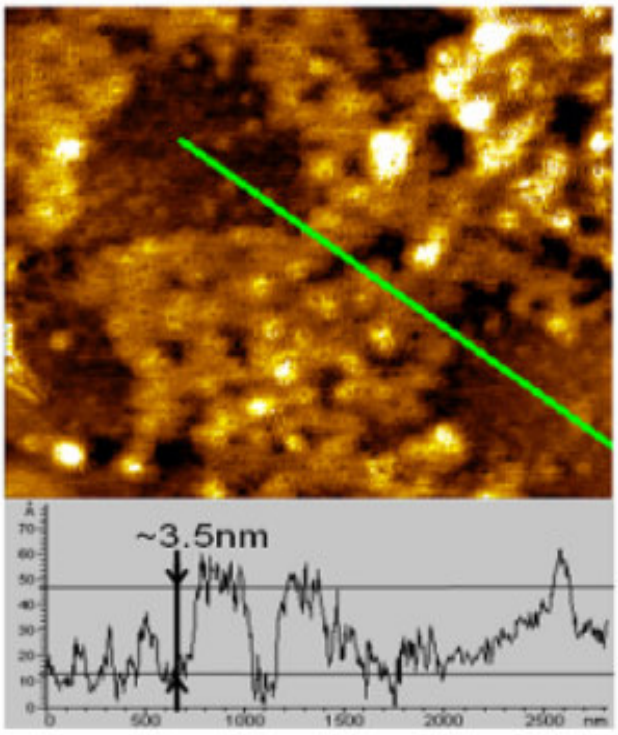

Figure 3- 3: AFM image of Cys-T6-Fc monolayer showing two kinds of domains with height difference ~3.5 nm.[126]

3.2. Electrochemical Characterization

The hypothesis that the two groups of charge transfer species observed in CV experiments with different charge transfer rate refer to the lying-down and standing-up phases of PNA is confirmed by CV results of PNA SAM with only the lying-down phase prepared by short time incubation. The CV results of PNA SAM without the standing-up phase show only the fast response species, suggesting that the slow species is the standing-up PNA, which is the key object of interest.

The Pitt group utilized the charge transfer rate difference between the two species to prepare a PNA SAM for the charge transfer study.[126] In this SAM only the standing-up species responds to the CV measurements. After a ferrocene group is

oxidized during the forward scan, a reverse scan reduces ferrocenium back to ferrocene. However, some ferrocenium can be lost through a chemical step, especially when chloride ion is present in the solution (**Figure 3- 4**). This degradation of ferrocene group only happens after it is oxidized by the forward scan, i.e. after electron transfer from the ferrocene to the electrode. A protocol was proposed to preferentially destroy the lying-down species by performing the CV scan of the SAM covered electrode in NaCl solution with a fast scan rate (> 1 V/s).[126] At this scan rate, electrons do not have enough time to be transferred through the PNA chain from the ferrocene groups to the electrode in the standing-up phase, while ferrocenes in the lying-down phase can react. The fast CV scan is repeated until the ferrocene in the lying-down phase is completely destroyed. Without the electrochemical probe, ferrocene, the lying-down phase, while still present does not contribute to the electrochemical signal.

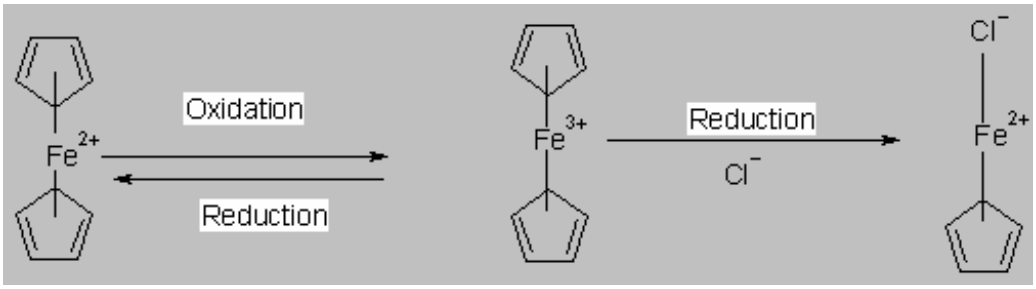

Figure 3- 4: Ferrocene Reaction during Cyclic Voltammetry cycles.[126]

Following the destroying procedure, a series of PNA molecules was studied by electrochemistry.[126] **Figure 3- 5** is the tunneling decay plot for this series of thymine single stranded PNA molecules with various lengths.[126] The distance contribution by a thymine base was taken to be 3.5 Å and the data was fit to $k_0 = A\exp(-\beta d)$. The semi-log fit to the data gives a tunneling decay constant of $\beta = 0.87$ Å^{-1} (3.05 / Base) for these thymine (T) containing single stranded PNA molecules. This value of β is similar to that reported for peptides and alkanethiols.[10, 125, 214-216]

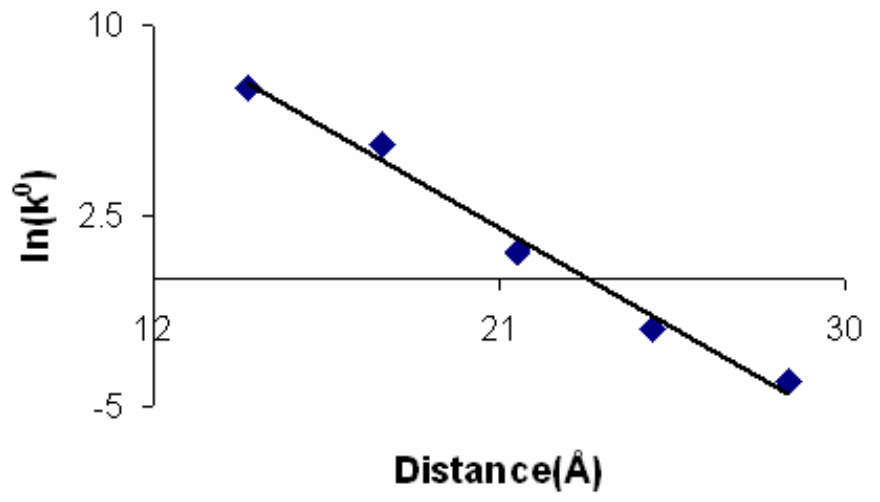

Figure 3- 5: Tunneling decay constant (β) determination for Thymine (T) containing single stranded PNA molecules (error bars are smaller than symbols).[126]

3.3. Single Molecule Conductivity Measurement of PNA

In order to understand the true single molecule behavior of PNA molecules, STM break-junction experiments were performed to measure the electronic properties of single PNA strands. An example of typical data for one of the PNA molecules we studied, cys-T4-cys (**Figure 3- 6**a) is shown in **Figure 3- 6**, where cys represents a cysteine group which binds to the gold electrode surface through a thiol-Au bond, and Tn indicates that the number of thymine (T) groups in PNA is n. A well defined peak is observed in the histogram analysis (**Figure 3- 6**a) of a large number of current-distance (IS) curves. Typical IS curves with clear conductance steps are shown in **Figure 3- 6**b. The linear fitting of the current peaks acquired at multiple biases reveals the conductance of cys-T4-cys (**Figure 3- 6**c) to be 2.5 $\pm$0.4 x10^{-5} G_0, where G_0 is the quantized conductance unit (77μS).

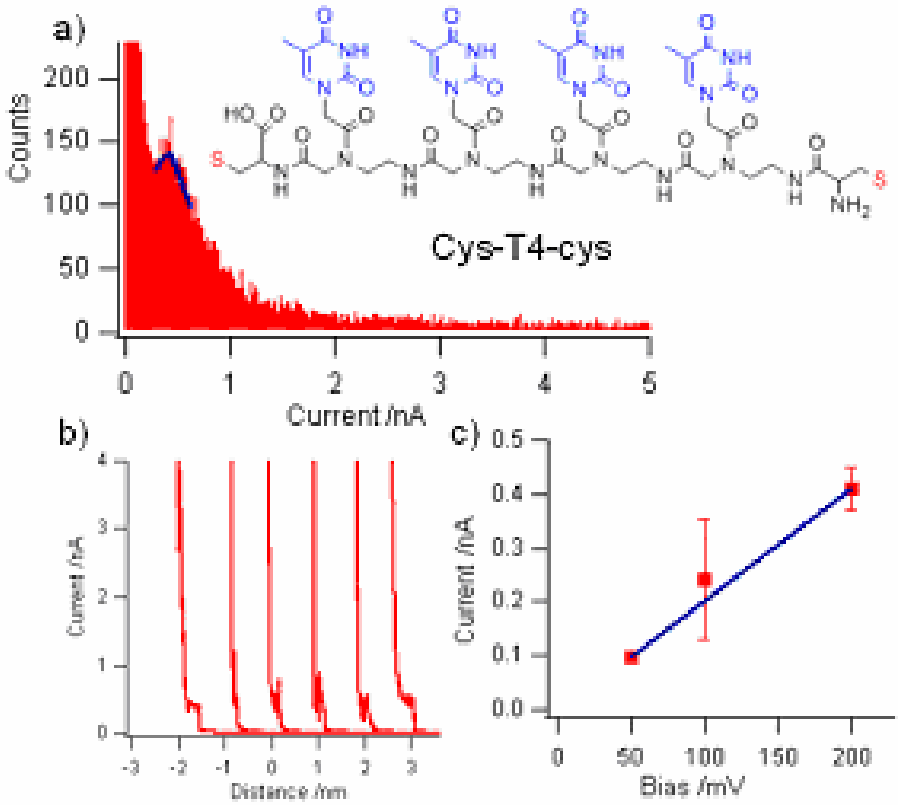

Figure 3- 6: Molecular conductance measurement of cys-T4-cys.[217]

We measured the conductance of PNA molecules with increasing number of thymine groups, i.e. length, to study the distance dependence of PNA conductance. The conductivity measurement results are summarized in **Table 3- 1**. We found that the conductance of cys-T3-cys (3.1 $\pm$0.3 x10^{-4} G_0) is similar to a much shorter molecule, cys-BK-cys (3.5 $\pm$0.4 x10^{-4} G_0), which has no thymine groups. This indicates that PNA with nucleobases is much more conductive than backbone only PNA, which confirms that charge transfer though PNA is mainly assisted by the nucleobases. Without the nucleobases, the peptide backbone, which has mostly saturated σ bonds, is poorly conductive. The conductivity of PNA is comparable to the reported conductance value of DNA.[218] This further supports the picture of nucleobase assisted charge transfer mechanism, because the structures of PNA and DNA are very similar except for their

backbones. The similar conductance value over a relatively long distance (several nanometers) appeaers to originate from the similar nucleobases in the PNA and DNA structures.

Table 3- 1: Conductance of PNA molecules. (BK means backbone only , i.e. PNA molecule without nucleobases) [217]

PNA	Length /nm	Conductance /G_0
Cys-T2-Cys	~1.5	$3.6 \pm 0.3 \times 10^{-3}$
Cys-T3-Cys	~1.9	$3.1 \pm 0.3 \times 10^{-4}$
Cys-T4-Cys	~2.3	$2.5 \pm 0.4 \times 10^{-5}$
Cys-T5-Cys	~2.6	$6.7 \pm 0.6 \times 10^{-6}$
Cys-BK-Cys	~1.1	$3.5 \pm 0.4 \times 10^{-4}$

The conductivity decay constant, β, calculated through the semi-logarithmic plot of resistance and molecule length based on $R = R_0 \exp(\beta L)$, where R_0 is the contact resistance, and L is the length of molecule is shown in **Figure 3- 7**). The β of PNA molecules with thymine groups is 0.58 ± 0.03/Å, which is in good agreement with macroscopic electrochemical results, where the charge transfer through a PNA self-assembled monolayer (SAM) is studied using cyclic voltammetry (CV) monitoring of a redox active probe, ferrocene, covalently attached to the other end of PNA.

It should be pointed out that while the conductivity of PNA chains is improved by the presence of nucleobases, the decay constant is still similar to peptides and alkanethiols.[10, 125, 214-216] This indicates that, although nucleobases contribute significantly to the conductance, the overall charge transfer in the molecule studied in our measurements is still in the tunneling regime, not hopping. The reason is likely to be the

short length of the PNA molecules studied in this work, since the hopping mechanism usually dominates at longer distances.[37, 40, 92] More experiments need to be done to explore the hopping regime for the charge transfer of longer PNA molecules.

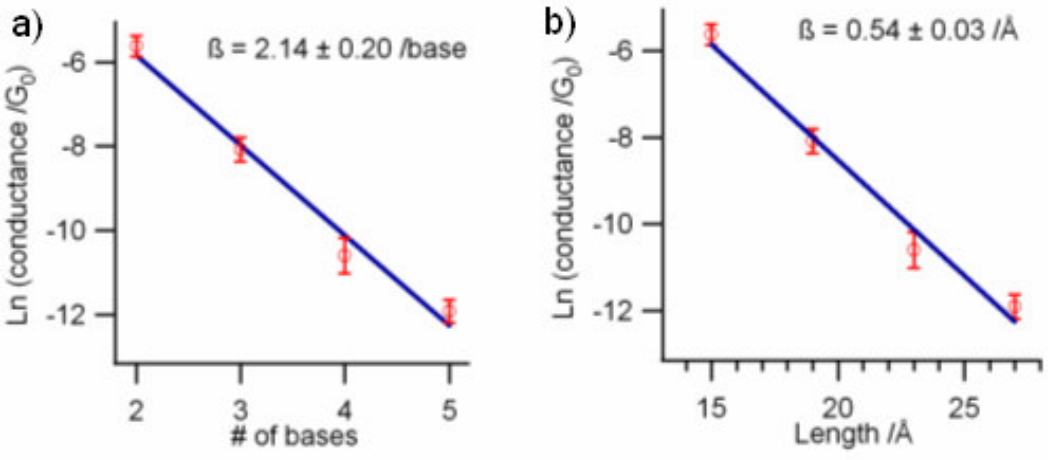

Figure 3- 7: Natural logarithmic plot of the conductance of PNA versus number of bases (a) and length (b).[217]

It was reported that the nucleobase type in the DNA structure affects the charges transfer due to the different redox states of the nucleobases.[91, 92, 195, 197-199] The effect of nucleobases is also seen in PNA systems.[219] With this in mind, we performed single molecule conductance measurements on single stranded PNA molecules with different nucleobases at the center. The results are summarized in **Table 3- 2**.

Table 3- 2: Conductance of same length PNA molecules with various nucleobases.

PNA	Length /nm	Conductance /G_0
Cys-TTT-Cys	~1.9	$3.1 \pm 0.3 \times 10^{-4}$
Cys-TCT-Cys	~1.9	$\sim 1.97 \pm 0.2 \times 10^{-4}$
Cys-TGT-Cys	~1.9	$4.2 \pm 0.9 \times 10^{-4}$

It has been reported that the charge transfer rate of a PNA with seven thymine bases is improved by several times if the center thymine is replaced by guanine.[219] This effect is attributed to the lower oxidation potential of guanine compared to thymine.[219] Theoretical simulations also suggest that the conductance of the purine (guanine and adenine) mixed PNA is an order of magnitude larger than that for the pyrimidines (cytosine and thymine).[219] However, in contrast to the reported results, our single molecule measurements show very similar conductance values for PNA molecules with TTT, TCT and TGT core.(**Table 3- 2**) The different behavior of PNA molecules in our measurements and in the reported results likely originates from the completely different experimental methods. Our STM break-junction measurement probes the behavior of single molecules, while the reported results are from macroscopic electrochemical measurements.[219]

The conformation of the PNA molecules in the break-junction measurements may be quite different than in the voltammetry experiments. The long single stranded PNA between two electrodes in solution could be quite floppy, compared to the PNA molecules in a self-assembled monolayer. In the voltammetry experiments the surface coverage is dense enough that all the PNA molecules are rigid and stand up on the electrode surface. In the break-junction measurements, if the nucleobase at the center is moving too much, it might play a weak role in the total conductance. Consider the following two situations for charge transfer through the PNA chain:

1) If the single stranded PNA has a rigid conformation and all three bases stack well, then the electrons have a well established π-stack to tunnel through and make little use of the backbone of PNA and the cysteine groups on both ends. In this case, the effect of various nucleobases is maximized, as see in electrochemical experiments.

2) If single stranded PNA is floppy and the bases do not stack well, the π-stack is disrupted, and the electrons passing through the backbone of cysteines and PNA might become competitive with the π-stack channel. It is hard to tell whether the backbone dominates the resistance or both channels contribute to the conductance. In either case, the conductance of single PNA molecules would be smaller than in scenario 1) where the π-stack is stable and provides sufficient support for the electron tunneling. In addition, the conductivity of single PNA molecules would be insensitive to the change of central base.

The observation of PNA conductance insensitivity to nucleobase is important for developing molecular wires. It highlights an important factor that affects the performance of molecular wires, the rigidity of molecule. This factor is important for designing long range charge transfer molecular wires, since longer molecules may be more vulnerable to structure fluctuations. This leads to an important feature of PNA that we discussed previously. The double stranded PNA is much more stable than DNA, which makes PNA more suitable for long range charge transfer.

It should be pointed out that another difference between our single molecule measurements and the reported electrochemical results may account for the different charge transfer behavior of PNA. The molecules we studied by break-junction methods are three nucleobase PNA, while the PNA molecules in [219] are longer. For longer PNA molecules, the hopping mechanism may start to dominate the charge transfer process, i.e. the electrons hop between the nucleobases and the energy levels of these bases are populated during the process. In the hopping mechanism, energy levels of nucleobases are important for the charge transfer. Nucleobases with lower redox potential, for example, guanine, should improve charge transfer. In the tunneling regime, the electrons do not sit on the energy levels of the nucleobases, which influence the charge transfer in an indirect way by mixing with the energy states of the backbone. In

our break-junction measurements, the three-base PNA molecules may primarily operate in the tunneling regime. The effect of the nucleobases may be limited. Theoretical study is needed to find out the extent of orbital mixing between nucleobases and the backbone.

4. Conclusions and Future Work

4.1. Conclusions

In this work, peptide nucleic acid was analyzed by cyclic voltammetry, atomic force microscopy, and the STM break-junction method. Single molecule and electrochemical measurements of thymine PNA with various lengths show similar β values, which are also similar to those of peptide linkages.

The electron transfer rate measured for the thymine containing single stranded PNA molecules may be slower than the reported rate for duplex DNA for a number of reasons. Single stranded PNA molecules are flexible and so base stacking in single stranded molecules might be poor. In the case of DNA, long range charge transfer has been explained by the hopping mechanism, i.e. thermal occupation of holes in the energy states of nucleobases, for example guanine. Once guanine is oxidized, the charge can travel a long distance. But thymine has much higher energy states than guanine. Therefore, the PNA strands composed of thymine in our study may mainly transport charge by superexchange mediated tunneling mechanism, i. e. they should show a strong decay with increasing distance between donor and acceptor similar to alkanethiols and peptide chains, as observed both by electrochemical experiments and our STM break-junction measurements.

Our single molecular measurements of three base PNA molecules with various center base show similar conductance results. The insensitivity may result from the floppy single stranded PNA chain, which has poor π-stacking. This finding highlights the importance of the rigidity of the molecular wire.

4.2. Future Work

4.2.1. Length Dependence of PNA Charge Transfer

We measured the conductance of thymine PNA with lengths from two to five nucleobases. The experimental results suggest that the electron transfer is mainly by the superexchange mechanism. It is important to study longer PNA molecules to observe the transition from the superexchange mechanism to the hopping mechanism.

4.2.2. pH Effect

All our measurements were performed in pH 7 buffer solution. It would be interesting to know how charge transfer is affected by various pH conditions.

4.2.3. Effect of Nucleobases at Longer Distances

We did not observe a change in conductance of the three nucleobase PNA molecules on varying the center base. Does this base type insensitivity persist for longer PNA when the hopping mechanism is the main charge transfer pathway? Will we observe a noticeable difference in conductance when all the nucleobases in a PNA are changed?

4.2.4. Conductance of PNA Duplex

We expect PNA duplex to provide stability, better π-stacking, and more electron transfer pathways. Therefore, the conductance of PNA should be improved significantly. However, until we perform the single molecule measurements, we would not know how single PNA duplex molecules behave between the two electrodes in solution.

4.2.5. Conductance of PNA with Metal Ions

The ultimate goal is to perform single molecule measurements of PNA duplex molecules with metal binding ligands and measure the conductivity with and without the presence of metal ions. A whole series of experiments should be performed to study the effect of 1) metal ion type; 2) pH; 3) nucleobase type; and 4) length of PNA.

CHAPTER 4

MOLECULAR SCALE VISUALIZATION OF PORPHYRIN CHARGE TRANSFER REACTIONS

1. Introduction

1.1. Introduction to Electrochemical Systems

1.1.1. Electrochemical Interface and Double Layer

A major research area in the field of electrochemistry is charge transfer and related phenomena, since electrochemical reactions all involve gaining or losing electrons.[220, 221] Since many electrodes used are solids, the electrochemical interface is, in many circumstances, recognized as a solid-liquid interface. At the interface, many ions specifically adsorb at the surface of the electrode, bringing in a layer of ionic excess charge, which is balanced by a layer of charge that resides in the electrode.[221] These two layers, together, are called the electrical double layer. The double layer concept is important for understanding electrochemical phenomena because most electrochemical reactions occur at the electrode surface, in the double layer.[220] The potential drop between the two electrodes also happens primarily in the double layer region. A simple model of the double layer is shown in **Figure 4- 1**.

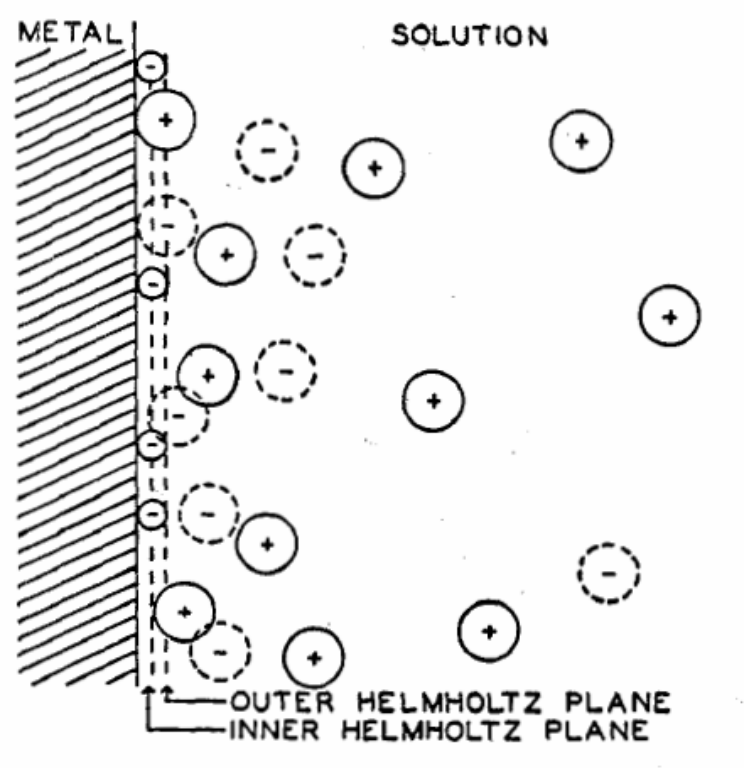

Figure 4- 1: The simplest model of electrochemical double layer.[221]

Electrochemical processes strongly depend on the structure and properties of the electrode surfaces. Noble metal electrodes are often used in electrochemical research of charge transfer for molecular systems because of their unique properties. In our studies, an Au(111) surface was chosen to perform most of the work because the following reasons: 1) the Au electrode is inert under most electrochemical conditions; 2) the Au electrode is easy to clean. After each experiment, a piranha solution cleaning procedure, described in previous chapters, is enough to remove all organic molecules on the surface; 3) the Au electrode surface is reproducible. A chemical cleaning followed by flame annealing usually provides nearly identical surfaces for experiments; 4) the Au(111) surface is well known and has been studied extensively.[222, 223] Au(111) has two stable phases: an unreconstructed and a reconstructed phase. [222, 223] The reconstruction refers to the reorganization of surface Au atoms when the symmetry of Au

crystal is broken at the surface. The reconstructed phase on Au(111) is a $(22 \times \sqrt{3})$ structure which has 23 surface atoms registered to the space of 22 bulk atoms underneath.[222, 223] The extra atoms at the surface cause microscopic roughness, seen as bumps in scanning tunneling microscopy (STM) images. The vertical corrugation of the reconstruction lines is ~ 0.1 Å (**Figure 4- 2**).

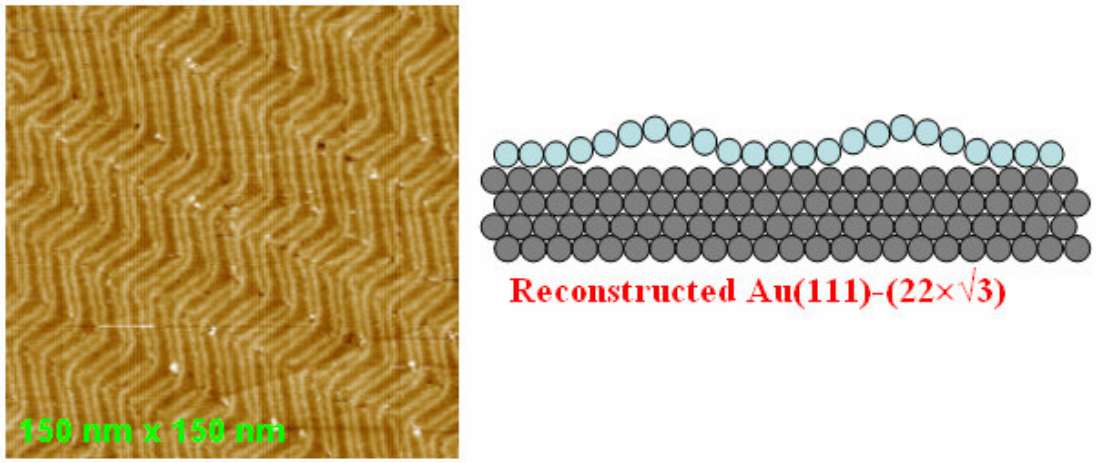

Figure 4- 2: STM image of the Au(111) reconstructed surface. The double strips are reconstruction lines as shown in the cartoon on the right.

The gold reconstruction is sensitive to contamination on the surface. Observation of a clean, reconstructed Au(111) surface is an important control experiment for further STM imaging under electrochemical conditions. In addition, our STM work involves high resolution imaging that requires sub-molecular recognition. The observation of reconstruction lines, usually ~0.1 Å high, is an indication of a good instrument and a good STM tip condition for single molecule study.

1.1.2. Electrochemical Scanning Tunneling Microscopy (EC-STM)

Traditional electrochemical techniques probe the macroscopic behavior of molecules on the electrode surfaces. They can be combined with spectroscopic

techniques, such as surface enhanced Raman spectroscopy, infrared spectroscopy, and surface X-ray scattering, to directly probe various aspects of the structure and properties of adsorbates under electrochemical environments.[224] However, all these techniques do not have molecular spatial resolution. Electrochemical scanning tunneling microscopy (EC-SPM) provides molecular insight for the observation of the behavior of single molecules under electrochemical conditions. EC-SPM has been used to study a number of potential driven processes at the electrode surface, for example surface reconstruction,[222] electrodeposition,[225] and molecular adsorption.[226-228]

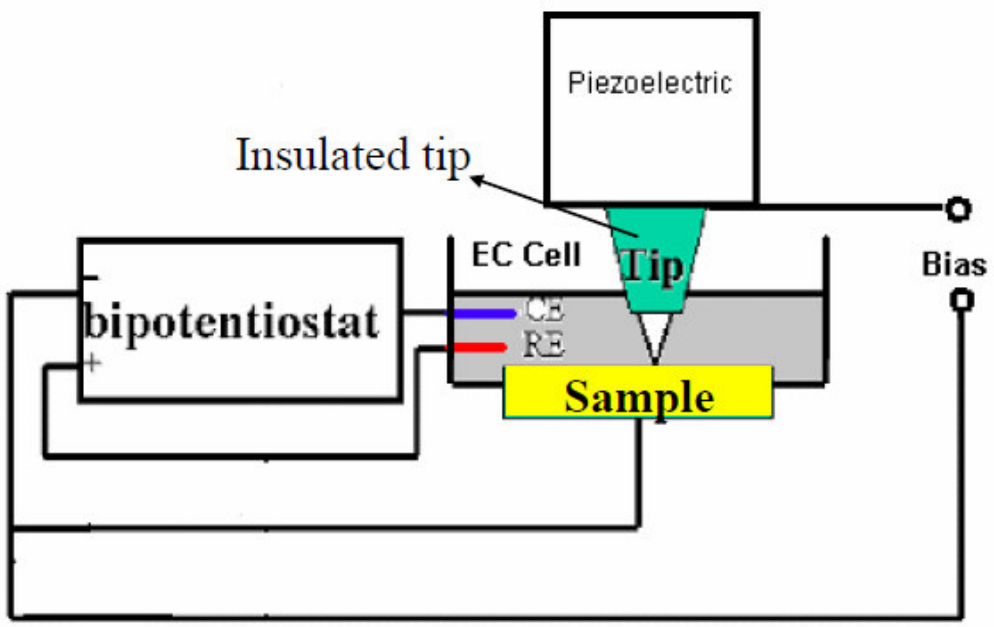

Figure 4- 3: Schematic of EC-STM. A bipotentiostat is used to control the electrode potential in a four electrode setup, including CE: counter electrode, RE: reference electrode.[229]

STM is a surface characterization technique. It was first developed for studies under vacuum and ambient environments.[230] Shortly after, STM was used for in-situ probing of electrochemical interfaces when tip coating techniques were developed.[231]

The metal STM tip generates a faradaic current, which can overwhelm the tunneling current if not suppressed. Therefore, it is necessary to coat the tip with an insulating material leaving only the very end of the tip uncoated.[231] The uncoated portion of the tip allows the tunneling current to pass through, and since the exposed surface is very small, the faradaic current (usually called leakage current) is usually less than 10 pA (the bias used is usually 10-40 mV) in our experiments. Another difference between EC-STM and normal STM is in the control of the tip-sample bias. The bias is the voltage difference applied between the tip and substrate in normal STM. However, in EC-STM the sample potential also needs to be controlled. Therefore a bipotentiostat is required to independently control the potential of the tip and the potential of the substrate relative to a reference electrode.

1.2. Motivation: The Importance of Porphyrins

The unique electronic properties and reactivity of porphyrins to have led to a wide range of applications from biology, molecular devices, artificial photosynthesis, information storage to fuel cells.[1, 29, 232-238] Due to their importance in fundamental and applied studies, the formation and characterization of ordered porphyrin adlayers have been extensively studied in the last two decades by scanning tunneling microscopy (STM) under various conditions, including ultra high vacuum (UHV), air and electrochemical environments.[226-228, 239-263]

1.3. STM Study of Porphyrin Self-assembly

Most early studies of porphyrin assemblies were performed under UHV environment. For example, Gimzewski's group showed that the self-assembled structures of Cu-tetra-(3, 5 di-tertiary-butyl-phenyl) porphyrin (CuTBPP) strongly depend on the substrate materials (Cu, Au, Ag).[239, 264] Various structures such as

trimers, tetramers, and a 1D wire-like structure induced by dipole-dipole interaction or intra-molecular hydrogen bonds were also observed by Yokoyama et al. using -CN or -COOH group substituted TBPP molecules.[240, 241] The Hipps group, combining theoretical calculations and STM observations in UHV of sublimed layers of one or multiple kinds of metal coordinated porphyrin on surfaces, found that the metal ion valence configuration, especially the status of the dz^2 orbital, strongly affects the observed tunneling contrast of STM images.[242, 243] Recently, several examples of supramolecular architectures formed by assembly of fullerenes and porphyrins have been studied under UHV. For instance, Bonifazi el al. reported a correlated arrangement between fullerene in 2nd layer and the porphyrin arrays underneath.[244] In addition, several interesting STM experiments involving multi-porphyrin supramolecular arrays have been carried out under UHV. [245-247]

There are several reports about the adlayer structures of porphyrin under ambient conditions. Bai and Wan et al. reported a two-dimensional hydrogen bonding network of 5, 10, 15, 20-tetrakis (4-carboxylphenyl)-21H, 23H-porphyrin (TCPP) on HOPG by using stearic acid lamellae as stabilizing barrier.[265] They also demonstrated the stabilizing effect of linear alkanes on the assembly of a planar organic molecule by using alkylated porphyrin to achieve highly stable structures on inert surfaces(HOPG).[248] Hou's group reported a novel "edge-on" stacking structure on HOPG surface besides the well-known "face-on" adsorption style by using a novel porphyrin derivative, 5-hydroxyphenyl-10, 15, 20-trikis(4-dodecyloxyphenyl) porphyrinatozinc(II) (ZnDPPOH). It is claimed that the van der Waals forces and the hydrogen-bonds, as well as π-π interactions between the conjugated porphyrin cores, together, contribute to the stability of the monolayer. [266]

STM has also been extensively used in investigating the structures of porphyrin adlayers in electrochemical environments.[226-228, 249-263] At the electrode-solution interface, the molecular self-assembly process depends on the balance between inter

molecule, molecule-substrate and molecule-solvent interactions.[226-228, 239-263, 265, 266] Compared to the vacuum-solid or gas-solid interfaces tuning the working electrode potential provides a convenient way to adjust the molecule-substrate interaction and surface mobility of molecules at electrolyte-solid interface.[226] In addition, the electrochemical environment allows investigation of the unique electronic and chemical properties of porphyrins, such as interfacial electron transfer, coordination and electro-catalysis.[227, 255, 256, 258, 262] [167, 227, 255, 256, 258] Itaya's group reported a series of experiments on highly ordered porphyrin arrays including single, multiple-component and fullerene-porphyrin supramolecular assemblies.[226-228, 249-258] For example, they found that iodine or sulfur modified metal surfaces provide weakened adsorbate-substrate binding and therefore result in ordered porphyrin arrays instead of disordered structures as observed on bare metal surfaces.[226, 249-254] A group of interesting electrocatalytical enhancements of O_2 reduction at the single molecule level on porphyrin modified Au interface has also been discovered.[227, 255, 256, 258] Tao et al. showed that a similar adlayer structure were formed by iron(III) protoporphyrin(FePP), zinc(II) protoporphyrin(ZnPP), protoporphyrin IX(PP) in aqueous solutions.[259, 260] Recently, potential controlled manipulation of surface mobility and redox activity of a metal-free, water soluble tetra-pyridyl-porphyrin (TPyP) on Au(111) were demonstrated in acid solutions.[261-263]

1.4. Single Molecular Redox Reaction Study of Porphyrins

Among studies of porphyrin SAM using STM, only a small number of papers addressed the interfacial electron transfer of porphyrin molecules although it is an essential step for electronics, electrochemistry, and solar-energy conversion, etc.[228, 260, 262, 263] For example, Itaya et al. reported the observation of ZnTPP reduction at Au(111)/electrolyte interface.[228] The results shown by Tao et al. is one of earliest

experiments dealing with the redox behavior of porphyrins using EC-STM with molecular resolution.[260] In STM images, it is easy to obtain high spatial resolution in the lateral direction with absolute measurement of the distance if the STM scanner is well calibrated. However, the vertical height in STM is always a relative height. Without a reference, it is not easy to tell whether a molecule has changed its height between images. In addition, the vertical height in STM images is not only related to the topography of the molecules but also to the electronic states, since the tunneling current can be significantly altered by electronic properties of the molecules. To observe the chemical change of the molecule FePP as a function of the potential using EC-STM, Tao *et. al.* prepared a mixed monolayer of FePP and PP molecules, in which PP does not undergo chemical change in the potential range explored and was used a reference.[260] They found that the Fermi levels of the substrate and tip can be easily shifted relative to the energy levels of molecules by tuning the working electrode potential.[260] The FePP molecules showed the highest contrast when the electrode potential was tuned close to the redox potential of FePP.[260]

A single molecule redox reaction study has also been studied by imaging the redox reaction of TPyP using EC-STM.[262, 263] It was found that the reduction of adsorbed TPyP is orders of magnitude slower than that of solution-phase TPyP.[262, 263] This work was done by the former members in our research group, Dr. Tao Ye and Dr. Yufan He. It was found that when TPyP molecules are adsorbed on the surface, the redox activity is suppressed, especially the reduction process. Additionally, the oxidation of TPyP molecules in a SAM shows a strong neighbor effect.[262, 263] In their work electrochemical and EC-STM measurements were combined to explore the redox properties of the surface adsorbed TPyP molecules.

The EC-STM experiments presented by the Tao group and the Borguet group involve very different systems. Tao probed the behavior of a metal coordinated

porphyrin and found that the redox reaction is due to the iron ion at the center of porphyrin.[260] The Borguet group used a metal-free porphyrin, so that the redox reaction observed was entirely due to the change of porphyrin core.[262, 263] This reaction might be common in many metal free porphyrin systems.

1.5. Previous EC-STM Study of TPyP

The self-assembly and redox behavior of TPyP was studied in the Borguet group using EC-STM under potential control.[261-263] The experiments were initially designed to study the interaction between TPyP molecules and the electrode under various conditions. It was found that at higher electrode potential (0.5 V_{SCE}), TPyP molecules interact strongly with the electrode surface and can not move freely on the surface to form a self-assembled monolayer, as shown in **Figure 4- 4**A, in which the TPyP molecules distribute randomly on the surface. When the surface potential is switched to -0.3 V_{SCE}, TPyP disappeared in the STM images (lower part, **Figure 4- 4**B) indicating that the molecules might be desorbed. However, when switching potential back to 0.5 V_{SCE}, the molecules immediately reappeared in the STM image, (lower part, **Figure 4- 4**C), suggesting that the molecules did not leave the surface and the reason they did not appear in STM images at -0.3 V_{SCE} is because the molecule-substrate interaction is not strong enough to sustain the STM imaging process, since STM tip always disturbs the surface during scanning.

Under intermediate potentials (around 0.0 V_{SCE} to 0.3 V_{SCE}), ordered arrays of TPyP SAM were observed. Interestingly, during the experiments, Dr. Yufan He often observed dark spots in the TPyP SAM. Those dark spots were initially attributed to missing molecules in the SAM. However, high resolution images showed clear molecular structure in the missing spots with the height contrast lower than the rest of monolayer, suggesting that the dark spots are not molecular vacancies.(**Figure 4- 5**) In

addition, the appearance of dark spots is closely related to the potential of the substrate. The coexistence of dark and bright TPyP molecules was only observed at negative potentials when the molecule should be in its reduced form.

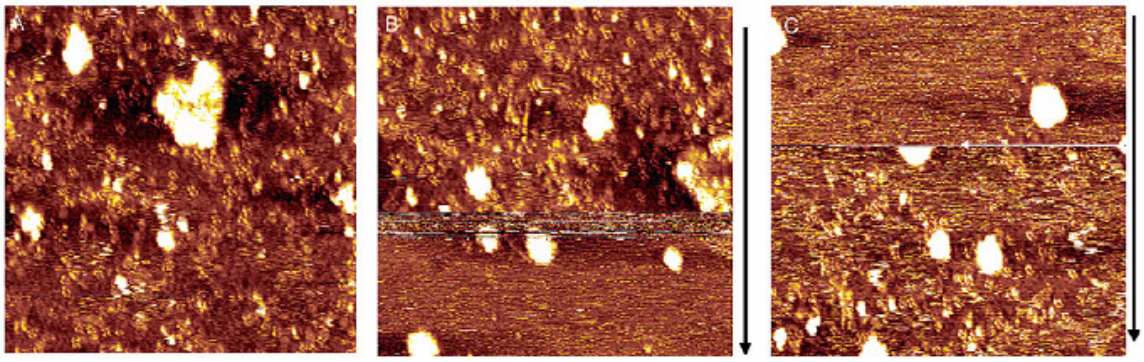

Figure 4- 4: In-situ STM images (50 x 50 nm^2) of TPyP (A) Electrode potential 0.5 V_{SCE}; (B) Electrode potential 0.5 V_{SCE} (upper part) and -0.3 V_{SCE} (lower part); (C) -0.3 V_{SCE} (upper part) and +0.5 V_{SCE}(lower part).[261]

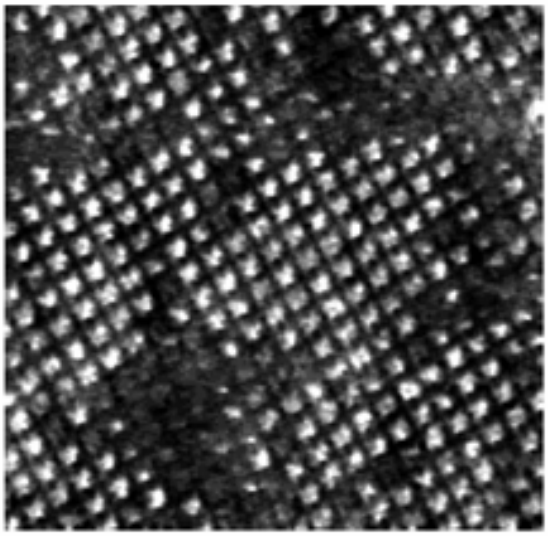

Figure 4- 5: Pre-adsorbed TPyP on Au(111) in 0.1 M H_2SO_4 at 0.1 V_{SCE} (27 x 27 nm^2) after partially oxidized.[263]

It was found that the number of dark spots can be controlled by the duration and amplitude of a short, positive potential pulse, i.e. an oxidation pulse.[263] This suggested that the dark spot was associated with the oxidized form of TPyP, while the bright spot are the reduced form. The observation of both oxidized and reduced TPyP at the same time at a negative potential is only possible if the reduction of TPyP is very slow, on a time scale longer than the STM imaging period, which is usually in the order of a few minutes in our study. The STM observation is confirmed by electrochemical experiments.[262] In these experiments, the potential of the TPyP modified electrode was initially changed to a positive potential (0.6 V_{SCE}) to oxidize all the TPyP molecules, followed by holding at -0.5 V_{SCE} for various time durations. After the potential step treatment, a cyclic voltammetry (CV) scan was performed to probe the redox state of the TPyP monolayer.(**Figure 4- 6**) It was found that the height of redox peaks in CV is very small when the holding time is about 0.5 minute, indicating that only a small percentage of TPyP molecules were reduced during this negative potential holding period. The peak height continuously increases with longer holding durations.

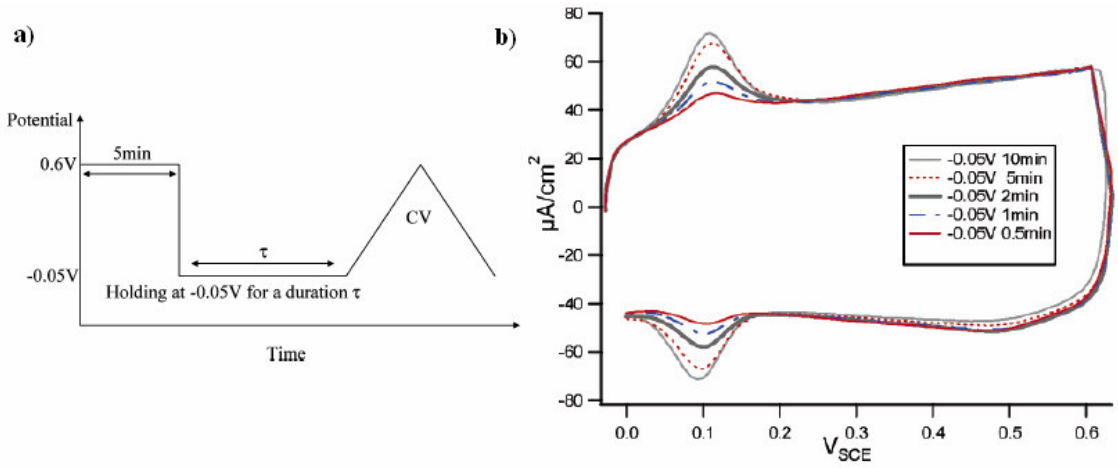

Figure 4- 6: Electrochemical experiments designed to probe the reduction time scale of a TPyP monolayer.[262]

It was proposed that the slow redox behavior of TPyP is due to a rate limiting protonation step in the redox reaction pathway.[262] Our understanding of the electrochemical dynamics and redox properties of adsorbed porphyrins is still limited, especially the precise details of the mechanism of porphyrin electrochemical reactions on surfaces.

2. Experimental Section

2.1. Electrode Preparation

A single-crystal gold bead was used as substrate. Before each experiment, the substrate was cleaned by immersion in hot piranha solution (1:3 H_2O_2 (J. T. Baker, CMOS) and H_2SO_4 (J. T. Baker, CMOS)) for 1 hr. (**Caution! The piranha solution is a very strong oxidizing agent and extremely dangerous**), followed by rinsing by sonication in ultrapure water (> 18 MΩ.cm, Barnstead, Nanopure Infinity system). Finally, annealing in a hydrogen flame and cooling down in a funnel protected atmosphere produced a bead where well-defined Au(111) facets with wide (> 100 nm) terraces could be easily found.

2.2. Sample Preparation

5,10,15,20-Tetra(4-pyridyl)-21H,23H-porphine (TPyP) and 5, 10, 15, 20-tetrakis (4-carboxylphenyl)-21H, 23H-porphyrin (TCPP) were purchased from Frontier Scientific and used without further purification. The chemical structures of the two molecules are shown in **Figure 4- 7**.

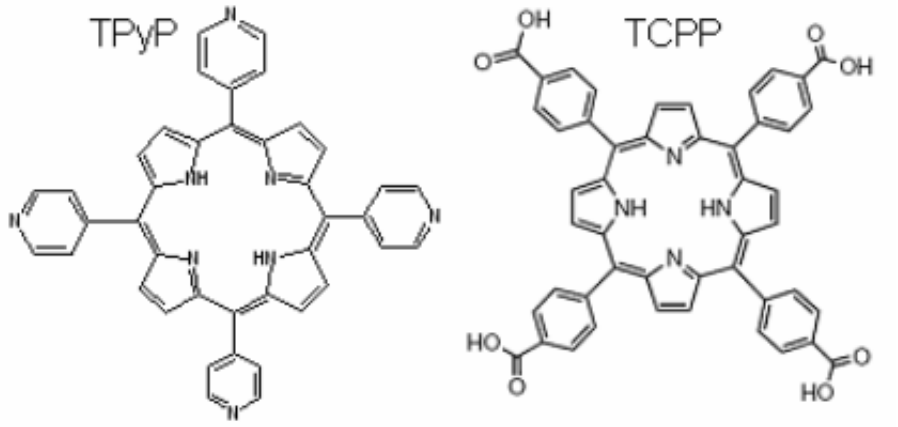

Figure 4- 7: Chemical structure of TPyP and TCPP molecules

The water soluble TPyP was used by dissolving in 0.1 M H_2SO_4 (Fisher Scientific Co., trace metal grade). A TPyP modified electrode was made in situ by adding ~ 10^{-5} M TPyP solution in to the electrochemical cell. Details of SAM formation will be discussed in the results section.

Ethanol was used to dissolve TCPP because of its poor solubility in aqueous solution. Self-assembled layers were prepared by immersing the gold bead in a TCPP/ethanol(Alfa Aesar, Spectrophotometric Grade) solution (10^{-5} M) for 2~3 min, rinsing thoroughly with ultrapure water, then promptly mounting it in a Teflon electrochemical cell containing $HClO_4$ (Fisher Scientific Co., trace metal grade) water solution under potential control (~0.1 V_{SCE}).

2.3. EC-STM Measurements

STM images were obtained using a PicoScan STM system with a bipotentiostat (Agilent, formally Molecular Imaging). Two platinum wires were used as counter and quasi-reference electrodes. All components (cell, O-ring and ceramic tweezers) involved in the STM experiments were chemically cleaned in the same manner as the single-crystal gold bead. The STM tips were electrochemically etched (3M KOH, 3~5V) from

tungsten wire (diameter 0.25mm) and insulated with paraffin wax. The faradaic current of the insulated tips under our imaging conditions was typically less than 10 pA at any bias used in our experiments. All the STM images were obtained under constant current mode with a high-resolution scanner, and without further processing (e.g., high-pass filtering) except necessary flattening. The setpoint in constant current mode for TPyP multilayer adsorption study was usually less than 0.1 nA. The setpoint for monolayer study of TPyP and TCPP was usually 0.1 -0.7 nA to obtain high resolution images.

3. Results and discussion

3.1. TPyP Self-assembly

A typical high resolution image of TPyP is shown in **Figure 4- 8**, in which each group of four bright spots corresponds to a single TPyP molecule. These bright spots are due to the titled pyridine rings in TPyP.[261] Similar images were reported by Hipps et al. for NiTPP in an UHV STM study.[267]

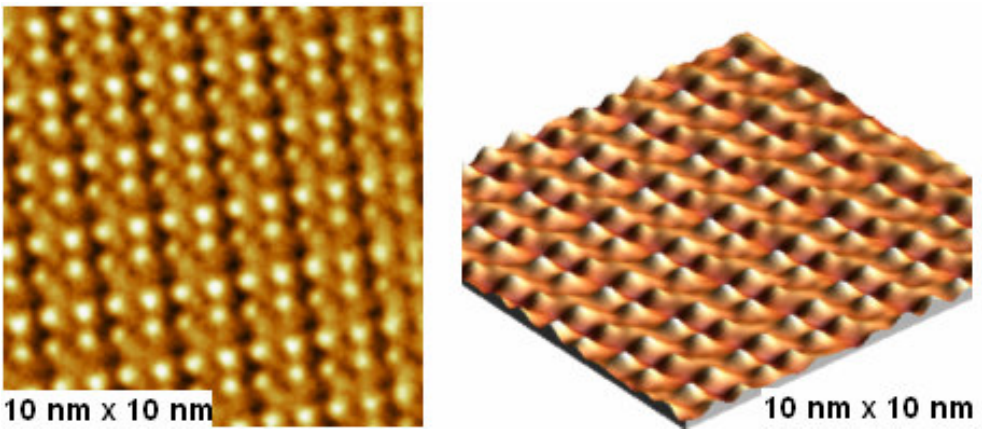

Figure 4- 8: Sub-molecular resolution STM image of TPyP monolayer acquired at 0.0 V_{SCE} in 0.1 M H_2SO_4.

We tuned the interaction between TPyP molecules and surface by varying the applied potential at the solid-liquid interface, which can alter the properties of TPyP as well. Earlier results from our group showed that TPyP forms multilayers at negative potential when reduced, while the oxidized form of TPyP forms only a monolayer on the surface.[262] However, no structures thicker than a bilayer structure were reported in the earlier studies and only small domains of TPyP were seen in the second layer, probably due to imaging conditions.[262] Here, we performed EC-STM measurements on the TPyP self-assembly to study the multilayer growth mechanism of TPyP. The experiments were done in 10^{-5} M TPyP solution under potential control. We found that TPyP, in its reduced state, can form more than two layers on the Au(111) surface. As shown in **Figure 4- 9**a, at least four layers of TPyP are present in the image. This multilayer growth could lead to a 3D crystal if enough TPyP molecules were provided by solution. When a limited amount of TPyP was supplied in the solution, we occasionally saw a two layer structure as shown in **Figure 4- 9**b. We think this image indicates a two layer adsorption structure because that the Au(111) reconstruction lines in the images (**Figure 4- 9**b) can only be seen if the bottom layer is the first layer adsorbed on the surface. In fact this partial two layer structure is rarely seen in our experiments. It only appears when the amount of TPyP added to the solution is well controlled, just slightly exceeding the amount required for monolayer formation. By increasing the substrate potential to > $0.2V_{SCE}$, TPyP is oxidized. The multilayer desorbs, leaving a perfect TPyP monolayer on the surface (**Figure 4- 9**c).

An interesting feature we observed in the STM images is that the monolayer of TPyP, or the first layer of TPyP multilayer, very rarely has missing molecules. But the top layers are usually imperfect, with a lot of vacancy holes present. This may be due to the different mechanism of adlayer formation. The first layer is formed because of the strong interaction between TPyP molecules and the substrate. The interaction between

the top layers is likely to be the π stacking between porphyrin cores, which might not be strong enough to hold all molecules in the adlayers. However, this π stacking, in principle, does not depend on which layer the TPyP molecule is in. Therefore, it can help TPyP adlayer grow continuously to form a many-layer structure.

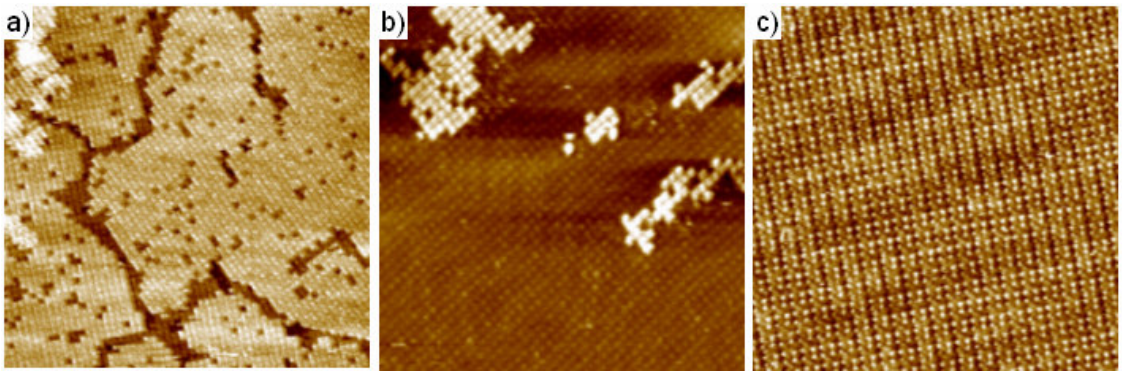

Figure 4- 9: STM images of TPyP adlayer on Au(111) in 0.1 M H_2SO_4 under potential control. a) Multilayer, 91 nm x 91 nm, 0.0 V_{SCE}; b) Two layers, 66 nm x 66 nm 0.0 V_{SCE}; c) Mono-layer, 30 nm x 30 nm, 0.2 V_{SCE}.[268]

The time scale for adlayer growth is in the order of several minutes. Usually multilayers of TPyP start to appear in STM images 15 minutes after the molecules are added to the solution. **Figure 4- 10**a shows an STM image acquired right after the injection of TPyP molecules into the electrochemical cell at 0.0 V_{SCE}. Clear Au(111) reconstruction lines are seen, indicating that the imaging condition is perfect and there is no adlayer adsorbed on the surface. However, the image appears to be quite noisy, with a lot of horizontal lines present in the image. These lines usually indicate molecular species dragged by the STM tip at the surface. In **Figure 4- 10**a, it is likely the isolated TPyP molecules which started to adsorbed onto the gold surface that were removed by the STM tip, since the interaction between a single TPyP molecule and the surface may not be strong enough to sustain a stable structure during STM imaging, even if the

smallest current setpoint is used. Fifteen minutes after the injection, a multilayer image of TPyP was observed (**Figure 4- 10**b). In the image, there are at least two well organized layers of TPyP, with an additional layer starting to grow on the top.

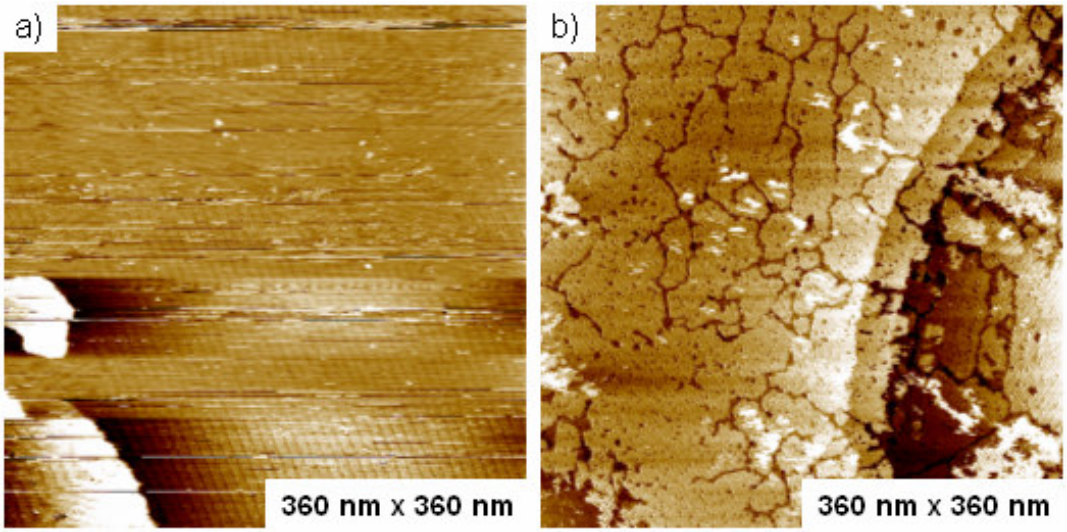

Figure 4- 10: STM images showing the growth of TPyP adlayers. a) Image acquired right after the injection of TPyP molecules into the electrochemical cell. b) 15 minutes after the injection, multilayer of TPyP formed. Both images are taken in 0.1 M H_2SO_4 at 0.0 V_{SCE} with TPyP concentration ~ 10^{-6} M.[268]

The TPyP self-assembly was also studied using a quartz crystal microbalance (QCM), as show in **Figure 4- 11**. While STM results provide more direct, structural view of the adlayer growth, the QCM results yield more quantitative information. After an initial dip in frequency due to the disturbance of solution by the injection process, the frequency continuously decreases due to the adsorption of TPyP.

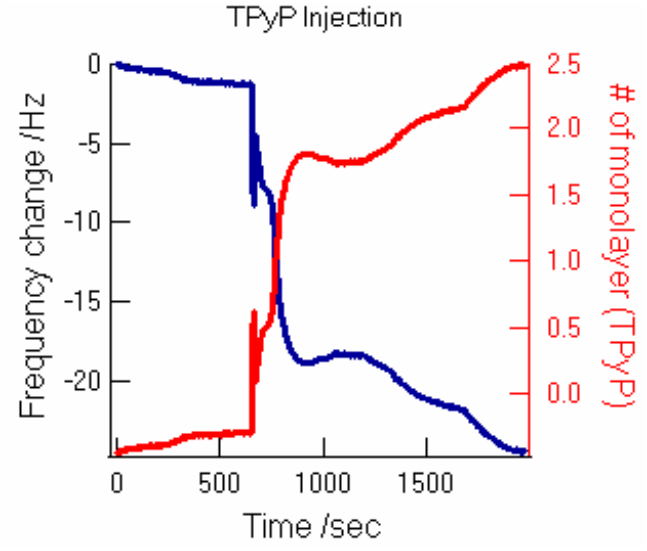

Figure 4- 11: TPyP adlayer formation studied by QCM in 0.1 M H_2SO_4 at 0.0 V_{SCE}. The Blue trace is the frequency change for TPyP adsorption. The sharp drop at around 650 sec is due to the injection of TPyP solution (final concentration after injection is ~ 10^{-6} M). The red trace is the calculated monolayer change based on the frequency plot.[268]

According to calculated TPyP growth dynamics (red curve in **Figure 4- 11**), the process of multilayer formation can be divided into two separate periods. In the initial 200 seconds, the adlayer grows rapidly, leading to an adsorption of about 1.8 layers. It is slightly less than two layers probably because the second layer is less dense than the first layer as seen in STM images. In addition, the plateau at 1.8 layers is probably due to a self-organization process in the second layer. After that, the adlayer continues to grow but with a much slower rate. The slower growth indicates a weaker interaction between the top layers. If the interaction is not strong enough to overwhelm the thermal motion of TPyP molecules, the thermal desorption of TPyP may compete with the multilayer growth process. This competition is seen in STM images, as show in **Figure 4- 12**. In the two successive STM images, the top layer of TPyP shows a dynamic behavior: some molecules have filled into the vacancy holes between the first image and the second

(indicated by red circles), while some molecules leave the surface (indicated by green circles).

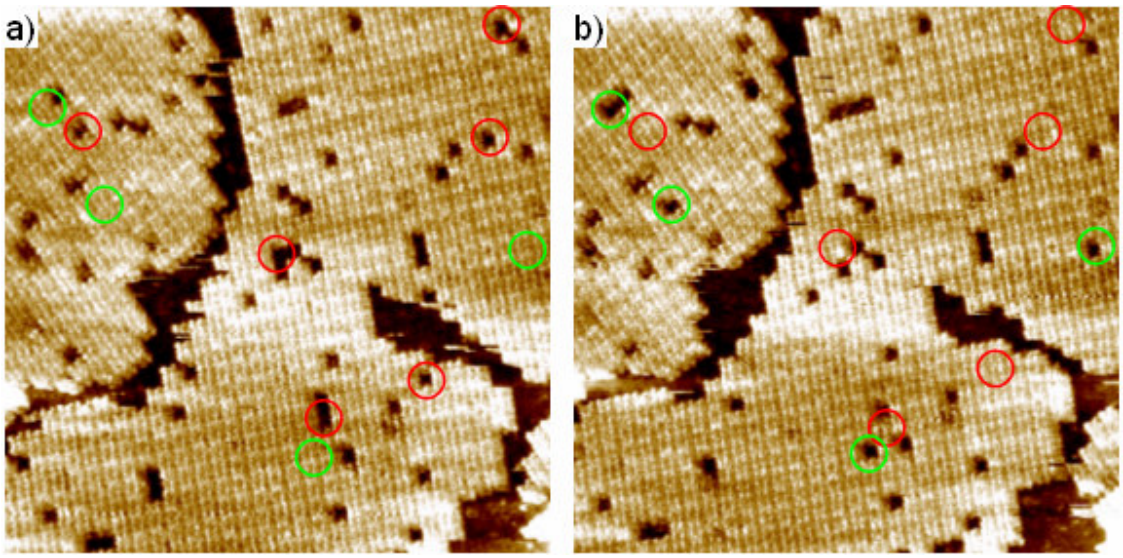

Figure 4- 12: Two STM successive image of TPyP multilayer in 0.1 M H_2SO_4 at 0.0 V_{SCE} (50 nm x 50 nm) separated by ~ 200 sec. Red circles show vacancy holes in the first image (a) being filled in the second image (b), while green circles show molecules leaving the surface.[268]

It should be pointed out that in the STM study of self-assembled monolayers, one should be very careful to choose imaging conditions to minimize the effect of the tip on the surface processes. The setpoint is one of the most important parameters and defines the current value when the STM is operated in the constant current mode. The higher the setpoint, the closer the tip is to the surface. Higher setpoint often gives clearer STM images, but the disturbance of the surface processes by the tip is also stronger. In our studies, we chose the lowest setpoint, which is just enough to maintain a good imaging condition while minimizing the tip effect. Usually, our setpoint is lower than 0.1 nA. Higher setpoints will lead to desorption of the adlayers. As shown in **Figure 4- 13**, the

center part of the image was scanned in previous images using a setpoint at 0.3 nA. Most of the molecules in the adlayer were removed by the STM tip.

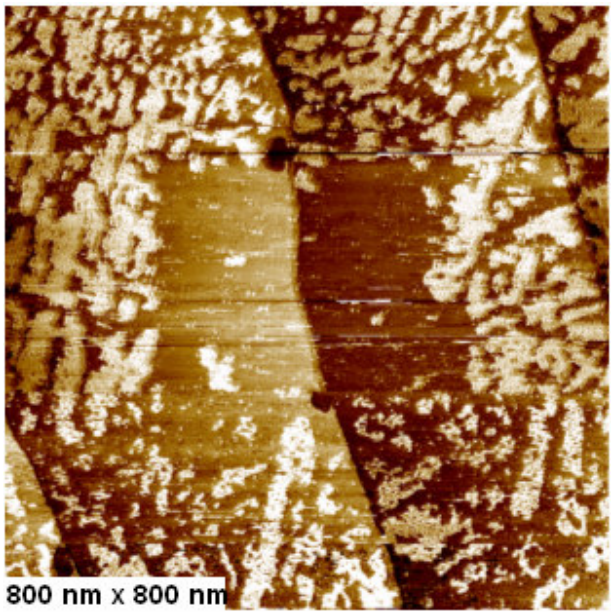

Figure 4- 13: STM images of TPyP adlayer on Au(111) in 0.1 M H_2SO_4 at 0.0 V_{SCE} (setpoint 0.1 nA). The center part of the image was previously scanned at 0.3 nA for several images.

3.2. TPyP Slow Reduction

The oxidized and reduced forms of TPyP molecules can be clearly distinguished by in-situ EC-STM. While TPyP oxidizes rapidly, on the order of seconds at 0.2 V_{SCE},[263] the reduction is much slower, on the order of tens of minutes.[262] The oxidation dynamics has been studied in our group using EC-STM.[263] However, the reduction dynamics has not been imaged by EC-STM. To study the reduction process, one needs to maintain good imaging conditions maintained for tens of minutes, up to hours. This is not easy in an electrochemical environment.

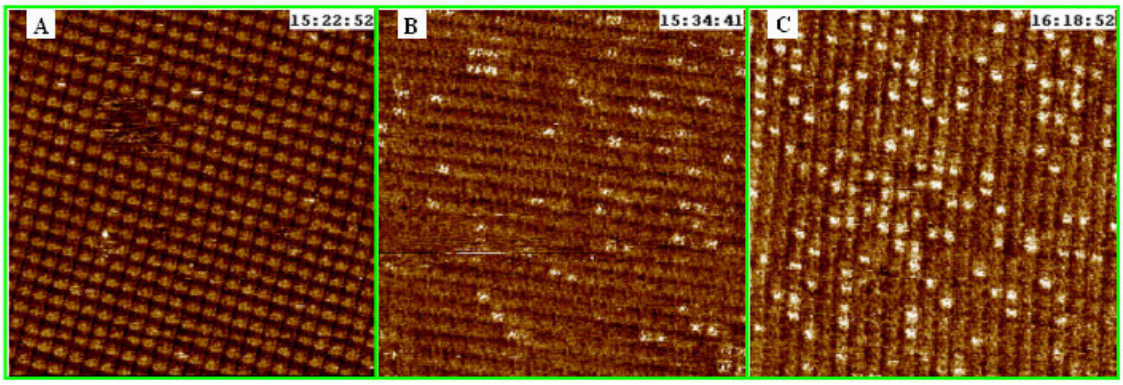

Figure 4- 14: The slow reduction of TPyP on an Au(111) surface in 0.1 M H_2SO_4 solution (30 x 30 nm^2). A: Oxidized TPyP monolayer at 0.2 V_{SCE}, B: 12 minutes of reduction at 0.0 V_{SCE}. C: 56 minutes of reduction at 0.0 V_{SCE}.[268]

The reduction of TPyP with single molecule sensitivity on Au(111) surface is shown in **Figure 4- 14**. After ten minutes at 0.0 V_{SCE}, 13% of the molecules were reduced (bright spots in **Figure 4- 14**B). About one hour later, 27% of the molecules were reduced (**Figure 4- 14**C). This reduction process is extremely slow. The images shown in **Figure 4- 15** were collected about 2 hours after the reduction process started and show that the monolayer is still not fully reduced. Only about 90% of the TPyP molecules have changed from dark to bright. Unlike the reported oxidation dynamics,[263] which showed a clear neighbor effect, the reduction of TPyP molecules in the monolayer showed no clear dependence on the redox states of molecules nearby.

When the TPyP monolayer is partially reduced, oxidized and reduced TPyP molecules coexist on the surface. Charge can diffuse in the monolayer, as shown in **Figure 4- 15**. From image A to image B, some molecules changed from bright to dark (at the same position, red square in A and green square in B), while some changed from dark to bright (green in A and red in B). The equal number of green and red squares indicates a local conservation of charge. This provides evidence for charge diffusion on the surface. The exact nature of the mechanism is under investigation. [268] This

phenomenon is not likely to be a consequence of molecular diffusion because in a close-packed SAM shown in **Figure 4- 15**, there is no room for the molecules to move and exchange position. In addition, there are no extra TPyP molecules in the solution so it is also not possible for the TPyP SAM to exchange molecules with the solution.

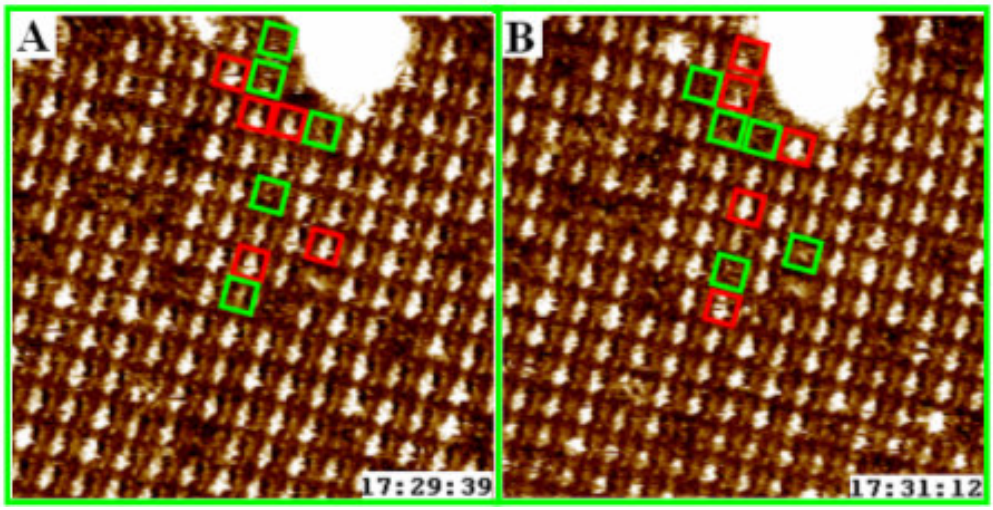

Figure 4- 15: TPyP monolayer in neat 0.1 M H_2SO_4, sample potential 0.0 V_{SCE}, 20 x 20 nm^2, 2 hours after reduction started.[268]

3.3. pH Dependent Reduction of Porphyrins

It has been suggested that the slow reduction of TPyP is due to a rate limiting, protonation step at the porphyrin core[262, 263], which, in principle, should depend on the pH value of the solution. However, the pH dependence with single molecule resolution afforded by ECSTM has not been investigated previously. Here, we report the results of experiments designed to systematically study the reduction dynamics of porphyrins to understand how the concentration of H^+ affects the reduction behavior of TCPP at an Au(111)/electrolyte interfaces. In addition we wished to show that the ability to distinguish oxidized and reduced porphyrins by EC-STM is not limited to TPyP. We choose TCPP instead of TPyP, because we hypothesized that the porphyrin redox

reaction previously observed take place at the porphyrin core, which should be observed in other porphyrins that have the same molecular core. We found that (1) TCPP molecules form three types of arrays, reflecting various ways for inter-molecular hydrogen bonds to stabilize molecular networks. (2) Absorbed TCPP molecules undergo a slow reduction process similar to the reported TPyP redox reaction. (3) Lower $[H^+]$ accelerates the reduction rate of TCPP, in other words, the slow reduction begins at a more positive potential than in the case of higher $[H^+]$.

Previous reports suggested that the first 2 electron transfer happens after a protonation-deprotonation process between $P(0)H_4^{2+}$ and $P(0)H_2$.[269, 270] It is reasonable to expect that the $[H^+]$ should affect the porphyrin reduction channel as involves a protonation-deprotonation step.[269, 270] However, the influence of $[H^+]$ on the slow reduction process after porphyrin adsorption is not well understood. The high resolution EC STM studies of TCPP arrays in 0.01 M, 0.1 M and 1M $HClO_4$ solution described here provide more information on the mechanism of this reduction.

After successfully imaging the structures of adsorbate layers, the potential of the working electrode was stepped to negative to check if any similar reduction reaction happens since TCPP bears a similar molecular structure with TPyP. During the scanning, all the TCPP molecules maintained the same tunneling contrast until a certain critical potential that was negative enough to reduce the oxidized species, was reached. As expected, the reduction potential varies depending on the H^+ concentration of the supporting electrolytes. **Figure 4- 16**A shows the TCPP arrays in 0.01 M $HClO_4$ right after the potential was stepped to 0.1 V_{SCE}. No bright spots are seen in the image. After a few minutes, it can be seen that some of adsorbed TCPP molecules (marked by white circles) turned to brighter contrast, i.e. being reduced (**Figure 4- 16**B, lower part), consistent with our previous observation for the related molecule TPyP. After the substrate potential was suddenly changed to 0.0 V_{SCE} at around half-scan position

(marked by white line in **Figure 4- 16**B, arrow indicates the scanning direction), the slow reduction process immediately speeded up and brighter dots appeared more quickly. At least 50% of the molecules immediately turned brighter in the rest upper part image, implying the formation of reduced TCPP.

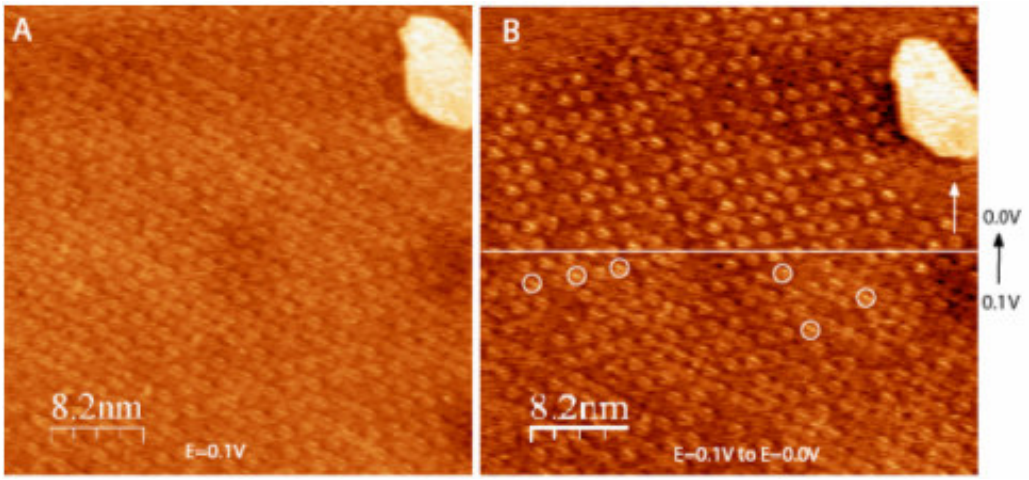

Figure 4- 16: (A) TCPP arrays in 0.01 M $HClO_4$ at potential of E = 0.1 V_{SCE} without any reduced form molecules. (B) Lower part, TCPP arrays in 0.01 M $HClO_4$ at potential of 0.1 V_{SCE} with only several reduced TCPP (bright spots) marked by white circles. Upper part, TCPP arrays immediately became brighter after potential change from 0.1 V_{SCE} to 0.0 V_{SCE} in the middle of image.[271]

Experiments have also been carried out in 0.1 M and 1 M $HClO_4$ solution in the same manner in order to investigate the $[H^+]$ influence on the reduction of TCPP arrays. In a 0.1 M $HClO_4$ solution, similar slow surface reduction (at around -0.05 V_{SCE}) and an acceleration of reduction rate (at around -0.15 V_{SCE}) were also observed. However, a more negative initial reduction potential is needed to start the reduction process. Here, the initial reduction potential is the starting potential at which slow reduction, determined by the appearance of first several bright spots during slow scanning (~7 lines/sec with a 512×512 image resolution), is observed. The initial reduction potential was ~0.15 V_{SCE},

more negative in 0.01 M $HClO_4$ than the value in 0.01 M $HClO_4$. In other words, the reduction happens faster in 0.01 M $HClO_4$ than in 0.1 M $HClO_4$ at the same reduction potential, for example 0.1 V_{SCE}. The same slow reduction process was observed in 1 M $HClO_4$ solution, too, with the initial reduction potential changeed to an even more negative value, around -0.15 V_{SCE} (**Figure 4- 17**).

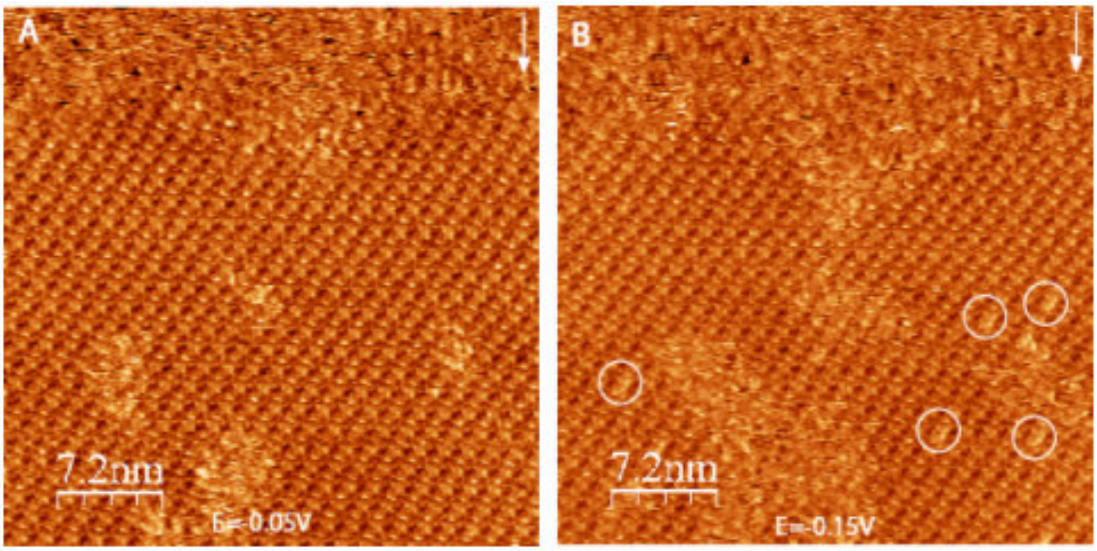

Figure 4- 17: (A) TCPP arrays in 1 M $HClO_4$ at potential of E = -0.05 V_{SCE} without bright spots. (B) Sequence STM images after (A) with several bright spots (marked by white circles) at potential of -0.15 V_{SCE}.[271]

According to the mechanism proposed by Wilson et al.[269], there are two steps including three porphyrin forms in this 2 electron transfer process. (1) A protonation and deprotonation reaction (PT) between two oxidized form $P(0)H_2$ and $P(0)H_4^{2+}$ and (2) An electron-transfer (ET) process between the oxidized forms ($P(0)H_4^{2+}$, $P(0)H_2$) and a reduced form ($P(-II)H_4$). The ET step can happen via two possible channels, either between $P(0)H_4^{2+}$ and $P(-II)H_4$ or between $P(0)H_2$ and $P(-II)H_4$, depending on the environmental H^+ concentration. Our results indicate that the reduction of TCPP

adsorbed on Au surface is inhibited by higher [H^+], which should promote the protonation process. Therefore, the protonated form of TCPP, $P(0)H_4^{2+}$, does not appear to be the reactive species that undergoes the charge transfer reaction to form reduced form of TCPP.

Based on the above discussion, it is reasonable to believe that $P(0)H_2$ is the active oxidized form of porphyrin in the slow reduction process, i.e. TCPP takes the reduction channel from $P(0)H_2$ to $P(-II)H_4$ (Eq. 4-1).

$$P(0)H_2 + 2e^- + 2H^+ \longleftrightarrow P(-II)H_4 \qquad \text{Eq. 4-1}$$

We propose a model to describe the mechanism of the slow reduction of porphyrin molecules adsorbed on the electrode surface.(**Figure 4- 18**) In this model, the H^+ concentration does not influence the charge transfer reaction directly. Instead, it suppresses the reduction process by protonating the original form of porphyrins ($P(0)H_2$) and turning it into $P(0)H_4^{2+}$, which has very limited electrochemical activity on the electrode surface. Although we propose that $P(0)H_4^{2+}$ does not react directly, it may be electrochemically reduced under other conditions that we did not explore. Alternatively, it may be reactive under the conditions in our experiments, but with a reaction rate much slower than the reduction of $P(0)H_2$. Our model is supported by the cyclic voltammetry (CV) results previously reported,[262] in which the authors started with an oxidized porphyrin monolayer and then held the electrode at a negative potential for various time durations, on the order of minutes, to reduce adsorbed porphyrins (**Figure 4- 6**). Successive CV curves (**Figure 4- 6**) show that the longer the holding time, the higher the redox peaks, clearly indicating a very slow reduction process. However, the CV curves themselves do not reflect the slow reduction because the reduction and oxidation peaks in each of the CV curve (**Figure 4- 6**) have the same amplitude, revealing a reversible reaction scheme. Our proposed model can explain this apparent contradiction easily. The observed slow reduction is an effect of $P(0)H_4^{2+}$ deprotonation, because the longer

the holding time at negative potential, the more $P(0)H_4^{2+}$ is deprotonated to $P(0)H_2$, recovering the electrochemical activity of the reduced TPyP. The reversible redox reaction observed in the CV curves is the fast reaction between $P(0)H_2$ and $P(-II)H_4$, which is reversible. It is also understandable that the reduction rate slows down at the longest holding times (asymptote of Figure 2 in [262]) because the number of $P(0)H_4^{2+}$ that can be deprotonated decreases as the protonated monolayer is depleted of protonated, electrochemically inactive species.

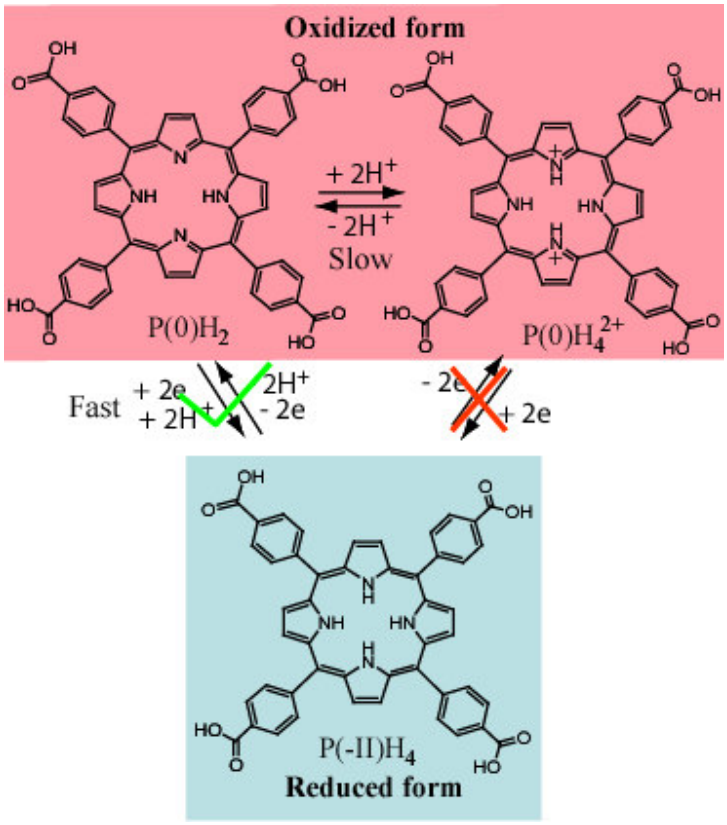

Figure 4- 18: Proposed mechanism of TCPP reduction on Au(111) in an acidic medium.[271]

Concerning the question which species corresponds to the bright or dark spot we observed in EC-STM, it is clear that after reduction, the TCPP molecules turns bright,

indicating that P(-II)H_4 are the bright spots in the STM images. Given the acidic condition during the experiments, most oxidized TCPP molecules are protonated. Therefore the dominant features we observe at the beginning of reduction, i.e. dark spots, are the protonated form of oxidized TCPP, P(0)H_4^{2+}. However, it is not obvious whether the original form of oxidized TCPP should be bright or dark spots. It is possible that P(0)H_2 turns bright right after deprotonated from P(0)H_4^{2+} before the reduction takes place. In this case, the bright spots represent P(0)H_2 and P(-II)H_4 in STM images, while P(0)H_4^{2+} is dark. In previous studies, it was reported that the oxidation of P(-II)H_4 is relatively fast compared to the reduction process.[263] It was shown that bright P(-II)H_4 changes to darker spots immediately after a short potential pulse, indicating that P(0)H_2 corresponds to dark spots in STM images. Combining both our results and previous reports, we conclude that both forms of the oxidized species (P(0)H_2 and P(0)H_4^{2+}) are the dark spots in STM images and the reduced form P(-II)H_4 is dark. Therefore our EC-STM observation of the contrast between bright and dark molecules in a TCPP monolayer is due to the different redox states of the molecules, i.e. the contrast is not introduced by the protonation/deprotonation step.

4. Conclusion and Future work

4.1. Conclusion

Redox processes driven by electric potentials in liquid environment are of great interest for chemists, biologists, surface engineers and many other specialists working in cutting edge areas. Scanning Probe Microscopy is an extremely useful tool for monitoring and controlled manipulations of nanometer-scaled objects, e.g. those affected by electrochemical transformations. SAMs of porphyrins are of great interest due to their diverse applications, including molecular devices, nano-templates, electrocatalysis, solar cells, and photosynthesis. However, most studies of the surface reactions of porphyrins

are based on optical spectroscopy and electrochemical measurements which probe the average properties of an ensemble of molecules. We combined a molecular level study of the self-assembly and redox reactions using EC-STM with a macroscopic electrochemical technique, cyclic voltammetry (CV), to study a redox active porphyrin molecule, TPyP (5,10,15,20-Tetra(4-Pyridyl)-21H,23H-Porphine) and other porphyrins.

We tuned the interaction between TPyP molecules and surface by varying the applied potential at the solid-liquid interface, which can alter the properties of TPyP as well. TPyP in its reduced state can form multilayers on Au(111) surface, possibly growing into a 3D crystal if enough TPyP molecules are present in solution. By increasing the substrate potential to >0.2 V_{SCE}, TPyP is oxidized. The multilayer desorbs, leaving a perfect TPyP monolayer on the surface.

The oxidized and reduced forms of TPyP molecules can be clearly distinguished by in-situ EC-STM. While TPyP oxidizes rapidly, on the order of seconds at 0.2V_{SCE}, the reduction is much slower, on the order of tens of minutes. Using EC-STM one can study a simple electron transfer reaction, the reduction of TPyP with single molecule sensitivity on an electrode surface. When the TPyP monolayer is partially reduced, oxidized and reduced TPyP molecules coexist on the surface. Charge can diffuse in the monolayer.

We propose that protonation and deprotonation processes at the center of porphyrin core play an important role in the surface redox reaction. Due to geometry restrictions of the molecules adsorbed on the surface, these processes are slowed down. To confirm, working together with Dr. Qunhui Yuan, we performed EC-STM studies on a similar porphyrin molecule, 5, 10, 15, 20-tetrakis (4-carboxylphenyl)-21H, 23H-porphine (TCPP), which has the same porphyrin core as TPyP with different substitution groups. We found that, similar to TPyP, the TCPP reduction reaction is very slow at 0.1 V_{SCE}. The reduction rate is increased after stepping the potential to a more negative

value, 0.0 V_{SCE}, demonstrating a potential dependence of the reduction rate. By changing pH to lower values, 1 M HClO4, we found that only a small number of molecules is reduced at a more negative potential, -0.15 V_{SCE}. The pH dependent results proof that protonation/deprotonation processes are correlated with charge transfer processes during the redox reaction of porphyrins.

4.2. Future Work

The observed slow reaction of TCPP is very similar to the reported TPyP redox reaction.[262, 263] Taking into account that TCPP and TPyP share the same porphyrin core and that the overall geometry structure is very similar, it is reasonable to believe that the slow reduction takes place at the center of porphyrin core, which supports the proposed model. We expect that this redox reaction mechanism can be generalized to other porphyrin molecules. Further investigation on a range of porphyrin molecules is needed to consolidate our knowledge of the redox reaction mechanism. It should be mentioned that the substitution groups in porphyrins may affect the redox reaction at the core. For example, TCPP is more acidic than TPyP, because the pyridyl groups can easily undergo protonation and add positive charges the to overall molecule structure.

REFERENCES

1. Balzani, V., *Electron Transfer in Chemistry*. 2001, Wiley-VCH: New York.
2. McLendon, G. and Hake, R., *INTERPROTEIN ELECTRON-TRANSFER.* Chemical Reviews, 1992. **92**(3): p. 481-490.
3. Nocek, J.M., Zhou, J.S., DeForest, S., Priyadarshy, S., Beratan, D.N., Onuchic, J.N., and Hoffman, B.M., *Theory and practice of electron transfer within protein-protein complexes: Application to the multidomain binding of cytochrome c by cytochrome c peroxidase.* Chemical Reviews, 1996. **96**(7): p. 2459-2489.
4. Davidson, V.L., *What controls the rates of interprotein electron-transfer reactions.* Accounts of Chemical Research, 2000. **33**(2): p. 87-93.
5. Ramirez, B.E., Malmstrom, B.G., Winkler, J.R., and Gray, H.B., *The currents of life: The terminal electron-transfer complex of respiration.* Proceedings of the National Academy of Sciences of the United States of America, 1995. **92**(26): p. 11949-11951.
6. Mitchell, P., *COUPLING OF PHOSPHORYLATION TO ELECTRON AND HYDROGEN TRANSFER BY A CHEMI-OSMOTIC TYPE OF MECHANISM.* Nature, 1961. **191**(478): p. 144-&.
7. Gust, D., Moore, T.A., and Moore, A.L., *Mimicking photosynthetic solar energy transduction.* Accounts of Chemical Research, 2001. **34**(1): p. 40-48.
8. Niyogi, K.K., *Photoprotection revisited: Genetic and molecular approaches.* Annual Review of Plant Physiology and Plant Molecular Biology, 1999. **50**: p. 333-359.
9. Britton, G., *Structure and properties of carotenoids in relation to function.* Faseb Journal, 1995. **9**(15): p. 1551-1558.
10. Adams, D.M., Brus, L., Chidsey, C.E.D., Creager, S., Creutz, C., Kagan, C.R., Kamat, P.V., Lieberman, M., Lindsay, S., Marcus, R.A., Metzger, R.M., Michel-Beyerle, M.E., Miller, J.R., Newton, M.D., Rolison, D.R., Sankey, O., Schanze, K.S., Yardley, J., and Zhu, X.Y., *Charge transfer on the nanoscale: Current status.* Journal of Physical Chemistry B, 2003. **107**(28): p. 6668-6697.
11. Lindsay, S.M. and Ratner, M.A., *Molecular transport junctions: Clearing mists.* Advanced Materials, 2007. **19**(1): p. 23-31.
12. Tao, N.J., *Electron transport in molecular junctions.* Nature Nanotechnology, 2006. **1**(3): p. 173-181.
13. Mirkin, C.A. and Ratner, M.A., *MOLECULAR ELECTRONICS.* Annual Review of Physical Chemistry, 1992. **43**: p. 719-754.
14. Kushmerick, J.G., Holt, D.B., Yang, J.C., Naciri, J., Moore, M.H., and Shashidhar, R., *Metal-molecule contacts and charge transport across monomolecular layers: Measurement and theory.* Physical Review Letters, 2002. **89**(8).
15. Reichert, J., Ochs, R., Beckmann, D., Weber, H.B., Mayor, M., and von Lohneysen, H., *Driving current through single organic molecules.* Physical Review Letters, 2002. **88**(17): p. 4.

16. Zhu, X.Y., *Electron transfer at molecule-metal interfaces: A two-photon photoemission study.* Annual Review of Physical Chemistry, 2002. **53**: p. 221-247.
17. Chen, F., Hihath, J., Huang, Z.F., Li, X.L., and Tao, N.J., *Measurement of single-molecule conductance.* Annual Review Of Physical Chemistry, 2007. **58**: p. 535-564.
18. Feynman, R.P., *"There's plenty of room at the bottom", a talk given to the annual meeting of the American Physical Society at Caltech, December 29, 1959.*
19. Adee, S., *37 years of Moore's law.* Ieee Spectrum, 2008. **45**(5): p. 56-56.
20. Thompson, S.E. and Parthasarathy, S., *Moore's law: the future of Si microelectronics.* Materials Today, 2006. **9**(6): p. 20-25.
21. Moore, G.E., *Cramming more components onto integrated circuits (Reprinted from Electronics, pg 114-117, April 19, 1965).* Proceedings of the Ieee, 1998. **86**(1): p. 82-85.
22. Heath, J.R. and Ratner, M.A., *Molecular electronics.* Physics Today, 2003. **56**(5): p. 43-49.
23. Wada, Y. *Prospects for single-molecule information-processing devices for the next paradigm*. 2002.
24. Melosh, N.A., Boukai, A., Diana, F., Gerardot, B., Badolato, A., Petroff, P.M., and Heath, J.R., *Ultrahigh-density nanowire lattices and circuits.* Science, 2003. **300**(5616): p. 112-115.
25. Frank, D.J., Dennard, R.H., Nowak, E., Solomon, P.M., Taur, Y., and Wong, H.S.P., *Device scaling limits of Si MOSFETs and their application dependencies.* Proceedings of the Ieee, 2001. **89**(3): p. 259-288.
26. Lu, W. and Lieber, C.M., *Nanoelectronics from the bottom up.* Nature Materials, 2007. **6**(11): p. 841-850.
27. Choi, H. and Mody, C.C.M., *The Long History of Molecular Electronics: Microelectronics Origins of Nanotechnology.* Social Studies of Science, 2009. **39**(1): p. 11-50.
28. Aviram, A. and Ratner, M.A., *MOLECULAR RECTIFIERS.* Chemical Physics Letters, 1974. **29**(2): p. 277-283.
29. Jortner, J. and Ratner, M., *Molecular Electronics*. 1997: Blackwell Science: Oxford, UK.
30. Tour, J.M., Wu, R., and Schumm, J.S., *EXTENDED ORTHOGONALLY FUSED CONDUCTING OLIGOMERS FOR MOLECULAR ELECTRONIC DEVICES.* Journal of the American Chemical Society, 1991. **113**(18): p. 7064-7066.
31. Waldeck, D.H. and Beratan, D.N., *MOLECULAR ELECTRONICS - OBSERVATION OF MOLECULAR RECTIFICATION.* Science, 1993. **261**(5121): p. 576-577.
32. Aviram, A., *MOLECULES FOR MEMORY, LOGIC, AND AMPLIFICATION.* Journal of the American Chemical Society, 1988. **110**(17): p. 5687-5692.
33. Ball, P. and Garwin, L., *SCIENCE AT THE ATOMIC SCALE.* Nature, 1992. **355**(6363): p. 761-766.
34. Davis, W.B., Svec, W.A., Ratner, M.A., and Wasielewski, M.R., *Molecular-wire behaviour in p-phenylenevinylene oligomers.* Nature, 1998. **396**(6706): p. 60-63.

35. Tian, W., Datta, S., Hong, S., Reifenberger, R., Henderson, J.I., and Kubiak, C.P., *Conductance spectra of molecular wires.* The Journal of Chemical Physics, 1998. **109**(7): p. 2874-2882.
36. Yaliraki, S.N. and Ratner, M.A., *Molecule-interface coupling effects on electronic transport in molecular wires.* Journal of Chemical Physics, 1998. **109**(12): p. 5036-5043.
37. Davis, W.B., Ratner, M.A., and Wasielewski, M.R., *Conformational gating of long distance electron transfer through wire-like bridges in donor-bridge-acceptor molecules.* Journal of the American Chemical Society, 2001. **123**(32): p. 7877-7886.
38. Tour, J.M., Rawlett, A.M., Kozaki, M., Yao, Y.X., Jagessar, R.C., Dirk, S.M., Price, D.W., Reed, M.A., Zhou, C.W., Chen, J., Wang, W.Y., and Campbell, I., *Synthesis and preliminary testing of molecular wires and devices.* Chemistry-a European Journal, 2001. **7**(23): p. 5118-5134.
39. Li, Z.Y. and Kosov, D.S., *Dithiocarbamate anchoring in molecular wire junctions: A first principles study.* Journal of Physical Chemistry B, 2006. **110**(20): p. 9893-9898.
40. Choi, S.H., Kim, B., and Frisbie, C.D., *Electrical resistance of long conjugated molecular wires.* Science, 2008. **320**(5882): p. 1482-1486.
41. Nitzan, A. and Ratner, M.A., *Electron transport in molecular wire junctions.* Science, 2003. **300**(5624): p. 1384-1389.
42. Visoly-Fisher, I., Daie, K., Terazono, Y., Herrero, C., Fungo, F., Otero, L., Durantini, E., Silber, J.J., Sereno, L., Gust, D., Moore, T.A., Moore, A.L., and Lindsay, S.M., *Conductance of a biomolecular wire.* Proceedings Of The National Academy Of Sciences Of The United States Of America, 2006. **103**(23): p. 8686-8690.
43. Bumm, L.A., Arnold, J.J., Cygan, M.T., Dunbar, T.D., Burgin, T.P., Jones, L., Allara, D.L., Tour, J.M., and Weiss, P.S., *Are single molecular wires conducting?* Science, 1996. **271**(5256): p. 1705-1707.
44. Parthenopoulos, D.A. and Rentzepis, P.M., *3-DIMENSIONAL OPTICAL STORAGE MEMORY.* Science, 1989. **245**(4920): p. 843-845.
45. Liu, Z.F., Hashimoto, K., and Fujishima, A., *PHOTOELECTROCHEMICAL INFORMATION-STORAGE USING AN AZOBENZENE DERIVATIVE.* Nature, 1990. **347**(6294): p. 658-660.
46. Hopfield, J.J., Onuchic, J.N., and Beratan, D.N., *A MOLECULAR SHIFT REGISTER BASED ON ELECTRON-TRANSFER.* Science, 1988. **241**(4867): p. 817-820.
47. Chen, J., Reed, M.A., Rawlett, A.M., and Tour, J.M., *Large on-off ratios and negative differential resistance in a molecular electronic device.* Science, 1999. **286**(5444): p. 1550-1552.
48. Xue, Y.Q., Datta, S., Hong, S., Reifenberger, R., Henderson, J.I., and Kubiak, C.P., *Negative differential resistance in the scanning-tunneling spectroscopy of organic molecules.* Physical Review B, 1999. **59**(12): p. R7852-R7855.
49. Xiao, X., Nagahara, L.A., Rawlett, A.M., and Tao, N., *Electrochemical gate-controlled conductance of single oligo(phenylene ethynylene)s.* Journal Of The American Chemical Society, 2005. **127**(25): p. 9235-9240.

50. Wassel, R.A., Credo, G.M., Fuierer, R.R., Feldheim, D.L., and Gorman, C.B., *Attenuating negative differential resistance in an electroactive self-assembled monolayer-based junction.* Journal of the American Chemical Society, 2004. **126**(1): p. 295-300.
51. Ashwell, G.J., *CHEMISTRY - PHOTOCHROMIC MEMORY DEVICES.* Nature, 1990. **347**(6294): p. 617-617.
52. Mitchell, R.H., Ward, T.R., Wang, Y.X., and Dibble, P.W., *Pi-switches: Synthesis of three-way molecular switches based on the dimethyldihydropyrene-metacyclophanediene valence isomerization.* Journal of the American Chemical Society, 1999. **121**(11): p. 2601-2602.
53. Silva, G.M.E. and Acioli, P.H., *Dynamics of charge transfer in molecular switches.* Synthetic Metals, 1997. **87**(3): p. 249-256.
54. Fabbrizzi, L. and Poggi, A., *SENSORS AND SWITCHES FROM SUPRAMOLECULAR CHEMISTRY.* Chemical Society Reviews, 1995. **24**(3): p. 197-202.
55. Kijima, H., Takeuchi, M., Robertson, A., Shinkai, S., Cooper, C., and James, T.D., *Exploitation of a novel 'on-off' photoinduced electron-transfer (PET) sensor against conventional 'off-on' PET sensors.* Chemical Communications, 1999(19): p. 2011-2012.
56. Huck, N.P.M., Jager, W.F., deLange, B., and Feringa, B.L., *Dynamic control and amplification of molecular chirality by circular polarized light.* Science, 1996. **273**(5282): p. 1686-1688.
57. Wiederrecht, G.P., Svec, W.A., and Wasielewski, M.R., *Triplet states with unusual spin polarization resulting from radical ion pair recombination at short distances.* Journal of the American Chemical Society, 1999. **121**(33): p. 7726-7727.
58. Klumpp, T., Linsenmann, M., Larson, S.L., Limoges, B.R., Burssner, D., Krissinel, E.B., Elliott, C.M., and Steiner, U.E., *Spin chemical control of photoinduced electron-transfer processes in ruthenium(II)-trisbipyridine-based supramolecular triads.* Journal of the American Chemical Society, 1999. **121**(5): p. 1076-1087.
59. Wu, Y.L., Mamiya, J., Kanazawa, A., Shiono, T., Ikeda, T., and Zhang, Q.J., *Photoinduced alignment of polymer liquid crystals containing azobenzene moieties in the side chain. 6. Biaxiality and three-dimensional reorientation.* Macromolecules, 1999. **32**(26): p. 8829-8835.
60. Ashton, P.R., Ballardini, R., Balzani, V., Credi, A., Dress, K.R., Ishow, E., Kleverlaan, C.J., Kocian, O., Preece, J.A., Spencer, N., Stoddart, J.F., Venturi, M., and Wenger, S., *A photochemically driven molecular-level abacus.* Chemistry-a European Journal, 2000. **6**(19): p. 3558-3574.
61. Ashton, P.R., Ballardini, R., Balzani, V., Baxter, I., Credi, A., Fyfe, M.C.T., Gandolfi, M.T., Gomez-Lopez, M., Martinez-Diaz, M.V., Piersanti, A., Spencer, N., Stoddart, J.F., Venturi, M., White, A.J.P., and Williams, D.J., *Acid-base controllable molecular shuttles.* Journal of the American Chemical Society, 1998. **120**(46): p. 11932-11942.

62. Jimenez, M.C., Dietrich-Buchecker, C., and Sauvage, J.P., *Towards synthetic molecular muscles: Contraction and stretching of a linear rotaxane dimer.* Angewandte Chemie-International Edition, 2000. **39**(18): p. 3284-+.
63. Balzani, V., Clemente-Leon, M., Credi, A., Semeraro, M., Venturi, M., Tseng, H.R., Wenger, S., Saha, S., and Stoddart, J.F., *A comparison of shuttling mechanisms in two constitutionally isomeric bistable rotaxane-based sunlight-powered nanomotors.* Australian Journal of Chemistry, 2006. **59**(3): p. 193-206.
64. Altieri, A., Bottari, G., Dehez, F., Leigh, D.A., Wong, J.K.Y., and Zerbetto, F., *Remarkable positional discrimination in bistable light- and heat-switchable hydrogen-bonded molecular shuttles.* Angewandte Chemie-International Edition, 2003. **42**(20): p. 2296-2300.
65. Green, J.E., Choi, J.W., Boukai, A., Bunimovich, Y., Johnston-Halperin, E., DeIonno, E., Luo, Y., Sheriff, B.A., Xu, K., Shin, Y.S., Tseng, H.R., Stoddart, J.F., and Heath, J.R., *A 160-kilobit molecular electronic memory patterned at 10(11) bits per square centimetre.* Nature, 2007. **445**(7126): p. 414-417.
66. Joachim, C., Gimzewski, J.K., and Aviram, A., *Electronics using hybrid-molecular and mono-molecular devices.* Nature, 2000. **408**: p. 541-548.
67. Heath, J.R., Kuekes, P.J., Snider, G.S., and Williams, R.S., *A defect-tolerant computer architecture: Opportunities for nanotechnology.* Science, 1998. **280**(5370): p. 1716-1721.
68. Stan, M.R., Franzon, P.D., Goldstein, S.C., Lach, J.C., and Ziegler, M.M., *Molecular electronics: From devices and interconnect to circuits and architecture.* Proceedings of the Ieee, 2003. **91**(11): p. 1940-1957.
69. Cohen, R., Stokbro, K., Martin, J.M.L., and Ratner, M.A., *Charge transport in conjugated aromatic molecular junctions: Molecular conjugation and molecule-electrode coupling.* Journal of Physical Chemistry C, 2007. **111**(40): p. 14893-14902.
70. Fan, F.R.F., Lai, R.Y., Cornil, J., Karzazi, Y., Bredas, J.L., Cai, L.T., Cheng, L., Yao, Y.X., Price, D.W., Dirk, S.M., Tour, J.M., and Bard, A.J., *Electrons are transported through phenylene-ethynylene oligomer monolayers via localized molecular orbitals.* Journal of the American Chemical Society, 2004. **126**(8): p. 2568-2573.
71. Heimel, G., Romaner, L., Bredas, J.L., and Zojer, E., *Interface energetics and level alignment at covalent metal-molecule junctions: pi-conjugated thiols on gold.* Physical Review Letters, 2006. **96**(19): p. 4.
72. Li, X.L., Xu, B.Q., Xiao, X.Y., Yang, X.M., Zang, L., and Tao, N.J., *Controlling charge transport in single molecules using electrochemical gate.* Faraday Discussions, 2006. **131**: p. 111-120.
73. Piccinin, S., Selloni, A., Scandolo, S., Car, R., and Scoles, G., *Electronic properties of metal-molecule-metal systems at zero bias: A periodic density functional study.* Journal of Chemical Physics, 2003. **119**(13): p. 6729-6735.
74. Tomfohr, J. and Sankey, O.F., *Theoretical analysis of electron transport through organic molecules.* Journal of Chemical Physics, 2004. **120**(3): p. 1542-1554.
75. Cui, X.D., Primak, A., Zarate, X., Tomfohr, J., Sankey, O.F., Moore, A.L., Moore, T.A., Gust, D., Harris, G., and Lindsay, S.M., *Reproducible measurement of single-molecule conductivity.* Science, 2001. **294**(5542): p. 571-574.

76. Dadosh, T., Gordin, Y., Krahne, R., Khivrich, I., Mahalu, D., Frydman, V., Sperling, J., Yacoby, A., and Bar-Joseph, I., *Measurement of the conductance of single conjugated molecules.* Nature, 2005. **436**(7051): p. 677-680.
77. Donhauser, Z.J., Mantooth, B.A., Kelly, K.F., Bumm, L.A., Monnell, J.D., Stapleton, J.J., Price, D.W., Rawlett, A.M., Allara, D.L., Tour, J.M., and Weiss, P.S., *Conductance switching in single molecules through conformational changes.* Science, 2001. **292**(5525): p. 2303-2307.
78. Li, C., Pobelov, I., Wandlowski, T., Bagrets, A., Arnold, A., and Evers, F., *Charge transport in single Au vertical bar alkanedithiol vertical bar Au junctions: Coordination geometries and conformational degrees of freedom.* Journal of the American Chemical Society, 2008. **130**: p. 318-326.
79. Reed, M.A., Zhou, C., Muller, C.J., Burgin, T.P., and Tour, J.M., *Conductance of a molecular junction.* Science, 1997. **278**: p. 252-254.
80. Reichert, J., *Driving current through single organic molecules.* Phys. Rev. Lett., 2002. **88**: p. 176804.
81. Xu, B.Q. and Tao, N.J.J., *Measurement of single-molecule resistance by repeated formation of molecular junctions.* Science, 2003. **301**(5637): p. 1221-1223.
82. Salomon, A., Cahen, D., Lindsay, S., Tomfohr, J., Engelkes, V.B., and Frisbie, C.D., *Comparison of electronic transport measurements on organic molecules.* Advanced Materials, 2003. **15**(22): p. 1881-1890.
83. Chen, I.W.P., Fu, M.D., Tseng, W.H., Chen, C.H., Chou, C.M., and Luh, T.Y., *The effect of molecular conformation on single molecule conductance: measurements of pi-conjugated oligoaryls by STM break junction.* Chemical Communications, 2007(29): p. 3074-3076.
84. Sedghi, G., Sawada, K., Esdaile, L.J., Hoffmann, M., Anderson, H.L., Bethell, D., Haiss, W., Higgins, S.J., and Nichols, R.J., *Single molecule conductance of porphyrin wires with ultralow attenuation.* Journal Of The American Chemical Society, 2008. **130**(27): p. 8582-+.
85. Yamada, R., Kumazawa, H., Noutoshi, T., Tanaka, S., and Tada, H., *Electrical conductance of oligothiophene molecular wires.* Nano Letters, 2008. **8**(4): p. 1237-1240.
86. Atkins, P. and Paula, J.d., *Physical Chemistry* 7th Ed. ed. 2002, New York: W. H. Freeman and Company.
87. Marcus, R.A., *THEORY OF OXIDATION-REDUCTION REACTIONS INVOLVING ELECTRON TRANSFER .1.* Journal of Chemical Physics, 1956. **24**(5): p. 966-978.
88. Hush, N.S., *HOMOGENEOUS AND HETEROGENEOUS OPTICAL AND THERMAL ELECTRON TRANSFER.* Electrochimica Acta, 1968. **13**(5): p. 1005-&.
89. Siddarth, P. and Marcus, R.A., *COMPARISON OF EXPERIMENTAL AND THEORETICAL ELECTRONIC MATRIX-ELEMENTS FOR LONG-RANGE ELECTRON-TRANSFER.* Journal of Physical Chemistry, 1990. **94**(7): p. 2985-2989.
90. Cui, X.D., Zarate, X., Tomfohr, J., Sankey, O.F., Primak, A., Moore, A.L., Moore, T.A., Gust, D., Harris, G., and Lindsay, S.M., *Making electrical contacts to molecular monolayers.* Nanotechnology, 2002. **13**(1): p. 5-14.

91. O'Neill, M.A. and Barton, J.K., *DNA mediated charge transport charege transfer chemistry and biology*, in *Long-Range Charge Transfer in DNA*, G.B. Schuster, Editor. 2004, Springer: Berlin/Heidelberg. p. pg 67-114.
92. Berlin, Y.A., Kurnikov, I.V., Beratan, D., Ratner, M.A., and Burin, A.L., *DNA electron transfer processes: Some theoretical notions*, in *Long-Range Charge Transfer in DNA Ii*. 2004, Springer-Verlag Berlin: Berlin. p. 1-36.
93. Steenken, S., *Electron transfer in DNA? Competition by ultra-fast proton transfer?* Biological Chemistry, 1997. **378**(11): p. 1293-1297.
94. Beratan, D.N., Priyadarshy, S., and Risser, S.M., *DNA: Insulator or wire?* Chemistry & Biology, 1997. **4**(1): p. 3-8.
95. Strachan, D.R., Smith, D.E., Johnston, D.E., Park, T.H., Therien, M.J., Bonnell, D.A., and Johnson, A.T., *Controlled fabrication of nanogaps in ambient environment for molecular electronics.* Applied Physics Letters, 2005. **86**(4).
96. Landauer, R., *ELECTRICAL RESISTANCE OF DISORDERED ONE-DIMENSIONAL LATTICES.* Philosophical Magazine, 1970. **21**(172): p. 863-&.
97. Landauer, R., *SPATIAL VARIATION OF CURRENTS AND FIELDS DUE TO LOCALIZED SCATTERERS IN METALLIC CONDUCTION.* Ibm Journal of Research and Development, 1957. **1**(3): p. 223-231.
98. Beenakker, C.W.J., *Random-matrix theory of quantum transport.* Reviews of Modern Physics, 1997. **69**(3): p. 731-808.
99. vanHouten, H. and Beenakker, C., *Quantum point contacts.* Physics Today, 1996. **49**(7): p. 22-27.
100. Xue, Y. and Ratner, M.A., *Microscopic study of electrical transport through individual molecules with metallic contacts. I. Band lineup, voltage drop, and high-field transport.* Phys. Rev. B, 2003. **68**: p. 115406-115418.
101. Newton, M.D. and Smalley, J.F., *Interfacial bridge-mediated electron transfer: mechanistic analysis based on electrochemical kinetics and theoretical modelling.* Physical Chemistry Chemical Physics, 2007. **9**(5): p. 555-572.
102. Mayor, M., Buschel, M., Fromm, K.M., Lehn, J.M., and Daub, J. *Electron transfer through bridging molecular structures*. 2002.
103. Greenfield, S.R., Svec, W.A., Gosztola, D., and Wasielewski, M.R., *Multistep photochemical charge separation in rod-like molecules based on aromatic imides and diimides.* Journal of the American Chemical Society, 1996. **118**(28): p. 6767-6777.
104. Balzani, V. and Scandola, F., *Supramolecular Photochemistry (Chapter 5 and 6).* 1991, Horwood, Chichester, UK.
105. Fromherz, P. and Rieger, B., *PHOTOINDUCED ELECTRON-TRANSFER IN DNA MATRIX FROM INTERCALATED ETHIDIUM TO CONDENSED METHYLVIOLOGEN.* Journal of the American Chemical Society, 1986. **108**(17): p. 5361-5362.
106. Kelley, S.O., Holmlin, R.E., Stemp, E.D.A., and Barton, J.K., *Photoinduced electron transfer in ethidium-modified DNA duplexes: Dependence on distance and base stacking.* Journal of the American Chemical Society, 1997. **119**(41): p. 9861-9870.
107. Brun, A.M. and Harriman, A., *ENERGY-TRANSFER AND ELECTRON-TRANSFER PROCESSES INVOLVING PALLADIUM PORPHYRINS BOUND*

TO DNA. Journal of the American Chemical Society, 1994. **116**(23): p. 10383-10393.
108. Brun, A.M. and Harriman, A., *DYNAMICS OF ELECTRON-TRANSFER BETWEEN INTERCALATED POLYCYCLIC MOLECULES - EFFECT OF INTERSPERSED BASES*. Journal of the American Chemical Society, 1992. **114**(10): p. 3656-3660.
109. Baguley, B.C., Denny, W.A., Atwell, G.J., and Cain, B.F., *POTENTIAL ANTI-TUMOR AGENTS .34. QUANTITATIVE RELATIONSHIPS BETWEEN DNA-BINDING AND MOLECULAR-STRUCTURE FOR 9-ANILINOACRIDINES SUBSTITUTED IN THE ANILINO RING*. Journal of Medicinal Chemistry, 1981. **24**(2): p. 170-177.
110. Siemeling, U., Vorfeld, U., Neumann, B., Stammler, H.G., Zanello, P., and de Biani, F.F. *Terpyridines functionalised with ferrocenyl groups of different redox potential*. 1999.
111. Benniston, A.C., Goulle, V., Harriman, A., Lehn, J.M., and Marczinke, B., *ELECTRON DELOCALIZATION IN POLYENE-BRIDGED BINUCLEAR COMPLEXES*. Journal of Physical Chemistry, 1994. **98**(32): p. 7798-7804.
112. Zheng, G.Y., Rillema, D.P., and Reibenspies, J.H., *Synthesis, X-ray structure, and physical and photophysical properties of the heterobimetallic complex Fe(eta(5)-C5H4PPh2)(2)Pt(bph)*. Inorganic Chemistry, 1999. **38**(4): p. 794-797.
113. Polese, A., Mondini, S., Bianco, A., Toniolo, C., Scorrano, G., Guldi, D.M., and Maggini, M., *Solvent-dependent intramolecular electron transfer in a peptide-linked [Ru(bpy)(3)](2+)-C-60 dyad*. Journal of the American Chemical Society, 1999. **121**(14): p. 3446-3452.
114. Martin, N., Sanchez, L., Illescas, B., and Perez, I., *C-60-based electroactive organofullerenes*. Chemical Reviews, 1998. **98**(7): p. 2527-2547.
115. Grigg, R., Holmes, J.M., Jones, S.K., and Norbert, W., *LUMINESCENT PH SENSORS BASED ON P-TERT-BUTYLCALIX[4]ARENE-LINKED RUTHENIUM(II) TRISBIPYRIDYL COMPLEXES*. Journal of the Chemical Society-Chemical Communications, 1994(2): p. 185-187.
116. Lucia, L.A., Whitten, D.G., and Schanze, K.S., *Photoinduced charge separation promoted by ring opening of a piperazine radical cation*. Journal of the American Chemical Society, 1996. **118**(12): p. 3057-3058.
117. Yonemoto, E.H., Saupe, G.B., Schmehl, R.H., Hubig, S.M., Riley, R.L., Iverson, B.L., and Mallouk, T.E., *ELECTRON-TRANSFER REACTIONS OF RUTHENIUM TRISBIPYRIDYL-VIOLOGEN DONOR-ACCEPTOR MOLECULES - COMPARISON OF THE DISTANCE DEPENDENCE OF ELECTRON-TRANSFER RATES IN THE NORMAL AND MARCUS INVERTED REGIONS*. Journal of the American Chemical Society, 1994. **116**(11): p. 4786-4795.
118. Goulle, V., Harriman, A., and Lehn, J.M., *AN ELECTRO-PHOTOSWITCH - REDOX SWITCHING OF THE LUMINESCENCE OF A BIPYRIDINE METAL-COMPLEX*. Journal of the Chemical Society-Chemical Communications, 1993(12): p. 1034-1036.
119. Miller, C., Cuendet, P., and Gratzel, M., *ADSORBED OMEGA-HYDROXY THIOL MONOLAYERS ON GOLD ELECTRODES - EVIDENCE FOR*

ELECTRON-TUNNELING TO REDOX SPECIES IN SOLUTION. Journal of Physical Chemistry, 1991. **95**(2): p. 877-886.
120. Slowinski, K., Chamberlain, R.V., Miller, C.J., and Majda, M., *Through-bond and chain-to-chain coupling. Two pathways in electron tunneling through liquid alkanethiol monolayers on mercury electrodes.* Journal of the American Chemical Society, 1997. **119**(49): p. 11910-11919.
121. Slowinski, K., Chamberlain, R.V., Bilewicz, R., and Majda, M., *Evidence for inefficient chain-to-chain coupling in electron tunneling through liquid alkanethiol monolayer films on mercury.* Journal of the American Chemical Society, 1996. **118**(19): p. 4709-4710.
122. Creager, S., Yu, C.J., Bamdad, C., O'Connor, S., MacLean, T., Lam, E., Chong, Y., Olsen, G.T., Luo, J.Y., Gozin, M., and Kayyem, J.F., *Electron transfer at electrodes through conjugated "molecular wire" bridges.* Journal of the American Chemical Society, 1999. **121**(5): p. 1059-1064.
123. Chidsey, C.E.D., *FREE-ENERGY AND TEMPERATURE-DEPENDENCE OF ELECTRON-TRANSFER AT THE METAL-ELECTROLYTE INTERFACE.* Science, 1991. **251**(4996): p. 919-922.
124. Tivanski, A.V., He, Y.F., Borguet, E., Liu, H.Y., Walker, G.C., and Waldeck, D.H., *Conjugated thiol linker for enhanced electrical conduction of gold-molecule contacts.* Journal of Physical Chemistry B, 2005. **109**(12): p. 5398-5402.
125. Carter, M.T., Rowe, G.K., Richardson, J.N., Tender, L.M., Terrill, R.H., and Murray, R.W., *DISTANCE DEPENDENCE OF THE LOW-TEMPERATURE ELECTRON-TRANSFER KINETICS OF (FERROCENYLCARBOXY)-TERMINATED ALKANETHIOL MONOLAYERS.* Journal of the American Chemical Society, 1995. **117**(10): p. 2896-2899.
126. Paul, A., Watson, R.M., Lund, P., Xing, Y.J., Burke, K., He, Y.F., Borguet, E., Achim, C., and Waldeck, D.H., *Charge transfer through single-stranded peptide nucleic acid composed of thymine Nucleotides.* Journal of Physical Chemistry C, 2008. **112**(18): p. 7233-7240.
127. Kushmerick, J.G., Naciri, J., Yang, J.C., and Shashidhar, R., *Conductance scaling of molecular wires in parallel.* Nano Letters, 2003. **3**(7): p. 897-900.
128. Kushmerick, J.G., Holt, D.B., Pollack, S.K., Ratner, M.A., Yang, J.C., Schull, T.L., Naciri, J., Moore, M.H., and Shashidhar, R., *Effect of bond-length alternation in molecular wires.* Journal of the American Chemical Society, 2002. **124**(36): p. 10654-10655.
129. Stewart, D.R., Ohlberg, D.A.A., Beck, P.A., Chen, Y., Williams, R.S., Jeppesen, J.O., Nielsen, K.A., and Stoddart, J.F., *Molecule-independent electrical switching in Pt/organic monolayer/Ti devices.* Nano Letters, 2004. **4**(1): p. 133-136.
130. Collier, C.P., Mattersteig, G., Wong, E.W., Luo, Y., Beverly, K., Sampaio, J., Raymo, F.M., Stoddart, J.F., and Heath, J.R., *A [2]catenane-based solid state electronically reconfigurable switch.* Science, 2000. **289**(5482): p. 1172-1175.
131. Park, H., Lim, A.K.L., Alivisatos, A.P., Park, J., and McEuen, P.L., *Fabrication of metallic electrodes with nanometer separation by electromigration.* Applied Physics Letters, 1999. **75**(2): p. 301-303.

132. Wu, Z.M., Steinacher, M., Huber, R., Calame, M., van der Molen, S.J., and Schonenberger, C., *Feedback controlled electromigration in four-terminal nanojunctions.* Applied Physics Letters, 2007. **91**(5).
133. Mahapatro, A.K., Ghosh, S., and Janes, D.B., *Nanometer scale electrode separation (nanogap) using electromigration at room temperature.* Ieee Transactions on Nanotechnology, 2006. **5**(3): p. 232-236.
134. Ho, P.S. and Kwok, T., *ELECTROMIGRATION IN METALS.* Reports on Progress in Physics, 1989. **52**(3): p. 301-348.
135. Weber, H.B., Reichert, J., Weigend, F., Ochs, R., Beckmann, D., Mayor, M., Ahlrichs, R., and von Lohneysen, H., *Electronic transport through single conjugated molecules.* Chemical Physics, 2002. **281**(2-3): p. 113-125.
136. Moreland, J. and Ekin, J.W., *ELECTRON-TUNNELING EXPERIMENTS USING NB-SN BREAK JUNCTIONS.* Journal of Applied Physics, 1985. **58**(10): p. 3888-3895.
137. Smit, R.H.M., *Measurement of the conductance of a hydrogen molecule.* Nature, 2002. **419**: p. 906-909.
138. Venkataraman, L., Klare, J.E., Nuckolls, C., Hybertsen, M.S., and Steigerwald, M.L., *Dependence of single-molecule junction conductance on molecular conformation.* Nature, 2006. **442**(7105): p. 904-907.
139. Haiss, W., Albrecht, T., van Zalinge, H., Higgins, S.J., Bethell, D., Hobenreich, H., Schiffrin, D.J., Nichols, R.J., Kuznetsov, A.M., Zhang, J., Chi, Q., and Ulstrup, J., *Single-molecule conductance of redox molecules in electrochemical scanning tunneling microscopy.* Journal of Physical Chemistry B, 2007. **111**(24): p. 6703-6712.
140. Nishikawa, A., Tobita, J., Kato, Y., Fujii, S., Suzuki, M., and Fujihira, M., *Accurate determination of multiple sets of single molecular conductance of Au/1,6-hexanedithiol/Au break junctions by ultra-high vacuum-scanning tunneling microscope and analyses of individual current-separation curves.* Nanotechnology, 2007. **18**.
141. He, J., Chen, F., Li, J., Sankey, O.F., Terazono, Y., Herrero, C., Gust, D., Moore, T.A., Moore, A.L., and Lindsay, S.M., *Electronic decay constant of carotenoid polyenes from single-molecule measurements.* Journal of the American Chemical Society, 2005. **127**(5): p. 1384-1385.
142. Xu, B.Q.Q., Li, X.L.L., Xiao, X.Y.Y., Sakaguchi, H., and Tao, N.J.J., *Electromechanical and conductance switching properties of single oligothiophene molecules.* Nano Letters, 2005. **5**(7): p. 1491-1495.
143. Huang, Z.F., Chen, F., Bennett, P.A., and Tao, N.J., *Single molecule junctions formed via au-thiol contact: Stability and breakdown mechanism.* Journal of the American Chemical Society, 2007. **129**(43): p. 13225-13231.
144. Venkataraman, L., Klare, J.E., Tam, I.W., Nuckolls, C., Hybertsen, M.S., and Steigerwald, M.L., *Single-molecule circuits with well-defined molecular conductance.* Nano Letters, 2006. **6**(3): p. 458-462.
145. Kushmerick, J.G., *Metal-molecule contacts.* Materials Today, 2005: p. 26-30.
146. Kim, B., Beebe, J.M., Jun, Y., Zhu, X.Y., and Frisbie, C.D., *Correlation between HOMO alignment and contact resistance in molecular junctions: Aromatic thiols*

versus aromatic isocyanides. Journal of the American Chemical Society, 2006. **128**(15): p. 4970-4971.
147. Liu, K., Li, G.R., Wang, X.H., and Wang, F.S., *Length dependence of electron conduction for oligo(1,4-phenylene ethynylene)s: A conductive probe-atomic force microscopy investigation.* Journal of Physical Chemistry C, 2008. **112**(11): p. 4342-4349.
148. Li, Z.Y. and Kosov, D.S., *Orbital interaction mechanisms of conductance enhancement and rectification by dithiocarboxylate anchoring group.* Journal of Physical Chemistry B, 2006. **110**(39): p. 19116-19120.
149. Seminario, J.M., De La Cruz, C.E., and Derosa, P.A., *A theoretical analysis of metal-molecule contacts.* Journal Of The American Chemical Society, 2001. **123**(23): p. 5616-5617.
150. Tulevski, G.S., Myers, M.B., Hybertsen, M.S., Steigerwald, M.L., and Nuckolls, C., *Formation of catalytic metal-molecule contacts.* Science, 2005. **309**(5734): p. 591-594.
151. Yaliraki, S.N., Kemp, M., and Ratner, M.A., *Conductance of molecular wires: Influence of molecule-electrode binding.* Journal of the American Chemical Society, 1999. **121**(14): p. 3428-3434.
152. Beebe, J.M., Engelkes, V.B., Miller, L.L., and Frisbie, C.D., *Contact resistance in metal-molecule-metal junctions based on aliphatic SAMs: Effects of surface linker and metal work function.* Journal of the American Chemical Society, 2002. **124**(38): p. 11268-11269.
153. Millar, D., Venkataraman, L., and Doerrer, L.H., *Efficacy of Au-Au contacts for scanning tunneling microscopy molecular conductance measurements.* Journal of Physical Chemistry C, 2007. **111**(47): p. 17635-17639.
154. Patrone, L., Palacin, S., and Bourgoin, J.P., *Direct comparison of the electronic coupling efficiency of sulfur and selenium alligator clips for molecules adsorbed onto gold electrodes.* Applied Surface Science, 2003. **212**: p. 446-451.
155. Patrone, L., Palacin, S., Charlier, J., Armand, F., Bourgoin, J.P., Tang, H., and Gauthier, S., *Evidence of the key role of metal-molecule bonding in metal-molecule-metal transport experiments.* Physical Review Letters, 2003. **91**(9).
156. Yasuda, S., Yoshida, S., Sasaki, J., Okutsu, Y., Nakamura, T., Taninaka, A., Takeuchi, O., and Shigekawa, H., *Bond fluctuation of S/Se anchoring observed in single-molecule conductance measurements using the point contact method with scanning tunneling microscopy.* Journal of the American Chemical Society, 2006. **128**(24): p. 7746-7747.
157. Colorado, R., Jr., Villazana, R.J., and Lee, T.R., *Self-assembled monolayers on gold generated from aliphatic dithiocarboxylic acids.* Langmuir, 1998. **14**(22): p. 6337-6340.
158. Park, T.H. and Therien, M.J., *Carbodithioate-terminated oligo(phenyleneethynylene)s: Synthesis and surface functionalization of gold nanoparticles.* Organic Letters, 2007. **9**(15): p. 2779-2782.
159. Querner, C., Reiss, P., Bleuse, J., and Pron, A., *Chelating Ligands for nanocrystals' surface functionalization.* Journal Of The American Chemical Society, 2004. **126**(37): p. 11574-11582.

160. Cai, L.T., Skulason, H., Kushmerick, J.G., Pollack, S.K., Naciri, J., Shashidhar, R., Allara, D.L., Mallouk, T.E., and Mayer, T.S., *Nanowire-based molecular monolayer junctions: Synthesis, assembly, and electrical characterization.* Journal Of Physical Chemistry B, 2004. **108**(9): p. 2827-2832.
161. Chen, J., Wang, W., Reed, M.A., Rawlett, A.M., Price, D.W., and Tour, J.M., *Room-temperature negative differential resistance in nanoscale molecular junctions.* Applied Physics Letters, 2000. **77**(8): p. 1224-1226.
162. Selzer, Y., Cai, L., Cabassi, M.A., Yao, Y., Tour, J.M., Mayer, T.S., and Allara, D.L., *Effect of local environment on molecular conduction: Isolated molecule versus self-assembled monolayer.* Nano Letters, 2005. **5**(1): p. 61-65.
163. Walzer, K., Marx, E., Greenham, N.C., Less, R.J., Raithby, P.R., and Stokbro, K., *Scanning tunneling microscopy of self-assembled phenylene ethynylene oligomers on Au(111) substrates.* Journal Of The American Chemical Society, 2004. **126**(4): p. 1229-1234.
164. Hsung, R.P., Babcock, J.R., Chidsey, C.E.D., and Sita, L.R., *THIOPHENOL PROTECTING GROUPS FOR THE PALLADIUM-CATALYZED HECK REACTION - EFFICIENT SYNTHESES OF CONJUGATED ARYLTHIOLS.* Tetrahedron Letters, 1995. **36**(26): p. 4525-4528.
165. Clavilier, J., Faure, R., Guinet, G., and Durand, R., *PREPARATION OF MONO-CRYSTALLINE PT MICROELECTRODES AND ELECTROCHEMICAL STUDY OF THE PLANE SURFACES CUT IN THE DIRECTION OF THE (111) AND (110) PLANES.* Journal of Electroanalytical Chemistry, 1980. **107**(1): p. 205-209.
166. Morita, T. and Lindsay, S., *Determination of single molecule conductances of alkanedithiols by conducting-atomic force microscopy with large gold nanoparticles.* Journal Of The American Chemical Society, 2007. **129**(23): p. 7262-+.
167. Lee, M.H., Speyer, G., and Sankey, O.F., *Electron transport through single alkane molecules with different contact geometries on gold.* Physica Status Solidi B-Basic Solid State Physics, 2006. **243**(9): p. 2021-2029.
168. Xiao, X.Y., Xu, B.Q., and Tao, N.J., *Measurement of single molecule conductance: Benzenedithiol and benzenedimethanethiol.* Nano Lett., 2004. **4**: p. 267-271.
169. Eng, M.P. and Albinsson, B., *Non-exponential distance dependence of bridge-mediated electronic coupling.* Angewandte Chemie-International Edition, 2006. **45**(34): p. 5626-5629.
170. Romaner, L., Heimel, G., Gruber, M., Bredas, J.L., and Zojer, E., *Stretching and breaking of a molecular junction.* Small, 2006. **2**: p. 1468-1475.
171. Giacalone, F., Segura, J.L., Martin, N., and Guldi, D.M., *Exceptionally small attenuation factors in molecular wires.* Journal Of The American Chemical Society, 2004. **126**(17): p. 5340-5341.
172. de la Torre, G., Giacalone, F., Segura, J.L., Martin, N., and Guldi, D.M., *Electronic communication through pi-conjugated wires in covalently linked porphyrin/C-60 ensembles.* Chemistry-A European Journal, 2005. **11**(4): p. 1267-1280.
173. Vail, S.A., Krawczuk, P.J., Guldi, D.M., Palkar, A., Echegoyen, L., Tome, J.P.C., Fazio, M.A., and Schuster, D.I., *Energy and electron transfer in polyacetylene-*

linked zinc-porphyrin[60]fullerene molecular wires. Chemistry-A European Journal, 2005. **11**(11): p. 3375-3388.
174. Bixon, M. and Jortner, J., *Electron transfer via bridges.* Journal of Chemical Physics, 1997. **107**(13): p. 5154-5170.
175. Hatcher, E., Balaeff, A., Keinan, S., Venkatramani, R., and Beratan, D.N., *PNA versus DNA: Effects of Structural Fluctuations on Electronic Structure and Hole-Transport Mechanisms.* J. Am. Chem. Soc., 2008(ASAP Article; DOI: 10.1021/ja802541e).
176. Sumi, H. and Kakitani, T., *Electron transfer via a midway molecule as seen in primary processes in photosynthesis; A new process describable as superexchange or sequential in mutually opposite limits.* Chemical Physics Letters, 1996. **252**(1-2): p. 85-93.
177. Datta, S., *Quantum Transport: Atom to Transistor*. 2005: Cambridge University Press.
178. Xue, Y.Q., Datta, S., and Ratner, M.A., *First-principles based matrix Green's function approach to molecular electronic devices: general formalism.* Chemical Physics, 2002. **281**(2-3): p. 151-170.
179. Brandbyge, M., Mozos, J.L., Ordejon, P., Taylor, J., and Stokbro, K., *Density-functional method for nonequilibrium electron transport.* Physical Review B, 2002. **65**(16).
180. Troisi, A. and Ratner, M.A., *Modeling the inelastic electron tunneling spectra of molecular wire junctions.* Physical Review B, 2005. **72**(3).
181. Paulsson, M., Frederiksen, T., and Brandbyge, M., *Inelastic transport through molecules: Comparing first-principles calculations to experiments.* Nano Letters, 2006. **6**(2): p. 258-262.
182. Andrews, D.Q., Van Duyne, R.P., and Ratner, M.A., *Stochastic modulation in molecular electronic transport junctions: Molecular dynamics coupled with charge transport calculations.* Nano Letters, 2008. **8**(4): p. 1120-1126.
183. Koentopp, M., Chang, C., Burke, K., and Car, R., *Density functional calculations of nanoscale conductance.* Journal of Physics-Condensed Matter, 2008. **20**(8).
184. Evers, F., Weigend, F., and Koentopp, M., *Conductance of molecular wires and transport calculations based on density-functional theory.* Physical Review B, 2004. **69**(23).
185. Ke, S.H., Baranger, H.U., and Yang, W.T., *Role of the exchange-correlation potential in ab initio electron transport calculations.* Journal of Chemical Physics, 2007. **126**(20).
186. Toher, C., Filippetti, A., Sanvito, S., and Burke, K., *Self-interaction errors in density-functional calculations of electronic transport.* Physical Review Letters, 2005. **95**(14).
187. Reimers, J.R., Cai, Z.L., Bilic, A., and Hush, N.S. *The appropriateness of density-functional theory for the calculation of molecular electronics properties*. 2003.
188. Koentopp, M., Burke, K., and Evers, F., *Zero-bias molecular electronics: Exchange-correlation corrections to Landauer's formula.* Physical Review B, 2006. **73**(12).

189. Li, Z. and Kosov, D.S., *Orbital interaction mechanisms of conductance enhancement and rectification by dithiocarboxylate anchoring group.* Journal Of Physical Chemistry B, 2006. **110**(39): p. 19116-19120.
190. Ghosh, A.W., Zahid, F., Datta, S., and Birge, R.R., *Charge transfer in molecular conductors - oxidation or reduction?* Chemical Physics, 2002. **281**(2-3): p. 225-230.
191. Ramachandran, G.K., Hopson, T.J., Rawlett, A.M., Nagahara, L.A., Primak, A., and Lindsay, S.M., *A bond-fluctuation mechanism for stochastic switching in wired molecules.* Science, 2003. **300**(5624): p. 1413-1416.
192. Galperin, M., Ratner, M.A., and Nitzan, A., *Hysteresis, switching, and negative differential resistance in molecular junctions: A polaron model.* Nano Letters, 2005. **5**(1): p. 125-130.
193. *Peptide Nucleic Acids: Protocols and Applications (Second Edition)*, P.E. Nielsen, Editor. 2004, Horizon Bioscience.
194. Dueholm, K.L., Egholm, M., Behrens, C., Christensen, L., Hansen, H.F., Vulpius, T., Petersen, K.H., Berg, R.H., Nielsen, P.E., and Buchardt, O., *SYNTHESIS OF PEPTIDE NUCLEIC-ACID MONOMERS CONTAINING THE 4 NATURAL NUCLEOBASES - THYMINE, CYTOSINE, ADENINE, AND GUANINE AND THEIR OLIGOMERIZATION.* Journal of Organic Chemistry, 1994. **59**(19): p. 5767-5773.
195. Blackburn, G.M. and Gait, M.J., *Nucleic Acids in Chemistry and Biology, 2nd ed.* 1996, Oxford: Oxford University Press.
196. Shabarova, Z. and Bogdanov, A., *Advanced Organic Chemistry of Nucleic Acids*. 1994, Weinheim: VCH.
197. Voityuk, A.A., *Assessment of semiempirical methods for the computation of charge transfer in DNA pi-stacks.* Chemical Physics Letters, 2006. **427**(1-3): p. 177-180.
198. Netzel, T.L., *Present status and future directions of research in electron-transfer mediated by DNA.* Journal of Biological Inorganic Chemistry, 1998. **3**(2): p. 210-214.
199. Netzel, T.L. *Electron transfer reactions in DNA*. 1997.
200. Arkin, M.R., Stemp, E.D.A., Holmlin, R.E., Barton, J.K., Hormann, A., Olson, E.J.C., and Barbara, P.F., *Rates of DNA-mediated electron transfer between metallointercalators.* Science, 1996. **273**(5274): p. 475-480.
201. Burrows, C.J. and Muller, J.G., *Oxidative nucleobase modifications leading to strand scission.* Chemical Reviews, 1998. **98**(3): p. 1109-1151.
202. Armitage, B., *Photocleavage of nucleic acids.* Chemical Reviews, 1998. **98**(3): p. 1171-1200.
203. deSilva, A.P., Gunaratne, H.Q.N., Gunnlaugsson, T., Huxley, A.J.M., McCoy, C.P., Rademacher, J.T., and Rice, T.E., *Signaling recognition events with fluorescent sensors and switches.* Chemical Reviews, 1997. **97**(5): p. 1515-1566.
204. Tour, J.M., *Conjugated macromolecules of precise length and constitution. Organic synthesis for the construction of nanoarchitectures.* Chemical Reviews, 1996. **96**(1): p. 537-553.

205. Priyadarshy, S., Risser, S.M., and Beratan, D.N., *DNA is not a molecular wire: Protein-like electron-transfer predicted for an extended pi-electron system.* Journal of Physical Chemistry, 1996. **100**(44): p. 17678-17682.
206. Mateo-Marti, E., Briones, C., Roman, E., Briand, E., Pradier, C.M., and Martin-Gago, J.A., *Self-assembled monolayers of peptide nucleic acids on gold surfaces: A spectroscopic study.* Langmuir, 2005. **21**(21): p. 9510-9517.
207. Briones, C., Mateo-Marti, E., Gomez-Navarro, C., Parro, V., Roman, E., and Martin-Gago, J.A. *Structural and functional characterization of self-assembled monolayers of peptide nucleic acids and its interaction with complementary DNA*. 2005.
208. Briones, C., Mateo-Marti, E., Gomez-Navarro, C., Parro, V., Roman, E., and Martin-Gago, J.A., *Ordered self-assembled monolayers of peptide nucleic acids with DNA recognition capability.* Physical Review Letters, 2004. **93**(20).
209. Reimers, J.R. and Hush, N.S., *ELECTRON-TRANSFER AND ENERGY-TRANSFER THROUGH BRIDGED SYSTEMS .3. TIGHT-BINDING LINKAGES WITH ZERO OR NONZERO ASYMPTOTIC BAND-GAP.* Journal of Photochemistry and Photobiology a-Chemistry, 1994. **82**(1-3): p. 31-46.
210. Dagama, A.A.S., *DONOR-ACCEPTOR INTERACTION IN METALLOPROTEINS.* Theoretica Chimica Acta, 1985. **68**(2): p. 159-169.
211. Wettig, S.D., Wood, D.O., Aich, P., and Lee, J.S., *M-DNA: A novel metal ion complex of DNA studied by fluorescence techniques.* Journal of Inorganic Biochemistry, 2005. **99**(11): p. 2093-2101.
212. Meyer, T.J. and Taube, H., *ELECTRON-TRANSFER REACTIONS OF RUTHENIUM AMMINES.* Inorganic Chemistry, 1968. **7**(11): p. 2369-&.
213. Goldman, C., *LONG-RANGE ELECTRON-TRANSFER IN PROTEINS - A RENORMALIZED-PERTURBATION-EXPANSION APPROACH.* Physical Review A, 1991. **43**(8): p. 4500-4509.
214. Sek, S., Sepiol, A., Tolak, A., Misicka, A., and Bilewicz, R., *Distance dependence of the electron transfer rate through oligoglycine spacers introduced into self-assembled monolayers.* Journal of Physical Chemistry B, 2004. **108**(24): p. 8102-8105.
215. Tao, N.J., *Measurement and control of single molecule conductance.* Journal of Materials Chemistry, 2005. **15**(32): p. 3260-3263.
216. Weber, K., Hockett, L., and Creager, S., *Long-range electronic coupling between ferrocene and gold in alkanethiolate-based monolayers on electrodes.* Journal of Physical Chemistry B, 1997. **101**(41): p. 8286-8291.
217. Xing, Y., Bezer, S., Watson, R.M., Lund, P., Paul, A., Waldeck, D., Achim, C., and Borguet, E., *Single Molecule Conductivity Measurement of Peptide Nucleic Acids.* (In preparation).
218. Xu, B.Q., Zhang, P.M., Li, X.L., and Tao, N.J., *Direct conductance measurement of single DNA molecules in aqueous solution.* Nano Letters, 2004. **4**(6): p. 1105-1108.
219. Paul, A., Bezer, S., Venkatramani, R., Kocsis, L., Wierzbinski, E., Balaeff, A., Keinan, S., Beratan, D.N., Achim, C., and Waldeck, D.H., *Role of Nucleobase Energetics and Nucleobase Interactions in Single-Stranded Peptide Nucleic Acid*

Charge Transfer. Journal of the American Chemical Society, 2009. **131**(18): p. 6498-6507.
220. Bard, A.J. and Faulkner, L.R., *Electrochemical Methods: Fundamentals and Applications*. 2000, New York: Wiley.
221. Grahame, D.C., *The electrical double layer and the theory of electro-capillarity.* Chemical Reviews, 1947. **41**: p. 441-501.
222. Kolb, D.M., *Reconstruction phenomena at metal-electrolyte interfaces.* Prog. Surf. Sci., 1996. **51**(2): p. 109-73.
223. Kolb, D.M. and Schneider, J., *Surface reconstruction in electrochemistry: gold(100)-(5 x 20), gold(111)-(1 x 23) and gold(110)-(1 x 2).* Electrochimica Acta, 1986. **31**(8): p. 929-36.
224. *Structure of electrified interfaces*, ed. J. Lipkowski and P.N. Ross. 1993, New York: VCH.
225. Herrero, E., Buller, L.J., and Abruna, H.D., *Underpotential deposition at single crystal surfaces of Au, Pt, Ag and other materials.* Chemical Reviews, 2001. **101**(7): p. 1897-1930.
226. Itaya, K., *In situ scanning tunneling microscopy in electrolyte solutions.* Progress in Surface Science, 1998. **58**(3): p. 121-247.
227. Yoshimoto, S. and Itaya, K., *Advances in supramolecularly assembled nanostructures of fullerenes and porphyrins at surfaces.* Journal of Porphyrins and Phthalocyanines, 2007. **11**(5-6): p. 313-333.
228. Yoshimoto, S., Yokoo, N., Fukuda, T., Kobayashi, N., and Itaya, K., *Formation of highly ordered porphyrin adlayers induced by electrochemical potential modulation.* Chemical Communications, 2006(5): p. 500-502.
229. Ye, T., *STRUCTURE, DYNAMICS, AND REACTIVITY OF MOLECULAR ASSEMBLIES*
AT INTERFACES, in *Department of Chemistry*. 2003, University of Pittsburgh: Pittsburgh.
230. Binnig, G. and Rohrer, H., *SURFACE IMAGING BY SCANNING TUNNELING MICROSCOPY.* Ultramicroscopy, 1983. **11**(2-3): p. 157-160.
231. Gewirth, A.A. and Niece, B.K., *Electrochemical applications of in situ scanning probe microscopy.* Chemical Reviews, 1997. **97**(4): p. 1129-1162.
232. Forrest, S.R., *Ultrathin organic films grown by organic molecular beam deposition and related techniques.* Chemical Reviews, 1997. **97**(6): p. 1793-1896.
233. Dolphin, V.D., *The Porphyrins*. 1979: Academic Press: New York.
234. Fukuzumi, S., *New perspective of electron transfer chemistry.* Organic & Biomolecular Chemistry, 2003. **1**(4): p. 609-620.
235. Guldi, D.M., *Fullerene-porphyrin architectures; photosynthetic antenna and reaction center models.* Chemical Society Reviews, 2002. **31**(1): p. 22-36.
236. Imahori, H., Mori, Y., and Matano, Y., *Nanostructured artificial photosynthesis.* Journal of Photochemistry and Photobiology C-Photochemistry Reviews, 2003. **4**(1): p. 51-83.
237. Yeager, E., *ELECTROCATALYSTS FOR O-2 REDUCTION.* Electrochimica Acta, 1984. **29**(11): p. 1527-1537.

238. Collman, J.P., Boulatov, R., Sunderland, C.J., and Fu, L., *Functional analogues of cytochrome c oxidase, myoglobin, and hemoglobin.* Chemical Reviews, 2004. **104**(2): p. 561-588.
239. Jung, T.A., Schlittler, R.R., and Gimzewski, J.K., *Conformational identification of individual adsorbed molecules with the STM.* Nature, 1997. **386**(6626): p. 696-698.
240. Yokoyama, T., Yokoyama, S., Kamikado, T., Okuno, Y., and Mashiko, S., *Selective assembly on a surface of supramolecular aggregates with controlled size and shape.* Nature, 2001. **413**(6856): p. 619-621.
241. Yokoyama, T., Kamikado, T., Yokoyama, S., and Mashiko, S., *Conformation selective assembly of carboxyphenyl substituted porphyrins on Au (111).* Journal of Chemical Physics, 2004. **121**(23): p. 11993-11997.
242. Scudiero, L., Barlow, D.E., and Hipps, K.W., *Physical properties and metal ion specific scanning tunneling microscopy images of metal(II) tetraphenylporphyrins deposited from vapor onto gold (111).* Journal of Physical Chemistry B, 2000. **104**(50): p. 11899-11905.
243. Scudiero, L., Barlow, D.E., Mazur, U., and Hipps, K.W., *Scanning tunneling microscopy, orbital-mediated tunneling spectroscopy, and ultraviolet photoelectron spectroscopy of metal(II) tetraphenylporphyrins deposited from vapor.* Journal of the American Chemical Society, 2001. **123**(17): p. 4073-4080.
244. Bonifazi, D., Spillmann, H., Kiebele, A., de Wild, M., Seiler, P., Cheng, F.Y., Guntherodt, H.J., Jung, T., and Diederich, F., *Supramolecular patterned surfaces driven by cooperative assembly of C-60 and porphyrins on metal substrates.* Angewandte Chemie-International Edition, 2004. **43**(36): p. 4759-4763.
245. Sugiura, K., Tanaka, H., Matsumoto, T., Kawai, T., and Sakata, Y., *A Mandala-patterned Bandanna-shaped porphyrin oligomer, C1244H1350N84Ni20O88, having a unique size and geometry.* Chemistry Letters, 1999(11): p. 1193-1194.
246. Kato, A., Sugiura, K., Miyasaka, H., Tanaka, H., Kawai, T., Sugimoto, M., and Yamashita, M., *A square cyclic porphyrin dodecamer: Synthesis and single-molecule characterization.* Chemistry Letters, 2004. **33**(5): p. 578-579.
247. Shoji, O., Tanaka, H., Kawai, T., and Kobuke, Y., *Single molecule visualization of coordination-assembled porphyrin macrocycles reinforced with covalent linkings.* Journal of the American Chemical Society, 2005. **127**(24): p. 8598-8599.
248. Qiu, X.H., Wang, C., Zeng, Q.D., Xu, B., Yin, S.X., Wang, H.N., Xu, S.D., and Bai, C.L., *Alkane-assisted adsorption and assembly of phthalocyanines and porphyrins.* Journal of the American Chemical Society, 2000. **122**(23): p. 5550-5556.
249. Kunitake, M., Batina, N., and Itaya, K., *SELF-ORGANIZED PORPHYRIN ARRAY ON IODINE-MODIFIED AU(111) IN ELECTROLYTE-SOLUTIONS - IN-SITU SCANNING-TUNNELING-MICROSCOPY STUDY.* Langmuir, 1995. **11**(7): p. 2337-2340.
250. Batina, N., Kunitake, M., and Itaya, K., *Highly ordered molecular arrays formed on iodine-modified Au(111) in solution: In situ STM imaging.* Journal of Electroanalytical Chemistry, 1996. **405**(1-2): p. 245-250.

251. Kunitake, M., Akiba, U., Batina, N., and Itaya, K., *Structures and dynamic formation processes of porphyrin adlayers on iodine-modified Au(111) in solution: In situ STM study.* Langmuir, 1997. **13**(6): p. 1607-1615.
252. Ogaki, K., Batina, N., Kunitake, M., and Itaya, K., *In situ scanning tunneling microscopy of ordering processes of adsorbed porphyrin on iodine-modified Ag(111).* Journal of Physical Chemistry, 1996. **100**(17): p. 7185-7190.
253. Sashikata, K., Sugata, T., Sugimasa, M., and Itaya, K., *In situ scanning tunneling microscopy observation of a porphyrin adlayer on an iodine-modified Pt(100) electrode.* Langmuir, 1998. **14**(10): p. 2896-2902.
254. Wan, L.J., Shundo, S., Inukai, J., and Itaya, K., *Ordered adlayers of organic molecules on sulfur-modified Au(111): In situ scanning tunneling microscopy study.* Langmuir, 2000. **16**(5): p. 2164-2168.
255. Yoshimoto, S., Inukai, J., Tada, A., Abe, T., Morimoto, T., Osuka, A., Furuta, H., and Itaya, K., *Adlayer structure of and electrochemical O-2 reduction on cobalt porphine-modiried and cobalt octaethylporphyrin-modifled Au(111) in HClO4.* Journal of Physical Chemistry B, 2004. **108**(6): p. 1948-1954.
256. Yoshimoto, S., Tada, A., Suto, K., Narita, R., and Itaya, K., *Adlayer structure and electrochemical reduction of O-2 on self-organized arrays of cobalt and copper tetraphenyl porphines on a Au(111) surface.* Langmuir, 2003. **19**(3): p. 672-677.
257. Yoshimoto, S., Tsutsumi, E., Suto, K., Honda, Y., and Itaya, K., *Molecular assemblies and redox reactions of zinc(II) tetraphenylporphyrin and zinc(II) phthalocyanine on Au(111) single crystal surface at electrochemical interface.* Chemical Physics, 2005. **319**(1-3): p. 147-158.
258. Yoshimoto, S., Sato, K., Sugawara, S., Chen, Y., Ito, O., Sawaguchi, T., Niwa, O., and Itaya, K., *Formation of supramolecular nanobelt arrays consisting of cobalt(II) "Picket-Fence" porphyrin on Au surfaces.* Langmuir, 2007. **23**(2): p. 809-816.
259. Tao, N.J., Cardenas, G., Cunha, F., and Shi, Z., *IN-SITU STM AND AFM STUDY OF PROTOPORPHYRIN AND IRON(III) AND ZINC(II) PROTOPORPHYRINS ADSORBED ON GRAPHITE IN AQUEOUS-SOLUTIONS.* Langmuir, 1995. **11**(11): p. 4445-4448.
260. Tao, N.J., *Probing potential-tuned resonant tunneling through redox molecules with scanning tunneling microscopy.* Physical Review Letters, 1996. **76**(21): p. 4066-4069.
261. He, Y., Ye, T., and Borguet, E., *Porphyrin self-assembly at electrochemical interfaces: Role of potential modulated surface mobility.* Journal of the American Chemical Society, 2002. **124**(40): p. 11964-11970.
262. Ye, T., He, Y.F., and Borguet, E., *Adsorption and electrochemical activity: An in situ electrochemical scanning tunneling microscopy study of electrode reactions and potential-induced adsorption of porphyrins.* Journal of Physical Chemistry B, 2006. **110**(12): p. 6141-6147.
263. He, Y. and Borguet, E., *Dynamics of porphyrin electron-transfer reactions at the electrode-electrolyte interface at the molecular level.* Angewandte Chemie-International Edition, 2007. **46**(32): p. 6098-6101.

264. Jung, T.A., Schlittler, R.R., Gimzewski, J.K., Tang, H., and Joachim, C., *Controlled room-temperature positioning of individual molecules: Molecular flexure and motion.* Science, 1996. **271**(5246): p. 181-184.
265. Lei, S.B., Wang, C., Yin, S.X., Wang, H.N., Xi, F., Liu, H.W., Xu, B., Wan, L.J., and Bai, C.L., *Surface stabilized porphyrin and phthalocyanine two-dimensional network connected by hydrogen bonds.* Journal of Physical Chemistry B, 2001. **105**(44): p. 10838-10841.
266. Zhou, Y.S., Wang, B., Zhu, M.Z., and Hou, J.G., *Observation of co-existence of 'face-on' and 'edge-on' stacking styles in a porphyrin monolayer.* Chemical Physics Letters, 2005. **403**(1-3): p. 140-145.
267. Hipps, K.W., Scudiero, L., Barlow, D.E., and Cooke, M.P., *A self-organized 2-dimensional bifunctional structure formed by supramolecular design.* Journal of the American Chemical Society, 2002. **124**(10): p. 2126-2127.
268. Xing, Y., He, Y., and Borguet, E., *Two dimensional charge diffusion in a self-assembled monolayer of redox active porphyrins.* (in preparation).
269. Wilson, G.S. and Neri, B.P., *CYCLIC VOLTAMMETRY OF PORPHYRINS AND METALLOPORPHYRINS.* Annals of the New York Academy of Sciences, 1973. **206**(OCT22): p. 568-578.
270. Neri, B.P. and Wilson, G.S., *ELECTROCHEMICAL STUDIES OF MESO-TETRA(4-N-METHYLPYRIDYL)PORPHIN IN ACID SOLUTION.* Analytical Chemistry, 1972. **44**(6): p. 1002-&.
271. Yuan, Q., Xing, Y., and Borguet, E., *An STM study of the pH dependent redox activity of a two dimensional hydrogen bonding porphyrin network at an electrochemical interface.* (Submitted).
272. Gingery, D. and Buhlmanna, P., *Single-step electrochemical method for producing very sharp Au scanning tunneling microscopy tips.* Review of Scientific Instruments, 2007. **78**(11).
273. Frisch, M.J.e.a., *Gaussian 03, Revision D.02*. 2004: Gaussian Inc.: Wallingford, CT, 2004.
274. Ridley, J. and Zerner, M., *INTERMEDIATE NEGLECT OF DIFFERENTIAL OVERLAP TECHNIQUE FOR SPECTROSCOPY - PYRROLE AND AZINES.* Theoretica Chimica Acta, 1973. **32**(2): p. 111-134.
275. Hutchison, G.R., Ratner, M.A., and Marks, T.J., *Accurate prediction of band gaps in neutral heterocyclic conjugated polymers.* Journal of Physical Chemistry A, 2002. **106**(44): p. 10596-10605.

BIBLIOGRAPHY

Adams, D. M., Brus, L., Chidsey, C. E. D., Creager, S., Creutz, C., Kagan, C. R., et al. (2003). Charge transfer on the nanoscale: Current status. *Journal of Physical Chemistry B, 107*(28), 6668-6697.

Adee, S. (2008). 37 years of Moore's law. *Ieee Spectrum, 45*(5), 56-56.

Altieri, A., Bottari, G., Dehez, F., Leigh, D. A., Wong, J. K. Y., & Zerbetto, F. (2003). Remarkable positional discrimination in bistable light- and heat-switchable hydrogen-bonded molecular shuttles. *Angewandte Chemie-International Edition, 42*(20), 2296-2300.

Andrews, D. Q., Van Duyne, R. P., & Ratner, M. A. (2008). Stochastic modulation in molecular electronic transport junctions: Molecular dynamics coupled with charge transport calculations. *Nano Letters, 8*(4), 1120-1126.

Arkin, M. R., Stemp, E. D. A., Holmlin, R. E., Barton, J. K., Hormann, A., Olson, E. J. C., et al. (1996). Rates of DNA-mediated electron transfer between metallointercalators. *Science, 273*(5274), 475-480.

Armitage, B. (1998). Photocleavage of nucleic acids. *Chemical Reviews, 98*(3), 1171-1200.

Ashton, P. R., Ballardini, R., Balzani, V., Baxter, I., Credi, A., Fyfe, M. C. T., et al. (1998). Acid-base controllable molecular shuttles. *Journal of the American Chemical Society, 120*(46), 11932-11942.

Ashton, P. R., Ballardini, R., Balzani, V., Credi, A., Dress, K. R., Ishow, E., et al. (2000). A photochemically driven molecular-level abacus. *Chemistry-a European Journal, 6*(19), 3558-3574.

Ashwell, G. J. (1990). CHEMISTRY - PHOTOCHROMIC MEMORY DEVICES. *Nature, 347*(6294), 617-617.

Atkins, P., & Paula, J. d. (2002). *Physical Chemistry* (7th Ed. ed.). New York: W. H. Freeman and Company.

Aviram, A. (1988). MOLECULES FOR MEMORY, LOGIC, AND AMPLIFICATION. *Journal of the American Chemical Society, 110*(17), 5687-5692.

Aviram, A., & Ratner, M. A. (1974). MOLECULAR RECTIFIERS. *Chemical Physics Letters, 29*(2), 277-283.

Baguley, B. C., Denny, W. A., Atwell, G. J., & Cain, B. F. (1981). POTENTIAL ANTI-TUMOR AGENTS .34. QUANTITATIVE RELATIONSHIPS BETWEEN DNA-BINDING AND MOLECULAR-STRUCTURE FOR 9-ANILINOACRIDINES SUBSTITUTED IN THE ANILINO RING. *Journal of Medicinal Chemistry, 24*(2), 170-177.

Ball, P., & Garwin, L. (1992). SCIENCE AT THE ATOMIC SCALE. *Nature, 355*(6363), 761-766.

Balzani, V. (2001). Electron Transfer in Chemistry. In (Vol. 3): Wiley-VCH: New York.

Balzani, V., Clemente-Leon, M., Credi, A., Semeraro, M., Venturi, M., Tseng, H. R., et al. (2006). A comparison of shuttling mechanisms in two constitutionally isomeric bistable rotaxane-based sunlight-powered nanomotors. *Australian Journal of Chemistry, 59*(3), 193-206.

Balzani, V., & Scandola, F. (1991). *Supramolecular Photochemistry (Chapter 5 and 6).* Horwood, Chichester, UK.

Bard, A. J., & Faulkner, L. R. (2000). *Electrochemical Methods: Fundamentals and Applications*. New York: Wiley.

Batina, N., Kunitake, M., & Itaya, K. (1996). Highly ordered molecular arrays formed on iodine-modified Au(111) in solution: In situ STM imaging. *Journal of Electroanalytical Chemistry, 405*(1-2), 245-250.

Beebe, J. M., Engelkes, V. B., Miller, L. L., & Frisbie, C. D. (2002). Contact resistance in metal-molecule-metal junctions based on aliphatic SAMs: Effects of surface linker and metal work function. *Journal of the American Chemical Society, 124*(38), 11268-11269.

Beenakker, C. W. J. (1997). Random-matrix theory of quantum transport. *Reviews of Modern Physics, 69*(3), 731-808.

Benniston, A. C., Goulle, V., Harriman, A., Lehn, J. M., & Marczinke, B. (1994). ELECTRON DELOCALIZATION IN POLYENE-BRIDGED BINUCLEAR COMPLEXES. *Journal of Physical Chemistry, 98*(32), 7798-7804.

Beratan, D. N., Priyadarshy, S., & Risser, S. M. (1997). DNA: Insulator or wire? *Chemistry & Biology, 4*(1), 3-8.

Berlin, Y. A., Kurnikov, I. V., Beratan, D., Ratner, M. A., & Burin, A. L. (2004). DNA electron transfer processes: Some theoretical notions. In *Long-Range Charge Transfer in DNA Ii* (Vol. 237, pp. 1-36). Berlin: Springer-Verlag Berlin.

Binnig, G., & Rohrer, H. (1983). SURFACE IMAGING BY SCANNING TUNNELING MICROSCOPY. *Ultramicroscopy, 11*(2-3), 157-160.

Bixon, M., & Jortner, J. (1997). Electron transfer via bridges. *Journal of Chemical Physics, 107*(13), 5154-5170.

Blackburn, G. M., & Gait, M. J. (1996). *Nucleic Acids in Chemistry and Biology, 2nd ed.* Oxford: Oxford University Press.

Bonifazi, D., Spillmann, H., Kiebele, A., de Wild, M., Seiler, P., Cheng, F. Y., et al. (2004). Supramolecular patterned surfaces driven by cooperative assembly of C-60 and porphyrins on metal substrates. *Angewandte Chemie-International Edition, 43*(36), 4759-4763.

Brandbyge, M., Mozos, J. L., Ordejon, P., Taylor, J., & Stokbro, K. (2002). Density-functional method for nonequilibrium electron transport. *Physical Review B, 65*(16).

Briones, C., Mateo-Marti, E., Gomez-Navarro, C., Parro, V., Roman, E., & Martin-Gago, J. A. (2004). Ordered self-assembled monolayers of peptide nucleic acids with DNA recognition capability. *Physical Review Letters, 93*(20).

Briones, C., Mateo-Marti, E., Gomez-Navarro, C., Parro, V., Roman, E., & Martin-Gago, J. A. (2005). *Structural and functional characterization of self-assembled monolayers of peptide nucleic acids and its interaction with complementary DNA*.

Britton, G. (1995). Structure and properties of carotenoids in relation to function. *Faseb Journal, 9*(15), 1551-1558.

Brun, A. M., & Harriman, A. (1992). DYNAMICS OF ELECTRON-TRANSFER BETWEEN INTERCALATED POLYCYCLIC MOLECULES - EFFECT OF INTERSPERSED BASES. *Journal of the American Chemical Society, 114*(10), 3656-3660.

Brun, A. M., & Harriman, A. (1994). ENERGY-TRANSFER AND ELECTRON-TRANSFER PROCESSES INVOLVING PALLADIUM PORPHYRINS BOUND TO DNA. *Journal of the American Chemical Society, 116*(23), 10383-10393.

Bumm, L. A., Arnold, J. J., Cygan, M. T., Dunbar, T. D., Burgin, T. P., Jones, L., et al. (1996). Are single molecular wires conducting? *Science, 271*(5256), 1705-1707.

Burrows, C. J., & Muller, J. G. (1998). Oxidative nucleobase modifications leading to strand scission. *Chemical Reviews, 98*(3), 1109-1151.

Cai, L. T., Skulason, H., Kushmerick, J. G., Pollack, S. K., Naciri, J., Shashidhar, R., et al. (2004). Nanowire-based molecular monolayer junctions: Synthesis, assembly, and electrical characterization. *Journal Of Physical Chemistry B, 108*(9), 2827-2832.

Carter, M. T., Rowe, G. K., Richardson, J. N., Tender, L. M., Terrill, R. H., & Murray, R. W. (1995). DISTANCE DEPENDENCE OF THE LOW-TEMPERATURE ELECTRON-TRANSFER KINETICS OF (FERROCENYLCARBOXY)-TERMINATED ALKANETHIOL MONOLAYERS. *Journal of the American Chemical Society, 117*(10), 2896-2899.

Chen, F., Hihath, J., Huang, Z. F., Li, X. L., & Tao, N. J. (2007). Measurement of single-molecule conductance. *Annual Review Of Physical Chemistry, 58*, 535-564.

Chen, I. W. P., Fu, M. D., Tseng, W. H., Chen, C. H., Chou, C. M., & Luh, T. Y. (2007). The effect of molecular conformation on single molecule conductance: measurements of pi-conjugated oligoaryls by STM break junction. *Chemical Communications*(29), 3074-3076.

Chen, J., Reed, M. A., Rawlett, A. M., & Tour, J. M. (1999). Large on-off ratios and negative differential resistance in a molecular electronic device. *Science, 286*(5444), 1550-1552.

Chen, J., Wang, W., Reed, M. A., Rawlett, A. M., Price, D. W., & Tour, J. M. (2000). Room-temperature negative differential resistance in nanoscale molecular junctions. *Applied Physics Letters, 77*(8), 1224-1226.

Chidsey, C. E. D. (1991). FREE-ENERGY AND TEMPERATURE-DEPENDENCE OF ELECTRON-TRANSFER AT THE METAL-ELECTROLYTE INTERFACE. *Science, 251*(4996), 919-922.

Choi, H., & Mody, C. C. M. (2009). The Long History of Molecular Electronics: Microelectronics Origins of Nanotechnology. *Social Studies of Science, 39*(1), 11-50.

Choi, S. H., Kim, B., & Frisbie, C. D. (2008). Electrical resistance of long conjugated molecular wires. *Science, 320*(5882), 1482-1486.

Clavilier, J., Faure, R., Guinet, G., & Durand, R. (1980). PREPARATION OF MONO-CRYSTALLINE PT MICROELECTRODES AND ELECTROCHEMICAL STUDY OF THE PLANE SURFACES CUT IN THE DIRECTION OF THE (111) AND (110) PLANES. *Journal of Electroanalytical Chemistry, 107*(1), 205-209.

Cohen, R., Stokbro, K., Martin, J. M. L., & Ratner, M. A. (2007). Charge transport in conjugated aromatic molecular junctions: Molecular conjugation and molecule-electrode coupling. *Journal of Physical Chemistry C, 111*(40), 14893-14902.

Collier, C. P., Mattersteig, G., Wong, E. W., Luo, Y., Beverly, K., Sampaio, J., et al. (2000). A [2]catenane-based solid state electronically reconfigurable switch. *Science, 289*(5482), 1172-1175.

Collman, J. P., Boulatov, R., Sunderland, C. J., & Fu, L. (2004). Functional analogues of cytochrome c oxidase, myoglobin, and hemoglobin. *Chemical Reviews, 104*(2), 561-588.

Colorado, R., Jr., Villazana, R. J., & Lee, T. R. (1998). Self-assembled monolayers on gold generated from aliphatic dithiocarboxylic acids. *Langmuir, 14*(22), 6337-6340.

Creager, S., Yu, C. J., Bamdad, C., O'Connor, S., MacLean, T., Lam, E., et al. (1999). Electron transfer at electrodes through conjugated "molecular wire" bridges. *Journal of the American Chemical Society, 121*(5), 1059-1064.

Cui, X. D., Primak, A., Zarate, X., Tomfohr, J., Sankey, O. F., Moore, A. L., et al. (2001). Reproducible measurement of single-molecule conductivity. *Science, 294*(5542), 571-574.

Cui, X. D., Zarate, X., Tomfohr, J., Sankey, O. F., Primak, A., Moore, A. L., et al. (2002). Making electrical contacts to molecular monolayers. *Nanotechnology, 13*(1), 5-14.

Dadosh, T., Gordin, Y., Krahne, R., Khivrich, I., Mahalu, D., Frydman, V., et al. (2005). Measurement of the conductance of single conjugated molecules. *Nature, 436*(7051), 677-680.

Dagama, A. A. S. (1985). DONOR-ACCEPTOR INTERACTION IN METALLOPROTEINS. *Theoretica Chimica Acta, 68*(2), 159-169.

Datta, S. (2005). *Quantum Transport: Atom to Transistor*: Cambridge University Press.

Davidson, V. L. (2000). What controls the rates of interprotein electron-transfer reactions. *Accounts of Chemical Research, 33*(2), 87-93.

Davis, W. B., Ratner, M. A., & Wasielewski, M. R. (2001). Conformational gating of long distance electron transfer through wire-like bridges in donor-bridge-acceptor molecules. *Journal of the American Chemical Society, 123*(32), 7877-7886.

Davis, W. B., Svec, W. A., Ratner, M. A., & Wasielewski, M. R. (1998). Molecular-wire behaviour in p-phenylenevinylene oligomers. *Nature, 396*(6706), 60-63.

de la Torre, G., Giacalone, F., Segura, J. L., Martin, N., & Guldi, D. M. (2005). Electronic communication through pi-conjugated wires in covalently linked porphyrin/C-60 ensembles. *Chemistry-A European Journal, 11*(4), 1267-1280.

deSilva, A. P., Gunaratne, H. Q. N., Gunnlaugsson, T., Huxley, A. J. M., McCoy, C. P., Rademacher, J. T., et al. (1997). Signaling recognition events with fluorescent sensors and switches. *Chemical Reviews, 97*(5), 1515-1566.

Dolphin, V. D. (1979). *The Porphyrins*: Academic Press: New York.

Donhauser, Z. J., Mantooth, B. A., Kelly, K. F., Bumm, L. A., Monnell, J. D., Stapleton, J. J., et al. (2001). Conductance switching in single molecules through conformational changes. *Science, 292*(5525), 2303-2307.

Dueholm, K. L., Egholm, M., Behrens, C., Christensen, L., Hansen, H. F., Vulpius, T., et al. (1994). SYNTHESIS OF PEPTIDE NUCLEIC-ACID MONOMERS CONTAINING THE 4 NATURAL NUCLEOBASES - THYMINE, CYTOSINE, ADENINE, AND GUANINE AND THEIR OLIGOMERIZATION. *Journal of Organic Chemistry, 59*(19), 5767-5773.

Eng, M. P., & Albinsson, B. (2006). Non-exponential distance dependence of bridge-mediated electronic coupling. *Angewandte Chemie-International Edition, 45*(34), 5626-5629.

Evers, F., Weigend, F., & Koentopp, M. (2004). Conductance of molecular wires and transport calculations based on density-functional theory. *Physical Review B, 69*(23).

Fabbrizzi, L., & Poggi, A. (1995). SENSORS AND SWITCHES FROM SUPRAMOLECULAR CHEMISTRY. *Chemical Society Reviews, 24*(3), 197-202.

Fan, F. R. F., Lai, R. Y., Cornil, J., Karzazi, Y., Bredas, J. L., Cai, L. T., et al. (2004). Electrons are transported through phenylene-ethynylene oligomer monolayers via localized molecular orbitals. *Journal of the American Chemical Society, 126*(8), 2568-2573.

Feynman, R. P. "There's plenty of room at the bottom", a talk given to the annual meeting of the American Physical Society at Caltech, December 29, 1959.

Forrest, S. R. (1997). Ultrathin organic films grown by organic molecular beam deposition and related techniques. *Chemical Reviews, 97*(6), 1793-1896.

Frank, D. J., Dennard, R. H., Nowak, E., Solomon, P. M., Taur, Y., & Wong, H. S. P. (2001). Device scaling limits of Si MOSFETs and their application dependencies. *Proceedings of the Ieee, 89*(3), 259-288.

Frisch, M. J. e. a. (2004). *Gaussian 03, Revision D.02*: Gaussian Inc.: Wallingford, CT, 2004.

Fromherz, P., & Rieger, B. (1986). PHOTOINDUCED ELECTRON-TRANSFER IN DNA MATRIX FROM INTERCALATED ETHIDIUM TO CONDENSED METHYLVIOLOGEN. *Journal of the American Chemical Society, 108*(17), 5361-5362.

Fukuzumi, S. (2003). New perspective of electron transfer chemistry. *Organic & Biomolecular Chemistry, 1*(4), 609-620.

Galperin, M., Ratner, M. A., & Nitzan, A. (2005). Hysteresis, switching, and negative differential resistance in molecular junctions: A polaron model. *Nano Letters, 5*(1), 125-130.

Gewirth, A. A., & Niece, B. K. (1997). Electrochemical applications of in situ scanning probe microscopy. *Chemical Reviews, 97*(4), 1129-1162.

Ghosh, A. W., Zahid, F., Datta, S., & Birge, R. R. (2002). Charge transfer in molecular conductors - oxidation or reduction? *Chemical Physics, 281*(2-3), 225-230.

Giacalone, F., Segura, J. L., Martin, N., & Guldi, D. M. (2004). Exceptionally small attenuation factors in molecular wires. *Journal Of The American Chemical Society, 126*(17), 5340-5341.

Gingery, D., & Buhlmanna, P. (2007). Single-step electrochemical method for producing very sharp Au scanning tunneling microscopy tips. *Review of Scientific Instruments, 78*(11).

Goldman, C. (1991). LONG-RANGE ELECTRON-TRANSFER IN PROTEINS - A RENORMALIZED-PERTURBATION-EXPANSION APPROACH. *Physical Review A, 43*(8), 4500-4509.

Goulle, V., Harriman, A., & Lehn, J. M. (1993). AN ELECTRO-PHOTOSWITCH - REDOX SWITCHING OF THE LUMINESCENCE OF A BIPYRIDINE

METAL-COMPLEX. *Journal of the Chemical Society-Chemical Communications*(12), 1034-1036.

Grahame, D. C. (1947). The electrical double layer and the theory of electro-capillarity. *Chemical Reviews, 41*, 441-501.

Green, J. E., Choi, J. W., Boukai, A., Bunimovich, Y., Johnston-Halperin, E., DeIonno, E., et al. (2007). A 160-kilobit molecular electronic memory patterned at 10(11) bits per square centimetre. *Nature, 445*(7126), 414-417.

Greenfield, S. R., Svec, W. A., Gosztola, D., & Wasielewski, M. R. (1996). Multistep photochemical charge separation in rod-like molecules based on aromatic imides and diimides. *Journal of the American Chemical Society, 118*(28), 6767-6777.

Grigg, R., Holmes, J. M., Jones, S. K., & Norbert, W. (1994). LUMINESCENT PH SENSORS BASED ON P-TERT-BUTYLCALIX[4]ARENE-LINKED RUTHENIUM(II) TRISBIPYRIDYL COMPLEXES. *Journal of the Chemical Society-Chemical Communications*(2), 185-187.

Guldi, D. M. (2002). Fullerene-porphyrin architectures; photosynthetic antenna and reaction center models. *Chemical Society Reviews, 31*(1), 22-36.

Gust, D., Moore, T. A., & Moore, A. L. (2001). Mimicking photosynthetic solar energy transduction. *Accounts of Chemical Research, 34*(1), 40-48.

Haiss, W., Albrecht, T., van Zalinge, H., Higgins, S. J., Bethell, D., Hobenreich, H., et al. (2007). Single-molecule conductance of redox molecules in electrochemical scanning tunneling microscopy. *Journal of Physical Chemistry B, 111*(24), 6703-6712.

Hatcher, E., Balaeff, A., Keinan, S., Venkatramani, R., & Beratan, D. N. (2008). PNA versus DNA: Effects of Structural Fluctuations on Electronic Structure and Hole-Transport Mechanisms. *J. Am. Chem. Soc.*(ASAP Article; DOI: 10.1021/ja802541e).

He, J., Chen, F., Li, J., Sankey, O. F., Terazono, Y., Herrero, C., et al. (2005). Electronic decay constant of carotenoid polyenes from single-molecule measurements. *Journal of the American Chemical Society, 127*(5), 1384-1385.

He, Y., & Borguet, E. (2007). Dynamics of porphyrin electron-transfer reactions at the electrode-electrolyte interface at the molecular level. *Angewandte Chemie-International Edition, 46*(32), 6098-6101.

He, Y., Ye, T., & Borguet, E. (2002). Porphyrin self-assembly at electrochemical interfaces: Role of potential modulated surface mobility. *Journal of the American Chemical Society, 124*(40), 11964-11970.

Heath, J. R., Kuekes, P. J., Snider, G. S., & Williams, R. S. (1998). A defect-tolerant computer architecture: Opportunities for nanotechnology. *Science, 280*(5370), 1716-1721.

Heath, J. R., & Ratner, M. A. (2003). Molecular electronics. *Physics Today, 56*(5), 43-49.

Heimel, G., Romaner, L., Bredas, J. L., & Zojer, E. (2006). Interface energetics and level alignment at covalent metal-molecule junctions: pi-conjugated thiols on gold. *Physical Review Letters, 96*(19), 4.

Herrero, E., Buller, L. J., & Abruna, H. D. (2001). Underpotential deposition at single crystal surfaces of Au, Pt, Ag and other materials. *Chemical Reviews, 101*(7), 1897-1930.

Hipps, K. W., Scudiero, L., Barlow, D. E., & Cooke, M. P. (2002). A self-organized 2-dimensional bifunctional structure formed by supramolecular design. *Journal of the American Chemical Society, 124*(10), 2126-2127.

Ho, P. S., & Kwok, T. (1989). ELECTROMIGRATION IN METALS. *Reports on Progress in Physics, 52*(3), 301-348.

Hopfield, J. J., Onuchic, J. N., & Beratan, D. N. (1988). A MOLECULAR SHIFT REGISTER BASED ON ELECTRON-TRANSFER. *Science, 241*(4867), 817-820.

Hsung, R. P., Babcock, J. R., Chidsey, C. E. D., & Sita, L. R. (1995). THIOPHENOL PROTECTING GROUPS FOR THE PALLADIUM-CATALYZED HECK REACTION - EFFICIENT SYNTHESES OF CONJUGATED ARYLTHIOLS. *Tetrahedron Letters, 36*(26), 4525-4528.

Huang, Z. F., Chen, F., Bennett, P. A., & Tao, N. J. (2007). Single molecule junctions formed via au-thiol contact: Stability and breakdown mechanism. *Journal of the American Chemical Society, 129*(43), 13225-13231.

Huck, N. P. M., Jager, W. F., deLange, B., & Feringa, B. L. (1996). Dynamic control and amplification of molecular chirality by circular polarized light. *Science, 273*(5282), 1686-1688.

Hush, N. S. (1968). HOMOGENEOUS AND HETEROGENEOUS OPTICAL AND THERMAL ELECTRON TRANSFER. *Electrochimica Acta, 13*(5), 1005-&.

Hutchison, G. R., Ratner, M. A., & Marks, T. J. (2002). Accurate prediction of band gaps in neutral heterocyclic conjugated polymers. *Journal of Physical Chemistry A, 106*(44), 10596-10605.

Imahori, H., Mori, Y., & Matano, Y. (2003). Nanostructured artificial photosynthesis. *Journal of Photochemistry and Photobiology C-Photochemistry Reviews, 4*(1), 51-83.

Itaya, K. (1998). In situ scanning tunneling microscopy in electrolyte solutions. *Progress in Surface Science, 58*(3), 121-247.

Jimenez, M. C., Dietrich-Buchecker, C., & Sauvage, J. P. (2000). Towards synthetic molecular muscles: Contraction and stretching of a linear rotaxane dimer. *Angewandte Chemie-International Edition, 39*(18), 3284-+.

Joachim, C., Gimzewski, J. K., & Aviram, A. (2000). Electronics using hybrid-molecular and mono-molecular devices. *Nature, 408*, 541-548.

Jortner, J., & Ratner, M. (1997). *Molecular Electronics*: Blackwell Science: Oxford, UK.

Jung, T. A., Schlittler, R. R., & Gimzewski, J. K. (1997). Conformational identification of individual adsorbed molecules with the STM. *Nature, 386*(6626), 696-698.

Jung, T. A., Schlittler, R. R., Gimzewski, J. K., Tang, H., & Joachim, C. (1996). Controlled room-temperature positioning of individual molecules: Molecular flexure and motion. *Science, 271*(5246), 181-184.

Kato, A., Sugiura, K., Miyasaka, H., Tanaka, H., Kawai, T., Sugimoto, M., et al. (2004). A square cyclic porphyrin dodecamer: Synthesis and single-molecule characterization. *Chemistry Letters, 33*(5), 578-579.

Ke, S. H., Baranger, H. U., & Yang, W. T. (2007). Role of the exchange-correlation potential in ab initio electron transport calculations. *Journal of Chemical Physics, 126*(20).

Kelley, S. O., Holmlin, R. E., Stemp, E. D. A., & Barton, J. K. (1997). Photoinduced electron transfer in ethidium-modified DNA duplexes: Dependence on distance and base stacking. *Journal of the American Chemical Society, 119*(41), 9861-9870.

Kijima, H., Takeuchi, M., Robertson, A., Shinkai, S., Cooper, C., & James, T. D. (1999). Exploitation of a novel 'on-off' photoinduced electron-transfer (PET) sensor against conventional 'off-on' PET sensors. *Chemical Communications*(19), 2011-2012.

Kim, B., Beebe, J. M., Jun, Y., Zhu, X. Y., & Frisbie, C. D. (2006). Correlation between HOMO alignment and contact resistance in molecular junctions: Aromatic thiols versus aromatic isocyanides. *Journal of the American Chemical Society, 128*(15), 4970-4971.

Klumpp, T., Linsenmann, M., Larson, S. L., Limoges, B. R., Burssner, D., Krissinel, E. B., et al. (1999). Spin chemical control of photoinduced electron-transfer processes in ruthenium(II)-trisbipyridine-based supramolecular triads. *Journal of the American Chemical Society, 121*(5), 1076-1087.

Koentopp, M., Burke, K., & Evers, F. (2006). Zero-bias molecular electronics: Exchange-correlation corrections to Landauer's formula. *Physical Review B, 73*(12).

Koentopp, M., Chang, C., Burke, K., & Car, R. (2008). Density functional calculations of nanoscale conductance. *Journal of Physics-Condensed Matter, 20*(8).

Kolb, D. M. (1996). Reconstruction phenomena at metal-electrolyte interfaces. *Prog. Surf. Sci., 51*(2), 109-173.

Kolb, D. M., & Schneider, J. (1986). Surface reconstruction in electrochemistry: gold(100)-(5 x 20), gold(111)-(1 x 23) and gold(110)-(1 x 2). *Electrochimica Acta, 31*(8), 929-936.

Kunitake, M., Akiba, U., Batina, N., & Itaya, K. (1997). Structures and dynamic formation processes of porphyrin adlayers on iodine-modified Au(111) in solution: In situ STM study. *Langmuir, 13*(6), 1607-1615.

Kunitake, M., Batina, N., & Itaya, K. (1995). SELF-ORGANIZED PORPHYRIN ARRAY ON IODINE-MODIFIED AU(111) IN ELECTROLYTE-SOLUTIONS - IN-SITU SCANNING-TUNNELING-MICROSCOPY STUDY. *Langmuir, 11*(7), 2337-2340.

Kushmerick, J. G. (2005). Metal-molecule contacts. *Materials Today*, 26-30.

Kushmerick, J. G., Holt, D. B., Pollack, S. K., Ratner, M. A., Yang, J. C., Schull, T. L., et al. (2002). Effect of bond-length alternation in molecular wires. *Journal of the American Chemical Society, 124*(36), 10654-10655.

Kushmerick, J. G., Holt, D. B., Yang, J. C., Naciri, J., Moore, M. H., & Shashidhar, R. (2002). Metal-molecule contacts and charge transport across monomolecular layers: Measurement and theory. *Physical Review Letters, 89*(8).

Kushmerick, J. G., Naciri, J., Yang, J. C., & Shashidhar, R. (2003). Conductance scaling of molecular wires in parallel. *Nano Letters, 3*(7), 897-900.

Landauer, R. (1957). SPATIAL VARIATION OF CURRENTS AND FIELDS DUE TO LOCALIZED SCATTERERS IN METALLIC CONDUCTION. *Ibm Journal of Research and Development, 1*(3), 223-231.

Landauer, R. (1970). ELECTRICAL RESISTANCE OF DISORDERED ONE-DIMENSIONAL LATTICES. *Philosophical Magazine, 21*(172), 863-&.

Lee, M. H., Speyer, G., & Sankey, O. F. (2006). Electron transport through single alkane molecules with different contact geometries on gold. *Physica Status Solidi B-Basic Solid State Physics, 243*(9), 2021-2029.

Lei, S. B., Wang, C., Yin, S. X., Wang, H. N., Xi, F., Liu, H. W., et al. (2001). Surface stabilized porphyrin and phthalocyanine two-dimensional network connected by hydrogen bonds. *Journal of Physical Chemistry B, 105*(44), 10838-10841.

Li, C., Pobelov, I., Wandlowski, T., Bagrets, A., Arnold, A., & Evers, F. (2008). Charge transport in single Au vertical bar alkanedithiol vertical bar Au junctions: Coordination geometries and conformational degrees of freedom. *Journal of the American Chemical Society, 130*, 318-326.

Li, X. L., Xu, B. Q., Xiao, X. Y., Yang, X. M., Zang, L., & Tao, N. J. (2006). Controlling charge transport in single molecules using electrochemical gate. *Faraday Discussions, 131*, 111-120.

Li, Z., & Kosov, D. S. (2006). Orbital interaction mechanisms of conductance enhancement and rectification by dithiocarboxylate anchoring group. *Journal Of Physical Chemistry B, 110*(39), 19116-19120.

Li, Z. Y., & Kosov, D. S. (2006a). Dithiocarbamate anchoring in molecular wire junctions: A first principles study. *Journal of Physical Chemistry B, 110*(20), 9893-9898.

Li, Z. Y., & Kosov, D. S. (2006b). Orbital interaction mechanisms of conductance enhancement and rectification by dithiocarboxylate anchoring group. *Journal of Physical Chemistry B, 110*(39), 19116-19120.

Lindsay, S. M., & Ratner, M. A. (2007). Molecular transport junctions: Clearing mists. *Advanced Materials, 19*(1), 23-31.

Liu, K., Li, G. R., Wang, X. H., & Wang, F. S. (2008). Length dependence of electron conduction for oligo(1,4-phenylene ethynylene)s: A conductive probe-atomic force microscopy investigation. *Journal of Physical Chemistry C, 112*(11), 4342-4349.

Liu, Z. F., Hashimoto, K., & Fujishima, A. (1990). PHOTOELECTROCHEMICAL INFORMATION-STORAGE USING AN AZOBENZENE DERIVATIVE. *Nature, 347*(6294), 658-660.

Lu, W., & Lieber, C. M. (2007). Nanoelectronics from the bottom up. *Nature Materials, 6*(11), 841-850.

Lucia, L. A., Whitten, D. G., & Schanze, K. S. (1996). Photoinduced charge separation promoted by ring opening of a piperazine radical cation. *Journal of the American Chemical Society, 118*(12), 3057-3058.

Mahapatro, A. K., Ghosh, S., & Janes, D. B. (2006). Nanometer scale electrode separation (nanogap) using electromigration at room temperature. *Ieee Transactions on Nanotechnology, 5*(3), 232-236.

Marcus, R. A. (1956). THEORY OF OXIDATION-REDUCTION REACTIONS INVOLVING ELECTRON TRANSFER .1. *Journal of Chemical Physics, 24*(5), 966-978.

Martin, N., Sanchez, L., Illescas, B., & Perez, I. (1998). C-60-based electroactive organofullerenes. *Chemical Reviews, 98*(7), 2527-2547.

Mateo-Marti, E., Briones, C., Roman, E., Briand, E., Pradier, C. M., & Martin-Gago, J. A. (2005). Self-assembled monolayers of peptide nucleic acids on gold surfaces: A spectroscopic study. *Langmuir, 21*(21), 9510-9517.

Mayor, M., Buschel, M., Fromm, K. M., Lehn, J. M., & Daub, J. (2002). *Electron transfer through bridging molecular structures*.

McLendon, G., & Hake, R. (1992). INTERPROTEIN ELECTRON-TRANSFER. *Chemical Reviews, 92*(3), 481-490.

Melosh, N. A., Boukai, A., Diana, F., Gerardot, B., Badolato, A., Petroff, P. M., et al. (2003). Ultrahigh-density nanowire lattices and circuits. *Science, 300*(5616), 112-115.

Meyer, T. J., & Taube, H. (1968). ELECTRON-TRANSFER REACTIONS OF RUTHENIUM AMMINES. *Inorganic Chemistry, 7*(11), 2369-&.

Millar, D., Venkataraman, L., & Doerrer, L. H. (2007). Efficacy of Au-Au contacts for scanning tunneling microscopy molecular conductance measurements. *Journal of Physical Chemistry C, 111*(47), 17635-17639.

Miller, C., Cuendet, P., & Gratzel, M. (1991). ADSORBED OMEGA-HYDROXY THIOL MONOLAYERS ON GOLD ELECTRODES - EVIDENCE FOR ELECTRON-TUNNELING TO REDOX SPECIES IN SOLUTION. *Journal of Physical Chemistry, 95*(2), 877-886.

Mirkin, C. A., & Ratner, M. A. (1992). MOLECULAR ELECTRONICS. *Annual Review of Physical Chemistry, 43*, 719-754.

Mitchell, P. (1961). COUPLING OF PHOSPHORYLATION TO ELECTRON AND HYDROGEN TRANSFER BY A CHEMI-OSMOTIC TYPE OF MECHANISM. *Nature, 191*(478), 144-&.

Mitchell, R. H., Ward, T. R., Wang, Y. X., & Dibble, P. W. (1999). Pi-switches: Synthesis of three-way molecular switches based on the dimethyldihydropyrene-metacyclophanediene valence isomerization. *Journal of the American Chemical Society, 121*(11), 2601-2602.

Moore, G. E. (1998). Cramming more components onto integrated circuits (Reprinted from Electronics, pg 114-117, April 19, 1965). *Proceedings of the Ieee, 86*(1), 82-85.

Moreland, J., & Ekin, J. W. (1985). ELECTRON-TUNNELING EXPERIMENTS USING NB-SN BREAK JUNCTIONS. *Journal of Applied Physics, 58*(10), 3888-3895.

Morita, T., & Lindsay, S. (2007). Determination of single molecule conductances of alkanedithiols by conducting-atomic force microscopy with large gold nanoparticles. *Journal Of The American Chemical Society, 129*(23), 7262-+.

Neri, B. P., & Wilson, G. S. (1972). ELECTROCHEMICAL STUDIES OF MESO-TETRA(4-N-METHYLPYRIDYL)PORPHIN IN ACID SOLUTION. *Analytical Chemistry, 44*(6), 1002-&.

Netzel, T. L. (1997). *Electron transfer reactions in DNA*.

Netzel, T. L. (1998). Present status and future directions of research in electron-transfer mediated by DNA. *Journal of Biological Inorganic Chemistry, 3*(2), 210-214.

Newton, M. D., & Smalley, J. F. (2007). Interfacial bridge-mediated electron transfer: mechanistic analysis based on electrochemical kinetics and theoretical modelling. *Physical Chemistry Chemical Physics, 9*(5), 555-572.

Nishikawa, A., Tobita, J., Kato, Y., Fujii, S., Suzuki, M., & Fujihira, M. (2007). Accurate determination of multiple sets of single molecular conductance of Au/1,6-hexanedithiol/Au break junctions by ultra-high vacuum-scanning tunneling microscope and analyses of individual current-separation curves. *Nanotechnology, 18*.

Nitzan, A., & Ratner, M. A. (2003). Electron transport in molecular wire junctions. *Science, 300*(5624), 1384-1389.

Niyogi, K. K. (1999). Photoprotection revisited: Genetic and molecular approaches. *Annual Review of Plant Physiology and Plant Molecular Biology, 50*, 333-359.

Nocek, J. M., Zhou, J. S., DeForest, S., Priyadarshy, S., Beratan, D. N., Onuchic, J. N., et al. (1996). Theory and practice of electron transfer within protein-protein complexes: Application to the multidomain binding of cytochrome c by cytochrome c peroxidase. *Chemical Reviews, 96*(7), 2459-2489.

O'Neill, M. A., & Barton, J. K. (2004). DNA mediated charge transport charege transfer chemistry and biology. In G. B. Schuster (Ed.), *Long-Range Charge Transfer in DNA* (Vol. Vol.236, pp. pg 67-114): Springer: Berlin/Heidelberg.

Ogaki, K., Batina, N., Kunitake, M., & Itaya, K. (1996). In situ scanning tunneling microscopy of ordering processes of adsorbed porphyrin on iodine-modified Ag(111). *Journal of Physical Chemistry, 100*(17), 7185-7190.

Park, H., Lim, A. K. L., Alivisatos, A. P., Park, J., & McEuen, P. L. (1999). Fabrication of metallic electrodes with nanometer separation by electromigration. *Applied Physics Letters, 75*(2), 301-303.

Park, T. H., & Therien, M. J. (2007). Carbodithioate-terminated oligo(phenyleneethynylene)s: Synthesis and surface functionalization of gold nanoparticles. *Organic Letters, 9*(15), 2779-2782.

Parthenopoulos, D. A., & Rentzepis, P. M. (1989). 3-DIMENSIONAL OPTICAL STORAGE MEMORY. *Science, 245*(4920), 843-845.

Patrone, L., Palacin, S., & Bourgoin, J. P. (2003). Direct comparison of the electronic coupling efficiency of sulfur and selenium alligator clips for molecules adsorbed onto gold electrodes. *Applied Surface Science, 212*, 446-451.

Patrone, L., Palacin, S., Charlier, J., Armand, F., Bourgoin, J. P., Tang, H., et al. (2003). Evidence of the key role of metal-molecule bonding in metal-molecule-metal transport experiments. *Physical Review Letters, 91*(9).

Paul, A., Bezer, S., Venkatramani, R., Kocsis, L., Wierzbinski, E., Balaeff, A., et al. (2009). Role of Nucleobase Energetics and Nucleobase Interactions in Single-Stranded Peptide Nucleic Acid Charge Transfer. *Journal of the American Chemical Society, 131*(18), 6498-6507.

Paul, A., Watson, R. M., Lund, P., Xing, Y. J., Burke, K., He, Y. F., et al. (2008). Charge transfer through single-stranded peptide nucleic acid composed of thymine Nucleotides. *Journal of Physical Chemistry C, 112*(18), 7233-7240.

Paulsson, M., Frederiksen, T., & Brandbyge, M. (2006). Inelastic transport through molecules: Comparing first-principles calculations to experiments. *Nano Letters, 6*(2), 258-262.

Peptide Nucleic Acids: Protocols and Applications (Second Edition). (2004). In P. E. Nielsen (Ed.): Horizon Bioscience.

Piccinin, S., Selloni, A., Scandolo, S., Car, R., & Scoles, G. (2003). Electronic properties of metal-molecule-metal systems at zero bias: A periodic density functional study. *Journal of Chemical Physics, 119*(13), 6729-6735.

Polese, A., Mondini, S., Bianco, A., Toniolo, C., Scorrano, G., Guldi, D. M., et al. (1999). Solvent-dependent intramolecular electron transfer in a peptide-linked [Ru(bpy)(3)](2+)-C-60 dyad. *Journal of the American Chemical Society, 121*(14), 3446-3452.

Priyadarshy, S., Risser, S. M., & Beratan, D. N. (1996). DNA is not a molecular wire: Protein-like electron-transfer predicted for an extended pi-electron system. *Journal of Physical Chemistry, 100*(44), 17678-17682.

Qiu, X. H., Wang, C., Zeng, Q. D., Xu, B., Yin, S. X., Wang, H. N., et al. (2000). Alkane-assisted adsorption and assembly of phthalocyanines and porphyrins. *Journal of the American Chemical Society, 122*(23), 5550-5556.

Querner, C., Reiss, P., Bleuse, J., & Pron, A. (2004). Chelating Ligands for nanocrystals' surface functionalization. *Journal Of The American Chemical Society, 126*(37), 11574-11582.

Ramachandran, G. K., Hopson, T. J., Rawlett, A. M., Nagahara, L. A., Primak, A., & Lindsay, S. M. (2003). A bond-fluctuation mechanism for stochastic switching in wired molecules. *Science, 300*(5624), 1413-1416.

Ramirez, B. E., Malmstrom, B. G., Winkler, J. R., & Gray, H. B. (1995). The currents of life: The terminal electron-transfer complex of respiration. *Proceedings of the National Academy of Sciences of the United States of America, 92*(26), 11949-11951.

Reed, M. A., Zhou, C., Muller, C. J., Burgin, T. P., & Tour, J. M. (1997). Conductance of a molecular junction. *Science, 278*, 252-254.

Reichert, J. (2002). Driving current through single organic molecules. *Phys. Rev. Lett., 88*, 176804.

Reichert, J., Ochs, R., Beckmann, D., Weber, H. B., Mayor, M., & von Lohneysen, H. (2002). Driving current through single organic molecules. *Physical Review Letters, 88*(17), 4.

Reimers, J. R., Cai, Z. L., Bilic, A., & Hush, N. S. (2003). *The appropriateness of density-functional theory for the calculation of molecular electronics properties*.

Reimers, J. R., & Hush, N. S. (1994). ELECTRON-TRANSFER AND ENERGY-TRANSFER THROUGH BRIDGED SYSTEMS .3. TIGHT-BINDING LINKAGES WITH ZERO OR NONZERO ASYMPTOTIC BAND-GAP. *Journal of Photochemistry and Photobiology a-Chemistry, 82*(1-3), 31-46.

Ridley, J., & Zerner, M. (1973). INTERMEDIATE NEGLECT OF DIFFERENTIAL OVERLAP TECHNIQUE FOR SPECTROSCOPY - PYRROLE AND AZINES. *Theoretica Chimica Acta, 32*(2), 111-134.

Romaner, L., Heimel, G., Gruber, M., Bredas, J. L., & Zojer, E. (2006). Stretching and breaking of a molecular junction. *Small, 2*, 1468-1475.

Salomon, A., Cahen, D., Lindsay, S., Tomfohr, J., Engelkes, V. B., & Frisbie, C. D. (2003). Comparison of electronic transport measurements on organic molecules. *Advanced Materials, 15*(22), 1881-1890.

Sashikata, K., Sugata, T., Sugimasa, M., & Itaya, K. (1998). In situ scanning tunneling microscopy observation of a porphyrin adlayer on an iodine-modified Pt(100) electrode. *Langmuir, 14*(10), 2896-2902.

Scudiero, L., Barlow, D. E., & Hipps, K. W. (2000). Physical properties and metal ion specific scanning tunneling microscopy images of metal(II) tetraphenylporphyrins deposited from vapor onto gold (111). *Journal of Physical Chemistry B, 104*(50), 11899-11905.

Scudiero, L., Barlow, D. E., Mazur, U., & Hipps, K. W. (2001). Scanning tunneling microscopy, orbital-mediated tunneling spectroscopy, and ultraviolet photoelectron spectroscopy of metal(II) tetraphenylporphyrins deposited from vapor. *Journal of the American Chemical Society, 123*(17), 4073-4080.

Sedghi, G., Sawada, K., Esdaile, L. J., Hoffmann, M., Anderson, H. L., Bethell, D., et al. (2008). Single molecule conductance of porphyrin wires with ultralow attenuation. *Journal Of The American Chemical Society, 130*(27), 8582-+.

Sek, S., Sepiol, A., Tolak, A., Misicka, A., & Bilewicz, R. (2004). Distance dependence of the electron transfer rate through oligoglycine spacers introduced into self-assembled monolayers. *Journal of Physical Chemistry B, 108*(24), 8102-8105.

Selzer, Y., Cai, L., Cabassi, M. A., Yao, Y., Tour, J. M., Mayer, T. S., et al. (2005). Effect of local environment on molecular conduction: Isolated molecule versus self-assembled monolayer. *Nano Letters, 5*(1), 61-65.

Seminario, J. M., De La Cruz, C. E., & Derosa, P. A. (2001). A theoretical analysis of metal-molecule contacts. *Journal Of The American Chemical Society, 123*(23), 5616-5617.

Shabarova, Z., & Bogdanov, A. (1994). *Advanced Organic Chemistry of Nucleic Acids*. Weinheim: VCH.

Shoji, O., Tanaka, H., Kawai, T., & Kobuke, Y. (2005). Single molecule visualization of coordination-assembled porphyrin macrocycles reinforced with covalent linkings. *Journal of the American Chemical Society, 127*(24), 8598-8599.

Siddarth, P., & Marcus, R. A. (1990). COMPARISON OF EXPERIMENTAL AND THEORETICAL ELECTRONIC MATRIX-ELEMENTS FOR LONG-RANGE ELECTRON-TRANSFER. *Journal of Physical Chemistry, 94*(7), 2985-2989.

Siemeling, U., Vorfeld, U., Neumann, B., Stammler, H. G., Zanello, P., & de Biani, F. F. (1999). *Terpyridines functionalised with ferrocenyl groups of different redox potential*.

Silva, G. M. E., & Acioli, P. H. (1997). Dynamics of charge transfer in molecular switches. *Synthetic Metals, 87*(3), 249-256.

Slowinski, K., Chamberlain, R. V., Bilewicz, R., & Majda, M. (1996). Evidence for inefficient chain-to-chain coupling in electron tunneling through liquid alkanethiol monolayer films on mercury. *Journal of the American Chemical Society, 118*(19), 4709-4710.

Slowinski, K., Chamberlain, R. V., Miller, C. J., & Majda, M. (1997). Through-bond and chain-to-chain coupling. Two pathways in electron tunneling through liquid alkanethiol monolayers on mercury electrodes. *Journal of the American Chemical Society, 119*(49), 11910-11919.

Smit, R. H. M. (2002). Measurement of the conductance of a hydrogen molecule. *Nature, 419*, 906-909.

Stan, M. R., Franzon, P. D., Goldstein, S. C., Lach, J. C., & Ziegler, M. M. (2003). Molecular electronics: From devices and interconnect to circuits and architecture. *Proceedings of the Ieee, 91*(11), 1940-1957.

Steenken, S. (1997). Electron transfer in DNA? Competition by ultra-fast proton transfer? *Biological Chemistry, 378*(11), 1293-1297.

Stewart, D. R., Ohlberg, D. A. A., Beck, P. A., Chen, Y., Williams, R. S., Jeppesen, J. O., et al. (2004). Molecule-independent electrical switching in Pt/organic monolayer/Ti devices. *Nano Letters, 4*(1), 133-136.

Strachan, D. R., Smith, D. E., Johnston, D. E., Park, T. H., Therien, M. J., Bonnell, D. A., et al. (2005). Controlled fabrication of nanogaps in ambient environment for molecular electronics. *Applied Physics Letters, 86*(4).

Structure of electrified interfaces. (1993). New York: VCH.

Sugiura, K., Tanaka, H., Matsumoto, T., Kawai, T., & Sakata, Y. (1999). A Mandala-patterned Bandanna-shaped porphyrin oligomer, C1244H1350N84Ni20O88, having a unique size and geometry. *Chemistry Letters*(11), 1193-1194.

Sumi, H., & Kakitani, T. (1996). Electron transfer via a midway molecule as seen in primary processes in photosynthesis; A new process describable as superexchange or sequential in mutually opposite limits. *Chemical Physics Letters, 252*(1-2), 85-93.

Tao, N. J. (1996). Probing potential-tuned resonant tunneling through redox molecules with scanning tunneling microscopy. *Physical Review Letters, 76*(21), 4066-4069.

Tao, N. J. (2005). Measurement and control of single molecule conductance. *Journal of Materials Chemistry, 15*(32), 3260-3263.

Tao, N. J. (2006). Electron transport in molecular junctions. *Nature Nanotechnology, 1*(3), 173-181.

Tao, N. J., Cardenas, G., Cunha, F., & Shi, Z. (1995). IN-SITU STM AND AFM STUDY OF PROTOPORPHYRIN AND IRON(III) AND ZINC(II) PROTOPORPHYRINS ADSORBED ON GRAPHITE IN AQUEOUS-SOLUTIONS. *Langmuir, 11*(11), 4445-4448.

Thompson, S. E., & Parthasarathy, S. (2006). Moore's law: the future of Si microelectronics. *Materials Today, 9*(6), 20-25.

Tian, W., Datta, S., Hong, S., Reifenberger, R., Henderson, J. I., & Kubiak, C. P. (1998). Conductance spectra of molecular wires. *The Journal of Chemical Physics, 109*(7), 2874-2882.

Tivanski, A. V., He, Y. F., Borguet, E., Liu, H. Y., Walker, G. C., & Waldeck, D. H. (2005). Conjugated thiol linker for enhanced electrical conduction of gold-molecule contacts. *Journal of Physical Chemistry B, 109*(12), 5398-5402.

Toher, C., Filippetti, A., Sanvito, S., & Burke, K. (2005). Self-interaction errors in density-functional calculations of electronic transport. *Physical Review Letters, 95*(14).

Tomfohr, J., & Sankey, O. F. (2004). Theoretical analysis of electron transport through organic molecules. *Journal of Chemical Physics, 120*(3), 1542-1554.

Tour, J. M. (1996). Conjugated macromolecules of precise length and constitution. Organic synthesis for the construction of nanoarchitectures. *Chemical Reviews, 96*(1), 537-553.

Tour, J. M., Rawlett, A. M., Kozaki, M., Yao, Y. X., Jagessar, R. C., Dirk, S. M., et al. (2001). Synthesis and preliminary testing of molecular wires and devices. *Chemistry-a European Journal, 7*(23), 5118-5134.

Tour, J. M., Wu, R., & Schumm, J. S. (1991). EXTENDED ORTHOGONALLY FUSED CONDUCTING OLIGOMERS FOR MOLECULAR ELECTRONIC DEVICES. *Journal of the American Chemical Society, 113*(18), 7064-7066.

Troisi, A., & Ratner, M. A. (2005). Modeling the inelastic electron tunneling spectra of molecular wire junctions. *Physical Review B, 72*(3).

Tulevski, G. S., Myers, M. B., Hybertsen, M. S., Steigerwald, M. L., & Nuckolls, C. (2005). Formation of catalytic metal-molecule contacts. *Science, 309*(5734), 591-594.

Vail, S. A., Krawczuk, P. J., Guldi, D. M., Palkar, A., Echegoyen, L., Tome, J. P. C., et al. (2005). Energy and electron transfer in polyacetylene-linked zinc-porphyrin[60]fullerene molecular wires. *Chemistry-A European Journal, 11*(11), 3375-3388.

vanHouten, H., & Beenakker, C. (1996). Quantum point contacts. *Physics Today, 49*(7), 22-27.

Venkataraman, L., Klare, J. E., Nuckolls, C., Hybertsen, M. S., & Steigerwald, M. L. (2006). Dependence of single-molecule junction conductance on molecular conformation. *Nature, 442*(7105), 904-907.

Venkataraman, L., Klare, J. E., Tam, I. W., Nuckolls, C., Hybertsen, M. S., & Steigerwald, M. L. (2006). Single-molecule circuits with well-defined molecular conductance. *Nano Letters, 6*(3), 458-462.

Visoly-Fisher, I., Daie, K., Terazono, Y., Herrero, C., Fungo, F., Otero, L., et al. (2006). Conductance of a biomolecular wire. *Proceedings Of The National Academy Of Sciences Of The United States Of America, 103*(23), 8686-8690.

Voityuk, A. A. (2006). Assessment of semiempirical methods for the computation of charge transfer in DNA pi-stacks. *Chemical Physics Letters, 427*(1-3), 177-180.

Wada, Y. (2002). *Prospects for single-molecule information-processing devices for the next paradigm*.

Waldeck, D. H., & Beratan, D. N. (1993). MOLECULAR ELECTRONICS - OBSERVATION OF MOLECULAR RECTIFICATION. *Science, 261*(5121), 576-577.

Walzer, K., Marx, E., Greenham, N. C., Less, R. J., Raithby, P. R., & Stokbro, K. (2004). Scanning tunneling microscopy of self-assembled phenylene ethynylene oligomers on Au(111) substrates. *Journal Of The American Chemical Society, 126*(4), 1229-1234.

Wan, L. J., Shundo, S., Inukai, J., & Itaya, K. (2000). Ordered adlayers of organic molecules on sulfur-modified Au(111): In situ scanning tunneling microscopy study. *Langmuir, 16*(5), 2164-2168.

Wassel, R. A., Credo, G. M., Fuierer, R. R., Feldheim, D. L., & Gorman, C. B. (2004). Attenuating negative differential resistance in an electroactive self-assembled monolayer-based junction. *Journal of the American Chemical Society, 126*(1), 295-300.

Weber, H. B., Reichert, J., Weigend, F., Ochs, R., Beckmann, D., Mayor, M., et al. (2002). Electronic transport through single conjugated molecules. *Chemical Physics, 281*(2-3), 113-125.

Weber, K., Hockett, L., & Creager, S. (1997). Long-range electronic coupling between ferrocene and gold in alkanethiolate-based monolayers on electrodes. *Journal of Physical Chemistry B, 101*(41), 8286-8291.

Wettig, S. D., Wood, D. O., Aich, P., & Lee, J. S. (2005). M-DNA: A novel metal ion complex of DNA studied by fluorescence techniques. *Journal of Inorganic Biochemistry, 99*(11), 2093-2101.

Wiederrecht, G. P., Svec, W. A., & Wasielewski, M. R. (1999). Triplet states with unusual spin polarization resulting from radical ion pair recombination at short distances. *Journal of the American Chemical Society, 121*(33), 7726-7727.

Wilson, G. S., & Neri, B. P. (1973). CYCLIC VOLTAMMETRY OF PORPHYRINS AND METALLOPORPHYRINS. *Annals of the New York Academy of Sciences, 206*(OCT22), 568-578.

Wu, Y. L., Mamiya, J., Kanazawa, A., Shiono, T., Ikeda, T., & Zhang, Q. J. (1999). Photoinduced alignment of polymer liquid crystals containing azobenzene moieties in the side chain. 6. Biaxiality and three-dimensional reorientation. *Macromolecules, 32*(26), 8829-8835.

Wu, Z. M., Steinacher, M., Huber, R., Calame, M., van der Molen, S. J., & Schonenberger, C. (2007). Feedback controlled electromigration in four-terminal nanojunctions. *Applied Physics Letters, 91*(5).

Xiao, X., Nagahara, L. A., Rawlett, A. M., & Tao, N. (2005). Electrochemical gate-controlled conductance of single oligo(phenylene ethynylene)s. *Journal Of The American Chemical Society, 127*(25), 9235-9240.

Xiao, X. Y., Xu, B. Q., & Tao, N. J. (2004). Measurement of single molecule conductance: Benzenedithiol and benzenedimethanethiol. *Nano Lett., 4*, 267-271.

Xing, Y., Bezer, S., Watson, R. M., Lund, P., Paul, A., Waldeck, D., et al. Single Molecule Conductivity Measurement of Peptide Nucleic Acids. *(In preparation)*.

Xing, Y., He, Y., & Borguet, E. Two dimensional charge diffusion in a self-assembled monolayer of redox active porphyrins. *(in preparation)*.

Xu, B. Q., & Tao, N. J. J. (2003). Measurement of single-molecule resistance by repeated formation of molecular junctions. *Science, 301*(5637), 1221-1223.

Xu, B. Q., Zhang, P. M., Li, X. L., & Tao, N. J. (2004). Direct conductance measurement of single DNA molecules in aqueous solution. *Nano Letters, 4*(6), 1105-1108.

Xu, B. Q. Q., Li, X. L. L., Xiao, X. Y. Y., Sakaguchi, H., & Tao, N. J. J. (2005). Electromechanical and conductance switching properties of single oligothiophene molecules. *Nano Letters, 5*(7), 1491-1495.

Xue, Y., & Ratner, M. A. (2003). Microscopic study of electrical transport through individual molecules with metallic contacts. I. Band lineup, voltage drop, and high-field transport. *Phys. Rev. B, 68*, 115406-115418.

Xue, Y. Q., Datta, S., Hong, S., Reifenberger, R., Henderson, J. I., & Kubiak, C. P. (1999). Negative differential resistance in the scanning-tunneling spectroscopy of organic molecules. *Physical Review B, 59*(12), R7852-R7855.

Xue, Y. Q., Datta, S., & Ratner, M. A. (2002). First-principles based matrix Green's function approach to molecular electronic devices: general formalism. *Chemical Physics, 281*(2-3), 151-170.

Yaliraki, S. N., Kemp, M., & Ratner, M. A. (1999). Conductance of molecular wires: Influence of molecule-electrode binding. *Journal of the American Chemical Society, 121*(14), 3428-3434.

Yaliraki, S. N., & Ratner, M. A. (1998). Molecule-interface coupling effects on electronic transport in molecular wires. *Journal of Chemical Physics, 109*(12), 5036-5043.

Yamada, R., Kumazawa, H., Noutoshi, T., Tanaka, S., & Tada, H. (2008). Electrical conductance of oligothiophene molecular wires. *Nano Letters, 8*(4), 1237-1240.

Yasuda, S., Yoshida, S., Sasaki, J., Okutsu, Y., Nakamura, T., Taninaka, A., et al. (2006). Bond fluctuation of S/Se anchoring observed in single-molecule conductance measurements using the point contact method with scanning tunneling microscopy. *Journal of the American Chemical Society, 128*(24), 7746-7747.

Ye, T. (2003). *STRUCTURE, DYNAMICS, AND REACTIVITY OF MOLECULAR ASSEMBLIES*

AT INTERFACES. University of Pittsburgh, Pittsburgh.

Ye, T., He, Y. F., & Borguet, E. (2006). Adsorption and electrochemical activity: An in situ electrochemical scanning tunneling microscopy study of electrode reactions and potential-induced adsorption of porphyrins. *Journal of Physical Chemistry B, 110*(12), 6141-6147.

Yeager, E. (1984). ELECTROCATALYSTS FOR O-2 REDUCTION. *Electrochimica Acta, 29*(11), 1527-1537.

Yokoyama, T., Kamikado, T., Yokoyama, S., & Mashiko, S. (2004). Conformation selective assembly of carboxyphenyl substituted porphyrins on Au (111). *Journal of Chemical Physics, 121*(23), 11993-11997.

Yokoyama, T., Yokoyama, S., Kamikado, T., Okuno, Y., & Mashiko, S. (2001). Selective assembly on a surface of supramolecular aggregates with controlled size and shape. *Nature, 413*(6856), 619-621.

Yonemoto, E. H., Saupe, G. B., Schmehl, R. H., Hubig, S. M., Riley, R. L., Iverson, B. L., et al. (1994). ELECTRON-TRANSFER REACTIONS OF RUTHENIUM TRISBIPYRIDYL-VIOLOGEN DONOR-ACCEPTOR MOLECULES - COMPARISON OF THE DISTANCE DEPENDENCE OF ELECTRON-TRANSFER RATES IN THE NORMAL AND MARCUS INVERTED REGIONS. *Journal of the American Chemical Society, 116*(11), 4786-4795.

Yoshimoto, S., Inukai, J., Tada, A., Abe, T., Morimoto, T., Osuka, A., et al. (2004). Adlayer structure of and electrochemical O-2 reduction on cobalt porphine-modiried and cobalt octaethylporphyrin-modifled Au(111) in HClO4. *Journal of Physical Chemistry B, 108*(6), 1948-1954.

Yoshimoto, S., & Itaya, K. (2007). Advances in supramolecularly assembled nanostructures of fullerenes and porphyrins at surfaces. *Journal of Porphyrins and Phthalocyanines, 11*(5-6), 313-333.

Yoshimoto, S., Sato, K., Sugawara, S., Chen, Y., Ito, O., Sawaguchi, T., et al. (2007). Formation of supramolecular nanobelt arrays consisting of cobalt(II) "Picket-Fence" porphyrin on Au surfaces. *Langmuir, 23*(2), 809-816.

Yoshimoto, S., Tada, A., Suto, K., Narita, R., & Itaya, K. (2003). Adlayer structure and electrochemical reduction of O-2 on self-organized arrays of cobalt and copper tetraphenyl porphines on a Au(111) surface. *Langmuir, 19*(3), 672-677.

Yoshimoto, S., Tsutsumi, E., Suto, K., Honda, Y., & Itaya, K. (2005). Molecular assemblies and redox reactions of zinc(II) tetraphenylporphyrin and zinc(II) phthalocyanine on Au(111) single crystal surface at electrochemical interface. *Chemical Physics, 319*(1-3), 147-158.

Yoshimoto, S., Yokoo, N., Fukuda, T., Kobayashi, N., & Itaya, K. (2006). Formation of highly ordered porphyrin adlayers induced by electrochemical potential modulation. *Chemical Communications*(5), 500-502.

Yuan, Q., Xing, Y., & Borguet, E. An STM study of the pH dependent redox activity of a two dimensional hydrogen bonding porphyrin network at an electrochemical interface. *(Submitted)*.

Zheng, G. Y., Rillema, D. P., & Reibenspies, J. H. (1999). Synthesis, X-ray structure, and physical and photophysical properties of the heterobimetallic complex Fe(eta(5)-C5H4PPh2)(2)Pt(bph). *Inorganic Chemistry, 38*(4), 794-797.

Zhou, Y. S., Wang, B., Zhu, M. Z., & Hou, J. G. (2005). Observation of co-existence of 'face-on' and 'edge-on' stacking styles in a porphyrin monolayer. *Chemical Physics Letters, 403*(1-3), 140-145.

Zhu, X. Y. (2002). Electron transfer at molecule-metal interfaces: A two-photon photoemission study. *Annual Review of Physical Chemistry, 53*, 221-247.

APPENDICES

APPENDIX A

STM Tip Preparation for PNA Conductivity Measurements in Aqueous Solution

1. Cut tip vs Etched tip

The gold STM tips for break-junction measurements can be prepared by two different techniques: 1) cutting with scissors, and 2) electrochemical etching. The tips cut by scissors are usually very sharp and, with proper cutting technique, most of the cut tips show clear gold atomic steps when imaging the Au(111) surface by STM. The cut tips also work well for the break-junction measurements in organic solvents and under atmosphere.

For measurements in aqueous conditions, the tip has to be coated by an insulating material to prevent current passing through the solution to the tip. However, the very end of the tip should be left uncoated for the break-junction measurements. We found out that while the uncoated cut STM tips work well in air and in organic solutions, they do not perform well when coated with insulating materials, probably because the coating is too thick. On the other hand, the electrochemically etched gold tips show much higher success rate after coating. The different performance for coated tips from the two preparation methods is probably due to the difference in shape of the two kinds of tips.

2. Gold tip etching

The gold tips were etched in a 3 M sodium chloride solution with 1% perchloric acid.[272] As shown in Figure A-1, a 0.25 mm diameter gold tip is submerged in the etchant solution together with a carbon electrode (prepared by removing the wood cover from a pencil). An AC voltage, about 2-3 volts, is applied between the wire and the carbon electrode to drive electrochemical etching of gold. The etching rate at the etchant/air interface is much faster than the submerged part, leading to the formation of a narrow neck (enlarge view in Figure A-1) at the interface. Usually after ~ 5 minutes, the

neck becomes too thin to support the weight of the bottom part of wire and breaks, creating a sharp gold tip. The etching process stops when the submerged part of wire drops into the solution.

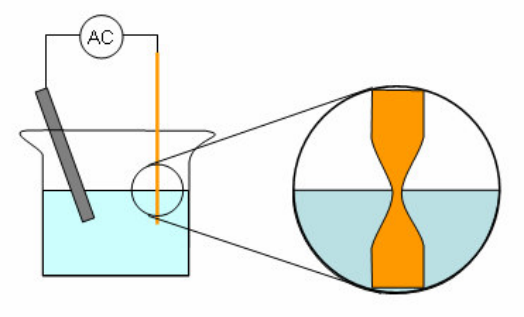

Figure A-1: Electrochemical etching setup for Au tips

3. Apiezon wax coating

The etched gold tips are coated by Apiezon wax using a home built setup (made by Dr. Tao Ye). A small copper heating block is screwed to the end of a soldering iron (Figure A-2). The screw on the back of the copper piece is used to attach a thermocouple to monitor the temperature during coating. A small amount of Apiezon wax is melted in the slit of the heating block. The gold tip is inserted into the melted wax and is pushed up through the wax. When the Apiezon cools down on the gold tip and shrinks slightly, the very end of the tip is exposed. The coated tip usually shows very low leaking current (< 0.01 nA) when immersed into aqueous solutions for break-junction experiments.

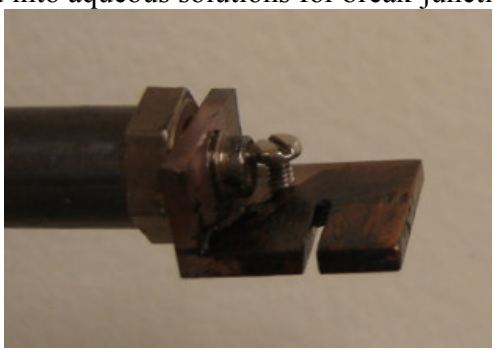

Figure A–2: Copper heating block for Apiezon wax coating.

APPENDIX B

Procedure for Preparation of a Gold Bead

1. Mount a 0.6 mm diameter gold wire on a stand using tweezers. Place a beaker of water below the wire to catch any gold that may drop.

2. Use an H_2 flame to melt the wire until a bead forms at the bottom.

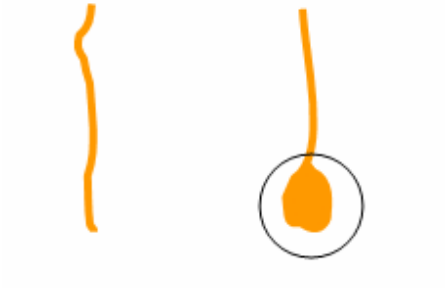

3. Direct the flame to heat the bead and wire until glowing and molten.

4. Use the flame to move the phase separation (see diagram below) up and down to drive contaminants to the surface.

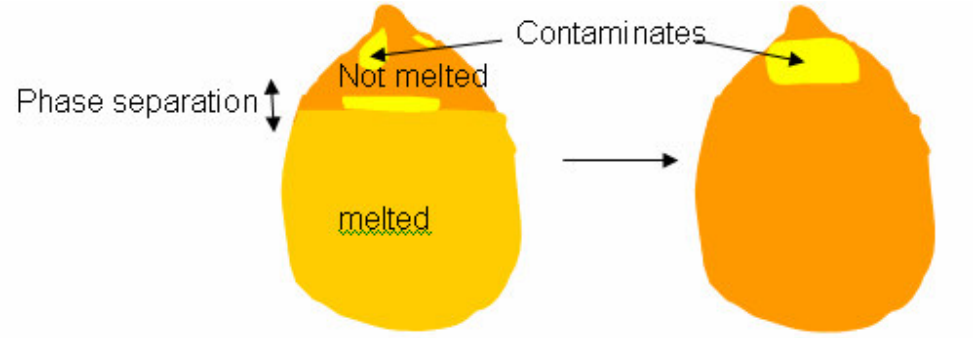

5. Submerge in Aqua Regia (1:3 HCl and HNO_3) for 20 seconds at room temperature to remove the contaminants from the surface.

6. Repeat steps 4 and 5 until all the contaminants are removed.

7. Clean the gold briefly in Piranha solution (1:3 H_2O_2 and H_2SO_4).

The gold bead prepared by the above procedure is attached to a gold foil with the Au(111) facet facing up (as shown in Figure B-1). A clean gold bead usually has Au(111) facets with dimensions of about 0.8 mm x 0.2 mm. A typical STM image is

shown Figure B-2. For a well prepared Au bead, usually every STM image shows atomicly flat Au(111) terraces at least a few hundred nanometers wide.

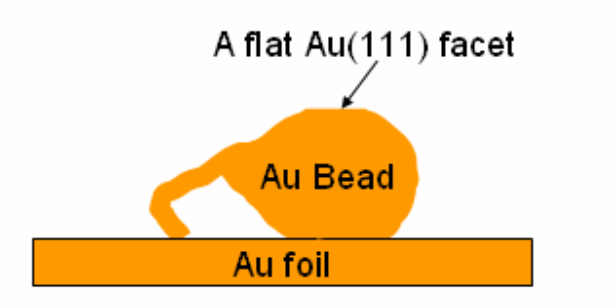

Figure B-1: An Au bead is attached to an Au foil with the Au(111) facet facing up.

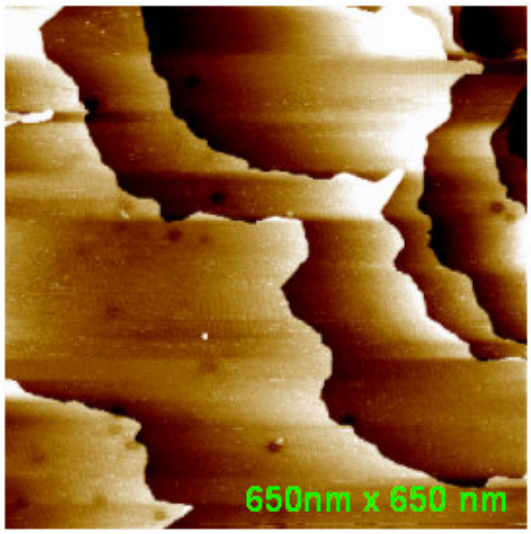

Figure B-2: A typical STM image of an Au(111) surface on a gold bead.

APPENDIX C

Synthesis and Deprotection of Carbodithioate OPE Molecules

This work was done by Dr. Tae-Hong Park in the Therien group at Duke University.

Synthesis of C1

The synthesis and characterization of 2-(Trimetylsilyl)ethyl ester of C1 are performed using the following procedure.

A suspension of NaOMe (246 mg, 4.56 mmol) and sulfur powder (146 mg, 4.56 mmol) in anhydrous THF (10 mL) was stirred for 30 min under Ar. To this mixture, α,α'-dichloro-p-xylene (200 mg, 1.14 mmol, Aldrich) was added, and after 24 h, (2-bromoethyl)trimethylsilane (0.73 mL, 4.53 mmol, TCI America) was added. After stirring for 24 h, the reaction mixture was quenched with water, and then extracted with CH_2Cl_2 (×3). The combined organic layers were dried over $MgSO_4$. After the solvent was evaporated, the residue was chromatographed on silica gel using hexane to afford red solid (22 mg, 4.5% yield based on α,α'-dichloro-p-xylene). 1H NMR ($CDCl_3$, 500 MHz): δ 7.94 (4H, s) 3.37 (4H, m), 1.05 (4H, m), and 0.11 (18H, s) ppm. 13C(1H) NMR ($CDCl_3$, 125 MHz): δ 227.7, 147.5, 126.8, 34.2, 14.9 and –1.59 ppm. Anal. calcd for $C_{18}H_{30}S_4Si_2$: C 50.18%, H 7.02%, found C 50.11%, H 6.79%.

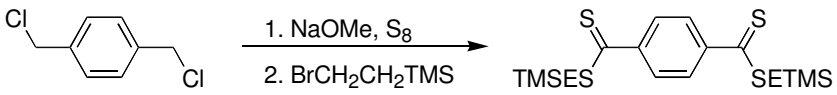

Figure C-1:: Synthesis of 1,4-benzenedicarbodithioic acid 2-(trimethylsilyl)ethyl ester.

a)

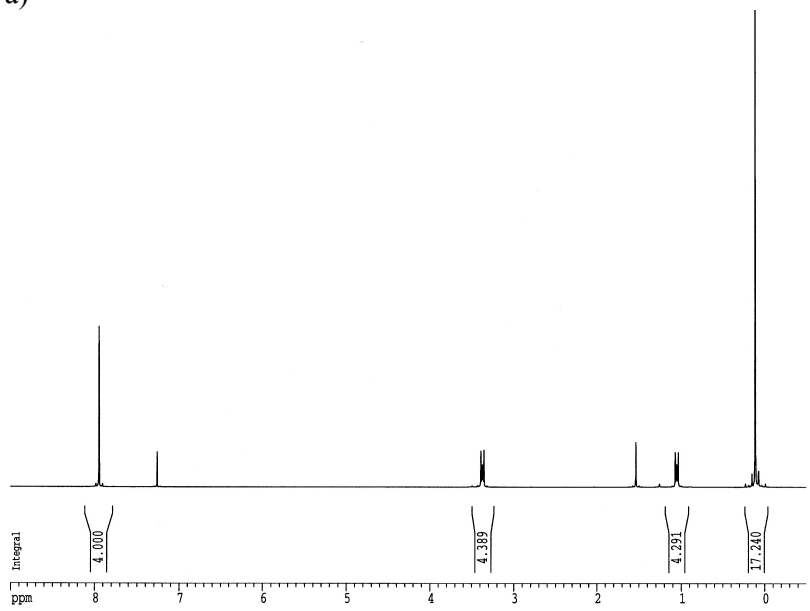

b)

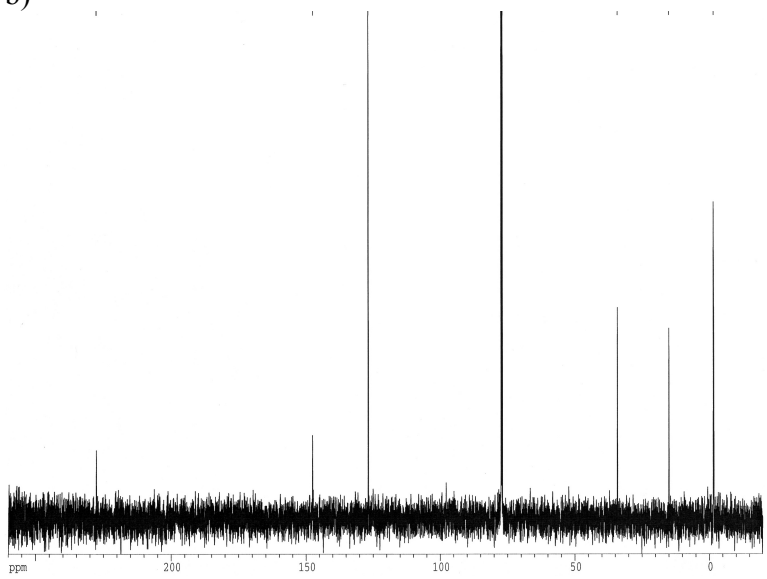

Figure C-2: 1H NMR (a) and 13C NMR (b) spectra of 1,4-benzenedicarbodithioic acid 2-(trimethylsilyl)ethyl ester.

Deprotection of precursor molecules

1,4-Benzenedithiol (T1) was used as received. Acetyl-protected precursor molecules of 4,4'-(ethyne-1,2-diyl)bisbenzenethiol (T2) and 4,4'-(1,4-phenylenedi(ethyne-2,1-diyl))bisbenzenethiol (T3) were deprotected using NaOH right before SAM preparation. Deprotection was accomplished by adding 10μL of 0.2 M NaOH (aq) to a 5 mL THF solution containing a precursor molecule (100 μM) immediately prior to these experiments.

TMSE-protected precursor molecules of 1,4-benzenedicarbodithioic acid (C1), 4,4'-(ethyne-1,2-diyl)bisdithiobenzoic acid (C2) and 4,4'-(1,4-phenylenedi(ethyne-2,1-diyl))bisdithiobenzoic acid (C3) were deprotected using tetra-n-butylammonium fluoride (TBAF) immediately prior to SAM preparation, by adding 200μL of TBAF solution (0.01 M in THF) to a 5 mL THF solution containing the precursor molecule (100 μM).

APPENDIX D

Synthesis of PNA Molecules

PNA oligomers were synthesized by solid phase synthesis (Boc protection strategy).[213] MBHA resin (Peptides International) with a loading of 0.18 meq/ gm was down-loaded using Boc-L-Cys-(4-MeOBzl)-OH (NovaBiochem) to an estimated loading of 0.04-0.06 meq/gm. Then three to seven Boc-T-OH PNA monomers (Applied Biosystems) were coupled using HCTU as a coupling agent. For the PNA molecules used in the electrochemical study, ferrocenecarboxylic acid was coupled to the N-terminus using the standard monomer coupling procedure, repeated twice to increase the yield of ferrocene-conjugated PNA. For the PNA molecules used in the STM break-junction study, another Cysteine group was added to the N-terminus. Oligomers were cleaved using TFMSA and were precipitated in ethyl ether and dried under nitrogen. Solid PNA products were dissolved in 15 % acetonitrile in water and were purified by reversed-phase HPLC using a solvent gradient from 15% to 35% acetonitrile in water over 40 minutes. The collected fractions were characterized by MALDI-TOF mass spectrometry on a PerSeptive Voyager STR MS.

APPENDIX E

Theoretical Simulation of the OPE Molecules

Electronic structure calculations: The six structures, three carbodithioate-terminated systems (CTS) and three dithiol-terminated systems (DTS), shown in chart 1 were built and geometry optimized with DFT and a B3LYP exchange correlation functional with a 6-31G* basis set, using Gaussian03.[273] The electronic structure of these geometry optimized structures was calculated using an INDO/s Hamiltonian[274] [197, 274, 275], and the molecular orbitals were used as input for the NEGF analysis of transport properties.

NEGF calculation: In the NEGF approach[177] the system is partitioned into three subsystems (Figure E-1): The device region (center) with the molecule and thiol, carbodithioate linkers and the left and right featureless electrodes (contacts) characterized purely in terms of the chemical potentials μ_L/μ_R. ε_F is the Fermi energy and V is the applied potential bias which is assumed to drop symmetrically across the two electrodes. The Green's function describes the molecule and its interactions with the electrodes:

$$\mathbf{G}(E) = \frac{1}{(E\mathbf{I} - \mathbf{H} - \mathbf{\Sigma}_L - \mathbf{\Sigma}_R)} \qquad \text{Eq. E-1}$$

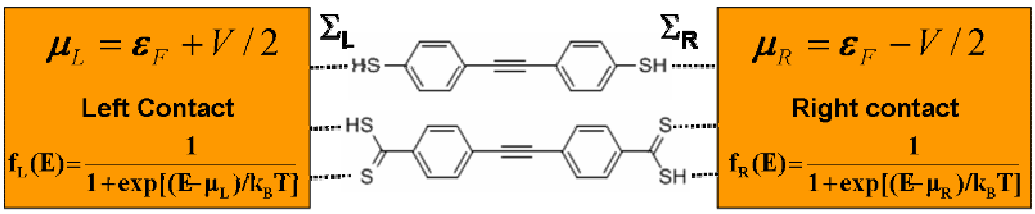

Figure E-1: Schematic for the separation of the system for NEGF calculations: a device region (the isolated molecule) and two featureless electrodes.

H is the Hamiltonian of the isolated molecule. The self-energies Σ describe the broadening and shifts in molecular energies induced by the right (R) and left (L)

electrodes. The transmission coefficient sums over all pathways for charge transport at energy E from one electrode to the other:

$$T(E) = Tr[\mathbf{\Gamma_L G \Gamma_R G}^{+}] \qquad \text{Eq. E-2}$$

The broadening matrix: $\Gamma = i\,[\Sigma - \Sigma+]$ is proportional to the imaginary part of the self energy.[74, 148, 178] We introduce the broadening matrix as a parameter represented in our calculations in the basis of atomic orbitals. The molecule is assumed to contact the metal electrodes only via the sulfur atoms, i.e. only orbitals of the sulfur atoms are broadened and the couplings among atomic orbitals are not affected by the contacts. The magnitude of the sulfur-gold coupling parameter (γ) was also chosen to be small so that the contacts do not strongly perturb the molecular eigenstates. This is the weak electrode-molecule coupling limit, and the transmission coefficient (or current) can be partitioned into contributions from individual molecular orbitals. The Green's function in the basis of molecular eigenstates is:

$$\mathbf{G}(E) = \frac{1}{\left[E\mathbf{I} - \mathbf{H}^{'} + \frac{i}{2}(\mathbf{\Gamma}_{\mathbf{L}}^{'} + \mathbf{\Gamma}_{R}^{'})\right]} \qquad \text{Eq. E-3}$$

where $\mathbf{H}^{'} = \mathbf{U}^{+}\mathbf{H}\mathbf{U}$; $\mathbf{\Gamma}_{\mathbf{L/R}}^{'} = \mathbf{U}^{+}\mathbf{\Gamma}_{\mathbf{L/R}}\mathbf{U}$; U diagonalizes the Fock matrix H. The current is given by the Landauer expression:

$$I(V) = \frac{q}{h}\int T(E)\left[f_L(E) - f_R(E)\right]dE \qquad \text{Eq. E-4}$$

The Fermi function defines the electron occupancy for each electrode (Figure E-1). The Fermi energy E_F is the same for both electrodes if they are made of the same metal, and V is an external potential bias (0-100 mV). The potential drop is assumed to be symmetric across the two electrodes. The small biases applied here are not expected to cause significant changes in molecular geometry or energies, and no potential drop is assumed across the molecule. In the weak molecule-electrode coupling limit, our

calculations are expected to capture relative trends and we analyze the relationship between the molecular structure and the conductance trends for the CTS and DTS.

APPENDIX F

List of Publications

1. Yangjun Xing, Tae-Hong Park, Ravindra Venkatramani, Shahar Keinan, David N. Beratan, Michael J. Therien, and Eric Borguet, *Optimizing Single Molecule Conductivity of Conjugated Organic Oligomers with Conjugated Carbodithioate Linkers.* (Submitted to the Journal of the American Chemical Society)
2. Yangjun Xing, Nikolay Dementev and Eric Borguet, *Chemical Labeling for Quantitative Characterization of Surface Chemistry*, Current Opinion in Solid State & Materials Science, **11**, 8691 (2007)
3. Yangjun Xing and Eric Borguet, *The Specificity and Sensitivity of Fluorescence Labeling of Surface Species,* Langmuir, **23**(2) 684-688 (2007)
4. Yangjun Xing, Yufan He, and Eric Borguet, *Two dimensional charge diffusion in a self assembled monolayer of redox active porphyrins.* (in preparation)
5. Yangjun Xing, Silvia Bezer, Richard M. Watson, David H. Waldeck, Catalina Achim, and Eric Borguet, *Single Molecule Conductivity Measurement of Peptide Nucleic Acids.* (In preparation)
6. Andrii Buvailo, Yangjun Xing, Jacqueline Hines, and Eric Borguet, *LiCl doped TiO2 thin films based SAW humidity sensors possessing ultrafast response and recovery dynamics.* (Submitted to Journal of the American Chemical Society)
7. Andrii Buvailo, Yangjun Xing, Jacqueline Hines, and Eric Borguet*, Thin polymer film based rapid and reversible wireless Surface Acoustic Wave humidity sensors.* (Submitted to Analytical Chemistry)
8. Qunhui Yuan, Yangjun Xing, and Eric Borguet, *An STM study of the pH dependent redox activity of a two dimensional hydrogen bonding porphyrin network at an electrochemical interface.* (Submitted to the Journal of the American Chemical Society)
9. Amit Paul, Richard M. Watson, Paul Lund, Yangjun Xing, Kathleen Burke, Yufan He, Eric Borguet, Catalina Achim, and David H. Waldeck, *Charge Transfer through Single Stranded Peptide Nucleic Acid Composed of Thymine Nucleotide,.* Journal of Physical Chemistry C, **112** (18) 7233-7240 (2008)
10. Guillaume Lamour, Ahmed Hamraoui, Andrii Buvailo, Yangjun Xing, Sean Keuleyan, Vivek Prakash, Ali Eftekhari, and Eric Borguet, *Contact angle measurements using a simplified experimental setup*, (Submitted to Journal of Chemical Education)